



2015

SEDIMENT ORGANIC CARBON FATE AND TRANSPORT IN A FLUVIOKARST WATERSHED IN THE BLUEGRASS REGION

Admin Husic

University of Kentucky, admin.husic@uky.edu

[Click here to let us know how access to this document benefits you.](#)

Recommended Citation

Husic, Admin, "SEDIMENT ORGANIC CARBON FATE AND TRANSPORT IN A FLUVIOKARST WATERSHED IN THE BLUEGRASS REGION" (2015). *Theses and Dissertations--Civil Engineering*. 30.
https://uknowledge.uky.edu/ce_etds/30

This Master's Thesis is brought to you for free and open access by the Civil Engineering at UKnowledge. It has been accepted for inclusion in Theses and Dissertations--Civil Engineering by an authorized administrator of UKnowledge. For more information, please contact UKnowledge@lsv.uky.edu.

STUDENT AGREEMENT:

I represent that my thesis or dissertation and abstract are my original work. Proper attribution has been given to all outside sources. I understand that I am solely responsible for obtaining any needed copyright permissions. I have obtained needed written permission statement(s) from the owner(s) of each third-party copyrighted matter to be included in my work, allowing electronic distribution (if such use is not permitted by the fair use doctrine) which will be submitted to UKnowledge as Additional File.

I hereby grant to The University of Kentucky and its agents the irrevocable, non-exclusive, and royalty-free license to archive and make accessible my work in whole or in part in all forms of media, now or hereafter known. I agree that the document mentioned above may be made available immediately for worldwide access unless an embargo applies.

I retain all other ownership rights to the copyright of my work. I also retain the right to use in future works (such as articles or books) all or part of my work. I understand that I am free to register the copyright to my work.

REVIEW, APPROVAL AND ACCEPTANCE

The document mentioned above has been reviewed and accepted by the student's advisor, on behalf of the advisory committee, and by the Director of Graduate Studies (DGS), on behalf of the program; we verify that this is the final, approved version of the student's thesis including all changes required by the advisory committee. The undersigned agree to abide by the statements above.

Admin Husic, Student

Dr. James Fox, Major Professor

Dr. Yi-Tin Wang, Director of Graduate Studies

SEDIMENT ORGANIC CARBON FATE AND TRANSPORT IN A FLUVIOKARST
WATERSHED IN THE BLUEGRASS REGION

THESIS

A thesis submitted in partial fulfillment of the
requirements for the degree of Master of Science in
Civil Engineering in the College of Engineering
at the University of Kentucky

By

Admin Husic

Lexington, Kentucky

Director: Dr. James Fox, Professor of Civil Engineering

Lexington, Kentucky

2015

Copyright © Admin Husic 2015

ABSTRACT OF THESIS

SEDIMENT ORGANIC CARBON FATE AND TRANSPORT IN A FLUVIOKARST WATERSHED IN THE BLUEGRASS REGION

Mature karst topography is well recognized within the hydrology and geology communities to include subterranean fluid pathways that act as turbulent conduits conveying fluid from surface stream sinks called swallets to sources called springs. However, we find that little knowledge has been reported with regards to the transport and fate of terrestrially-derived sediment organic carbon (SOC) within karst watersheds. This study investigated the hypothesis that karst pathways could act as biologically active conveyors of SOC that temporarily store sediment, turnover carbon at higher rates than otherwise considered, and recharge depleted SOC back to the surface stream within the fluvial system. Mixed research methods were applied within a mature karst network. Methods included high resolution measurements of water and sediment characteristics of surface streams, carbon and stable carbon isotope measurements of transported sediment, and numerical modeling of water and sediment pathways. The mixing of sediment during net zero deposition and erosion was investigated in this study using a parameter calibrated to SOC data. Results of this study showed that heterotrophic bacteria in the subsurface conduit oxidized $0.05 \text{ tCkm}^{-2}\text{y}^{-1}$ resulting from the temporary storage of terrestrial carbon in the karst conduit. The subsurface conduit transports $0.15 \text{ tCkm}^{-2}\text{y}^{-1}$ out of the fluviokarst watershed.

KEYWORDS: karst, fluvial system, organic carbon, watershed, sediment transport modeling

Admin Husic

10-20-2015

SEDIMENT ORGANIC CARBON FATE AND TRANSPORT IN A FLUVIOKARST
WATERSHED IN THE BLUEGRASS REGION

By

Admin Husic

James Fox

Director of Thesis

Y. T. Wang

Director of Graduate Studies

10-20-2015

Acknowledgements

The following thesis benefitted from the input of several people. Firstly, I would like to thank my Thesis Chair, Dr. James Fox, for his support and encouragement. I would also like to thank the other members of my Thesis Committee: Dr. Yi-Tin Wang and Dr. Carmen Agouridis. Jim Currens and others at the Kentucky Geological Survey have provided great support in the field and laboratory. Finally, I would like to thank the University of Kentucky Civil Engineering Department for providing me the academic support to develop and implement my ideas.

Table of Contents

Acknowledgements.....	iii
List of Tables	vii
List of Figures.....	viii
Chapter 1 Introduction	1
1.1 Background.....	1
1.2 Research Need	3
1.3 Objectives	5
1.4 Thesis Layout.....	6
Chapter 2 Literature Review.....	9
2.1 Karst Processes	9
2.1.1 Geologic.....	9
2.1.2 Hydrologic	11
2.1.3 Hydraulic.....	12
2.1.4 Darcy-Weisbach Friction Factor.....	14
2.2 Fluvial Processes.....	16
2.2.1 Sediment Production.....	16
2.2.2 Deposition and Sedimentation	17
2.2.3 Sediment Transport and Downstream Flux	17
2.3 Sediment Organic Carbon Processes	18
2.3.1 Source	20
2.3.2 Generation.....	21
2.3.3 Decomposition.....	22
2.4 Sediment Transport Studies in Karst	23
2.5 Sediment Organic Carbon Studies in Karst	24
2.6 Water, Sediment, and SOC Source, Fate, and Transport in Karst	26
2.6.1 Flow and Storage of Water in Karst	26
2.6.2 Dye Tracing	27
2.6.3 Mapping of Karst Features.....	28
2.6.4 Laboratory Studies.....	29

2.6.5 Hydrograph Separation	29
2.6.6 Isotope Analysis.....	30
2.6.7 Numerical Modeling	30
Chapter 3 Study Site	39
3.1 Physiogeographic Setting.....	40
3.2 Geology.....	41
3.3 Human Disturbances.....	42
3.4 Historic Study of System	43
3.5 Water Processes, Source, and Mechanics	45
3.6 Sediment Transport Sources and Processes	46
3.7 Carbon Mechanisms and Transport	47
Chapter 4 Methodology	51
4.1 Water Data	51
4.1.1 Stream Gages	51
4.1.2 Observation Wells.....	52
4.1.3 Dye Traces	54
4.2 Sediment Data.....	56
4.2.1 Total Suspended Solids Pumps and Samplers	56
4.2.2 Sediment Flux	57
4.2.3 Particle Size Distribution	60
4.3 Carbon Data	61
4.3.1 Source Sampling	61
4.3.2 Outlet Sampling	62
4.3.3 Lab Analysis	63
4.4 Numerical Modeling.....	64
4.4.1 Water Budget and Hydrologic Model.....	65
4.4.2 Hydraulic Model	66
4.4.3 Carbon Model	73
4.4.4 Model Inputs and Parameterization	79
4.4.5 Calibration and Validation.....	81
4.4.6 Sensitivity and Uncertainty Analysis.....	83
4.4.7 High Performance Computing	85

Chapter 5 Results	100
5.1 Model Evaluation.....	100
5.1.1 Water.....	100
5.1.2 Sediment	100
5.1.3 Sediment Organic Carbon.....	101
5.1.4 Sensitivity of P_{algae}	103
5.2 Temporal and Spatial Distributions of Water, Sediment, and Sediment Carbon.....	104
5.2.1 Water.....	104
5.2.2 Sediment	105
5.2.3 Sediment Organic Carbon.....	107
5.3 Long-term Budgets of Water, Sediment, and Sediment Carbon	108
5.3.1 Water.....	108
5.3.2 Sediment	109
5.3.3 Sediment Organic Carbon.....	110
Chapter 6 Discussion	128
6.1 Karst Conduits as Active Biologic Conveyors	128
6.2 Physical and Biogeochemical Processes in Karst Systems.....	129
6.3 Advancement of Water Quality Modeling.....	134
Chapter 7 Conclusions	136
References.....	139
Vita.....	161

List of Tables

Table 2-1: Table of Discharges and Catchment Areas for Karst Springs.....	32
Table 4-1: Flow rate relationships between stream gages in Cane Run Watershed	86
Table 4-2: Relationships between sediment concentration, C_{ss} , and stream flow rate, Q	86
Table 4-3: Conduit Bathymetry, Q_{SS} Inflow, and Land Use Information for Model Cells	87
Table 4-4: Un-mixing Results for Means of Data Inputs using Carbon Stable Isotope ...	87
Table 4-5: Inputs and parameter values for sediment transport model.....	88
Table 4-6: Carbon and $\delta^{13}C$ Uncertainty Analysis Inputs	89
Table 5-1: Sensitivity Analysis Percent Change in Sediment Yield (SY).....	112
Table 5-2: Sensitivity Analysis Percent Change in average Suspended Sediment SOC%	112
Table 5-3: Carbon Source Contribution for Fixed Algae Percent using Monte Carlo Simulation (n = 10,000)	113
Table 5-4: Carbon Model Calibration and Validation Uncertainty using Monte Carlo Simulation (n = 10,000)	113

List of Figures

Figure 2-1: Common Karst Topographical Features (KGS, 2002).....	34
Figure 2-2: Conceptual Model of Surface-Subsurface Hydraulics Using an Observed Hydrograph	35
Figure 2-3: The Fluvial System (Miller, 1990).....	36
Figure 2-4: In-stream sediment carbon physical and biogeochemical processes including advective flux in and out of the stream reach, dissolution, precipitation, erosion, deposition, invasion, evasion, assimilation, sloughing, decomposition, aggregation, and bacterial respiration. (Ford and Fox, 2012)	37
Figure 2-5: Conceptual Model of SOC Transport in Fluviokarst	38
Figure 3-1: Location Map of Cane Run Watershed and Royal Spring Basin.....	48
Figure 3-2: Cane Run Creek Land Use Map	49
Figure 3-3: Qualitative Dye Traces in Royal Spring (adapted from Lee, 2012)	50
Figure 4-1: Fluviokarst Sediment and Carbon Transport Calibration Method. STAGE 1: model preparation. Sediment pirated from tributaries (Q_{SS}), conduit flow rate (Q_i), and hydraulic and hydrologic inputs were supplied to the Sediment Transport Model. STAGE 2: sediment calibration. Transport coefficients (C_{tc}) are adjusted so that model results reflect TSS data. STAGE 3: carbon calibration. Sediment transport model results, carbon source unmixing, decomposition rates (k), and percent algae ($\%algae$) were used as inputs to the Carbon Model which was calibrated by adjusting the soil decomposition rate (k_{soil}) and sediment exchange rate (ex) to reflect SOC data.	90
Figure 4-2: TSS vs Turbidity Relationship for Groundwater Station Samples	91
Figure 4-3: Velocity and Concentration Profiles in Surface Streams.....	92
Figure 4-4: Velocity and Concentration Profiles in Karst Conduit	93
Figure 4-5: Particle Size Distributions a) urban tributary, b) agriculture tributary, c) surface outflow, d) subsurface outflow. (1) and (2) indicates multiple samples taken on same date.....	94
Figure 4-6: Sediment Trap Sampler (Phillips et al., 2000).....	95
Figure 4-7: Weekly Max Flows Royal Spring vs Conduit (Groundwater Station)	95

Figure 4-8: Modeling Framework for Coupled Surface-Subsurface Model.....	96
Figure 4-9: Conceptual Water Budget for Coupled Drainage Network	97
Figure 4-10: Friction Factor vs Conduit Velocity.....	98
Figure 4-11: Flow and Sediment into Subsurface Conduit Conceptualization (GW = Groundwater Station, RS = Royal Spring). Conduit geometry increases from Cell 1 – 10 then remains constant from Cell 10 – 16.	99
Figure 5-1: Suspended Sediment Discharge (Groundwater Station) Model Calibration and Validation.....	114
Figure 5-2: Sensitivity Analysis for Sediment Model	115
Figure 5-3: Calibration and Validation of Carbon Model. Model results are for the springhead in comparison with the sediment carbon trap measurements also collected at the springhead.	115
Figure 5-4: Sensitivity Analysis for Carbon Model.....	116
Figure 5-5: Monte Carlo Simulation (n = 10,000) Source Contribution Results for Fixed Algae Percentage	116
Figure 5-6: Inflows (a and b) and Outflows (c and d) to the Coupled Drainage Network Normalized by Maximum Flow Rate at Each Location	117
Figure 5-7: Well stage at the Groundwater Station (Cell #10).....	118
Figure 5-8: Tributary Suspended Sediment Flux with a) high flows and b) low flows..	119
Figure 5-9: Model Results (Groundwater Station) for 2011-2013 Water Years	120
Figure 5-10: Longitudinal Bed Depth Changes in Conduit.....	121
Figure 5-11: Sediment Organic Carbon Flux in Subsurface Conduit.....	122
Figure 5-12: Organic Carbon Percentage in Suspended Sediment and Bed Sediment..	122
Figure 5-13: Fractioning of Carbon Pools in Conduit Bed.....	123
Figure 5-14: Fractioning of Carbon Sources in Suspended Conduit Load.....	123
Figure 5-15: Bi-weekly Carbon Decomposition Yield in Subsurface Conduit	124
Figure 5-16: Water Budget for Cane Run Fluviokarst Watershed	125
Figure 5-17: Sediment Budget for Cane Run Fluviokarst Watershed	126
Figure 5-18: Carbon Budget for Cane Run Fluviokarst Watershed	127

Chapter 1 Introduction

1.1 Background

Fluvial networks are recognized to not only act as conveyors of sediment organic carbon, but also to serve as ecosystems that can actively turnover terrestrial-derived carbon and generate new autochthonous organic matter (Battin et al., 2008; Ford and Fox, 2012). Terrestrial-derived sediment organic carbon originates in the uplands within surface soils and streambank sediments where it is then transported downstream during hydrologic events. The upper layer of the stream bed, known as the surface fine grained laminae, can act to sequester carbon via algal and macrophyte production (Droppo and Stone, 1994; Ford and Fox, 2012). Mild sloping channels and low dissolved organic carbon concentrations coupled with the process of photosynthesis create depositional areas where autochthonous organic carbon can be synthesized from inorganic materials through primary production and other allochthonous carbon sources can be deposited or decomposed via heterotrophic bacteria (Leithold et al., 2005; Walling et al., 2006; Ford and Fox, 2012; Lane et al., 2013). The surface fine grained laminae can also act as a source of carbon dioxide due to breakdown of organic carbon by the active microbial pool (Aufdenkampe et al., 2011; Butman and Raymond, 2011). The process of organic carbon decomposition outgasses carbon dioxide to the atmosphere and is as important as primary production to the ecosystem (Moorhead et al., 1996). The impact that fluvial karst topography has on these hydrobiological processes is an area where relatively little is known due to system heterogeneity and complexity.

The realization of the biologically active nature of fine sediment has created the basis for much of the research activity in recent years due to the high uncertainty surrounding the fate of active sediments within fluvial carbon budgets that can be integrated into local ecosystem budgets (Griffiths et al., 2012) as well as regional and global carbon cycling models (Cole et al., 2007; Butman and Raymond, 2011). The uncertainty associated with the enrichment and degradation of organic carbon can also be incorporated into modeling the ability of sediment to fuel denitrifying bacteria that can transform and remove nutrients from stream water (Mulholland et al., 2008; Findlay et al., 2011; Newcomer et al., 2012). It is now recently recognized that sediment organic carbon microbial turnover in low order streams is a highly active constituent to the hydrobiological carbon cycle and constitutes 10% of the net ecosystem exchange of carbon in the United States (Battin et al., 2008; Butman and Raymond, 2011). Current unknowns within the literature include in-stream carbon transformation rates, CO₂ degassing rates, sediment carbon exports, interactions of carbon pools, and regional carbon budget estimates (Alvarez-Cobelas et al., 2010; Raymond et al., 2013; Creamer et al., 2015; Ford and Fox, 2015; Graça et al., 2015; Sobczak and Raymond, 2015). The topic of sediment organic carbon fate and transport in fluviokarst systems is one that requires further study and thus is the focus of this research.

In this thesis we investigate the role of karst topography in augmenting transit of fine sediment and the source-sink capacity of temporarily stored sediment organic within the coupled surface-subsurface drainage network. Karst landscapes are typified as solutionally dissolved landscapes that are dominated by secondary porosity via fractures and conduits that produce low-resistance pathways for water transport (Shuster and White,

1971; Thrailkill, 1974; Smart and Hobbs, 1986). Fine sediment (i.e., sediment with a diameter less than 53 micron) is naturally generated during hydrologic events through the erosion of upland areas, stream beds, and stream banks. Anthropogenic land use practices have exacerbated natural erosion rates and have elevated fine sediment delivery to streams which can often times prove deleterious to aquatic life by limiting light penetration thus smothering fish eggs and other aquatic organisms, killing aquatic flora, and transporting contaminants such as heavy metals (Brookes, 1986; Davies-Colley et al., 1992; Wood and Armitage, 1997; Owens et al., 2001). The organic portion of fine sediment is composed of particulate organic carbon (POC) and dissolved organic carbon (DOC). Organic carbon is a vital component of the aquatic food web, soil structure and strength, and in the buffering of harmful substances (Miller and Donahue, 1990; Conant et al., 2001).

The coupling of hydrogeological and hydraulic physical mechanisms with biological decomposition processes in a fluviokarst watershed is presented in this thesis to develop a new conceptual model of sediment organic carbon fate and transport in karst landscapes. The research investigates subsurface conduit processes such as erosion, transport, and deposition that impact bed level changes, organic carbon decomposition, and sediment mixing.

1.2 Research Need

Karst landscapes and aquifers are some of the most prevalent topographical features in the world. It is estimated that karst landscapes make-up over one fifth of the land area in the United States (Ford and Williams, 2007), and up to one quarter of the global population has been estimated to live in regions dominated by karst landforms and receive

their drinking water from karst aquifers (Leibundgut, 1998; Bakalowicz, 2005; Fleury, 2009). While the importance of karst hydrology is well-recognized, measurements of various processes are hindered by the lack of applicable sensing networks, extremely complex systems, difficult to reach locations, and simply by the fact that many of the underground processes cannot be visualized or mapped. Reaching the point of recording hydrologic, hydraulic, and biologic measurements remotely in a natural, underground conduit is an arduous process that requires intense resources, manpower, monitoring, and upkeep. A need for a conceptual fluviokarst sediment and carbon transport model to be developed based on data that can be collected with well-accepted borehole drilling techniques, monitoring instruments, and sampling methods is evident in making decisions with regards to karst water resources and land management.

Water transported through karst conduits often has high velocity, turbulent flows more analogous to freshwater streams than groundwater flow. Due to these fast transport mechanisms, pollutants originating from agricultural and urban runoff are flushed through the subterranean karst to springs and wells that often times serve as drinking water sources (Mikac et al., 2011). Carbon enriched sediments are then often times redirected from surface pathways to subsurface caves where deposition occurs resulting in storage of sediment and induced bacterial activity. Accumulated sediment in shallow temperate zone caves has been shown to have high carbon dioxide levels which indicate high microbial activity leading to organic carbon decomposition (Baldini et al., 2006). There is a need to investigate how sediment organic carbon is mobilized, deposited, and transformed in environments where surface pathways and subsurface conduits have a strong hydrologic

coupling so as to better understand the impact of land use practices on human and environmental health as well as carbon exchange dynamics.

1.3 Objectives

The primary objective of this research was to develop a model framework that would couple upland sediment erosion with hydrologic, hydraulic and carbon decomposition models to estimate the transformation of sediment during temporary storage in a fluviokarst watershed located in the Bluegrass Region of Kentucky, USA. The coupling of these different physical and biological processes would elucidate unknowns in fluviokarst hydrogeology and investigate new viewpoints to the biogeochemical transformations occurring within dual surface-subsurface fluviokarst systems. In order to meet this primary objective, several specific objectives were identified:

1. Review of the literature to understand the geological, hydrologic, and hydraulic properties of karst systems including how the systems are formed and how the systems react to hydrologic events.
2. Review of the literature to understand watershed and river sedimentation and erosion processes ranging from upland production and in-stream transport to eventual fate.
3. Review of stream biological processes to investigate carbon source, generation, and decomposition.
4. Selection of a study watershed and description of the methods for data and sample collection.

5. Description of laboratory methods for estimating sediment concentration and carbon density and isotope ratios.
6. Development of a physical model framework linking the surface stream hydrology with the subsurface closed-conduit hydraulic flow system.
7. Development of an organic carbon model framework linking carbon sources in the uplands with carbon decomposition and flux in the subsurface conduit.
8. Performing a water budget to assess the storage capacity of the karst aquifer
9. Performing a sediment budget to estimate the amount of surface sediment pirated by swallets and other karst features.
10. Performing a carbon budget to investigate the enrichment or decomposition of sediment organic carbon within the system and to estimate the sink or source capabilities of fluviokarst.
11. Testing the sensitivity of the sediment transport model by varying parameters against the calibrated values determined from field data collection.
12. Testing the uncertainty of the carbon model by performing 10,000 Monte Carlo realizations to estimate variability of carbon sources into the system.
13. Providing results of the study and preliminary estimates of sediment organic carbon decomposition within temperate, mature fluviokarst watersheds.

1.4 Thesis Layout

Chapter 1 provides the motivation for this research through detailing the state of current research on sediment and carbon transport in fluvial and karst systems, the need to fill knowledge gaps in this area of literature, and the objectives of this research effort.

Chapter 2 provides a literature review of karst processes including geologic, hydrologic, hydraulic, and processes related to energy loss in fluvio-karst networks. Afterwards, fluvial sediment mobilization, deposition, and transport processes are explained and visualized. Literature on organic carbon source, generation, and decomposition in watersheds is overviewed. Finally, methods for investigating the above are outlined.

Chapter 3 provides information on the study watershed including the physiogeographic setting, geology, disturbances, historic study, as well as water, sediment, and carbon transport processes occurring in the watershed.

Chapter 4 outlines the methodology used in the presented research. Included in this section are water and sediment field instrumentation and collection methods, laboratory sample analysis, and the numerical framework for sediment and carbon modeling.

Chapter 5 presents the results for the water budget from the field instrumentation, the sediment budget from sample collection and sediment transport modeling, and the carbon budget including source and decomposition.

Chapter 6 provides a discussion on the role of fluvio-karst in sediment transport and the physical impacts of fluvio-karst on sediment organic carbon. The role of fluvio-karst in the transformation of organic carbon and the biogeochemical impacts of fluvio-karst on sediment organic carbon are presented. The juxtaposition between carbon behavior in surface and subsurface streams is discussed. Finally, the implications the findings of this research have on global carbon budget modeling are explored.

Chapter 7 provides the conclusions of this thesis and potential future work on the research topic.

Chapter 2 Literature Review

2.1 Karst Processes

Karst landscapes are formed by the chemical dissolution of soluble calcium carbonate rock (White, 1988) as shown by



where, CaCO_3 is calcite, Ca^{2+} is the positive calcium ion, 2HCO_3^- is the bicarbonate ion, and H_2CO_3 is carbonic acid represented by the equation



where, H_2O is water and CO_2 is carbon dioxide. The chemical dissolution processes occur as rainfall delivers slightly acidic water that seeps through soil and dissolves calcium carbonate bedrock over time. The result is creation of surface features such as epikarst, sinkholes, and springs. It is estimated that karst landscapes make-up over one fifth of the land area in the United States and 12% of the land area globally (Ford and Williams, 2007).

2.1.1 Geologic

Calcium carbonate rock is originally formed by the accumulated precipitation of calcite and aragonite by marine animals for shell and skeleton building or precipitated in the tissues of algal plants. Through lithification, water pressure compacts the precipitated calcite and aragonite and, over time, forms limestone. Limestone and dolomite are the most common rock formations that are susceptible to karst development. These carbonate rocks are dissolved through weathering, erosion and chemical processes. Initially fractures (50-500 micrometers) are created in the bedrock and over time these fractures increase in size

as a result of dissolution and particle detachment by fluid shear forces. Once the fractures pass a certain threshold (typically about 1 cm), the rate of dissolution of the bedrock increases significantly and varying sizes of conduits are formed (White, 2002).

The classification of many karst systems, with respect to water-bearing properties, is determined by the distribution, frequency, and scale of void spaces, fractures, and conduits. The three types of porosity in karst are matrix permeability, fracture permeability, and conduit permeability (White, 2002; Scanlon et al., 2003). Matrix permeability consists of the intrinsic intergranular pore spaces formed during lithification and other micro-voids. Fractures are formed from mechanical joints and bedding plane partings which are later enlarged by solution. Conduits and caves are large openings ranging from 1 cm to 10+ meters which are formed by extensive preferential dissolution typically along bedding planes (White, 2002; Bonacci et al., 2009).

Figure 2-1 shows examples of different karst features created by dissolution of limestone bedrock. Topographical karst features such as sinkholes, swallets, and estavelles are formed by the dissolution of near-surface bedrock and washing out of underlying soils. Dolines, or sinkholes, can be formed by drawdown initiation in the subcutaneous zone where perched water in the epikarst is funneled towards higher permeability zones that result in forming a depression (Kemmerly, 1982). Sinkholes are also created through the suffosion of soil, which is an event in which loose, non-cohesive soil sits on top of fissures or joints of a karst landform, rainfall percolates through the layers of soil recreating the dissolving effect of the carbonate rock until, eventually, enough of the overlying rock has been dissolved to cause the soil to collapse into a cave void (Khomenko, 2006).

2.1.2 Hydrologic

There are various types of recharge that contribute flow into a karst aquifer and to the karst drainage network. Allogenic recharge is provided by surface streams that drain from non-carbonate regions of a watershed into sinkholes (Thraikill, 1991). Autogenic recharge is provided by rainfall infiltration into the karst aquifer *via* fracture and matrix permeability as well as percolation through the epikarst and soil (White, 2002). Storage within a limestone aquifer acts as a two-component system. A minor component to the storage system is in both abandoned and active conduits as well as subsurface caves. Conduits can be massive features with diameters in the tens of meters, but they are not as prevalent as smaller voids and macropores. The majority of the storage within the karst aquifer is in the form of groundwater that lies within the narrow fissures and openings in bedrock (Einsiedl, 2005).

While most of the water is stored in the narrow fissures within the rock, the flow velocities within these fissures, while not laminar, is very slow (Lapcevic et al., 1999; Qian et al., 1999, 2005). The bulk of the water conveyed underground is transmitted through solutionally enlarged conduits (Atkinson, 1977; Palanisamy and Workman, 2014). Conduits are often times closely connected to the surface through swallets and other large openings which bypass infiltration and provide direct recharge and quickflow to the karst aquifer. When coupled to the surface streams of the fluvial network, mature karst topography is well recognized to pirate as much as $0.26 \text{ m}^3 \text{ s}^{-1} \text{ km}^{-2}$ from the land surface only to resurface tens to hundreds of kilometers from the sink locations (Ford and Williams, 1989). Conduits also work to drain the sustained, diffuse flow from the surrounding rock

fracture matrix. This diffuse flow provides a constant flow to springheads in the system given that they are below the aquifer water table (Lee and Krothe, 2001).

Table 2-1 reviews the minimum, mean, and maximum spring discharges from karst aquifers around the world. The variability in drainage area and magnitude of discharge serve to show how many similarly sized aquifers can possess very different hydrogeologic properties due to the heterogeneity of karst evolution (i.e. some of the aquifers are dominated by primary or matrix porosity and others by secondary or tertiary porosity). Many of the springs are perennial and serve as drinking water sources.

2.1.3 Hydraulic

Phreatic conduits are typically below the water table and therefore have a downstream control structure, i.e., subterranean dam, or adverse conduit gradient in the streamwise direction that produce saturated conditions (Lauritzen et al., 1985; Jeannin, 2001). In terms of hydraulics, phreatic conduits have an upper limit for their energy gradient and thus upper limit for fluid conveyance due to the existence of the downstream controls. The “carrying capacity” principle of conduit drainage systems describes the process by which flow begins to overtop swallets due to the karst aquifer reaching a maximum flow capacity (White, 2002).

Karst conduits behave in a manner similar to that of pipes in a water distribution network (Ray, 2005). The similarities between karst systems and water distribution systems has led many researchers to apply concepts of water distribution to flow problems in karst aquifers (Jeannin, 2001; Liedl et al., 2003; Fiorillo, 2011). Flow in karst conduits is always turbulent and cannot be described by traditional groundwater laws such as Darcy’s Law and the Hagen-Poiseuille Law which are restricted to laminar flow. The Darcy-Weisbach

equation is used almost exclusively when referring to energy losses within karst aquifers (Gale, 1984; Lauritzen et al., 1985; Smart, 1988; Springer, 2004; Kaufmann, 2009). Friction factors, head losses, and roughness heights in karst conduits have extreme variability from not just one system to the next, but also within the same system depending on the method used to determine energy loss terms (Worthington, 1991; Jeannin 2001).

A key factor in the coupled system is the interaction between the karst subsurface drainage network with above-ground hydrologic processes such as stream flow, runoff and precipitation. Swallets provide a one-way point source of flow and sediment into the subsurface conduit. On the other hands, estavelles are karst features with a dual function that link and interact between the surface and subsurface drainage networks. There are two phases that the estavelle can act in: the estavelle is either acting as an intermittent spring (outflow) or as a ponor (inflow). Factors influencing in which phase the estavelle will act are stream stage, groundwater level, flow rate in the conduit, and maximum carrying capacity (Milanovic, 2004). Research performed by Bailly-Comte et al. (2008) suggests that when water is released through the estavelle, it is a result of previous entrapped water being flushed out (i.e., storage-release) by a rise in the water-table of the karstic aquifer.

Figure 2-2 depicts the various flow types in a coupled surface-subsurface network. Flow can be seen reversing depending on stream elevations and pressure heads within the conduit. The hydraulics of the system are heavily influenced by the surface hydrograph and swallet-flow interactions. In Phase 1, diffuse seepage from fractures and pores provides the entirety of the spring baseflow; discharge is a function of the water table elevation. In Phase 2, the onset of the storm event activates certain swallet features depending on spatial and temporal variability of precipitation and runoff. In Phase 3, the conduit and surface

channel are completely submerged in water and pipe-full conditions are realized throughout the system. Flow is strongly governed by the stage levels throughout the stream. In the final phase, Phase 4, the system begins to drain and the water-saturated epikarst supplies flow to the subsurface until normal baseflow conditions are once again satisfied.

2.1.4 Darcy-Weisbach Friction Factor

The Darcy-Weisbach friction factor, f , is an experimental value that attempts to predict the head loss in pipes and fittings (Moody, 1944; Brown, 2002). The Moody Diagram, from the work of Rouse (1976), was developed in an attempt to graphically ascertain the coefficient of friction for a pipe

$$f = \phi \left(Re, \frac{\varepsilon}{D} \right), \quad (3)$$

where, Re is the Reynolds number (unitless), ε is the roughness of the pipe (m), and D is the diameter of the pipe (m).

The Moody Diagram shows that for relatively smooth pipes the friction factor will remain constant in the turbulent zone ($Re > 4000$). Karst landscapes are often characterized by the presence of high Reynolds numbers. These turbulent flow pathways enable advection of fluid and sediments at rates often on par with surface streams and much higher than well-studied non-karst groundwater systems. The Darcy-Weisbach equation defines the friction factor as

$$f = h_L \frac{2gD}{v^2L}, \quad (4)$$

where, h_L is the head loss between two locations (m), g is the acceleration due to gravity (m s^{-2}), v is the velocity of the fluid (m s^{-1}), and L is the pipe length (m).

The friction factor is shown to differ greatly from location to location. Research studies done in the Mendip Hills, Great Britain region show that friction factor varied with discharge, from an f of 35 at the largest discharge to 140 for the lowest discharge at a location named Reservoir Hole (Atkinson, 1977). One potential reason for this large difference in friction factor is that air-filled voids in the water table change the average hydraulic radius of the conduit to some extent with discharge. Another hypothesis is that constrictions and changes of area within the conduit dramatically change the friction factor for different flows in a non-linear manner. However, Atkinson calculated f based on straight-line flow velocities and straight-line hydraulic gradients which will tend to overestimate f .

Scallops in cave conduits have also been used to calculate friction factors (Gale, 1984). Scallops are polygonal intersecting depressions whose form is hydraulically controlled. Scallops develop at a stable scallop Reynolds number of 1000-3000. Studies by many different researchers all confirm scallop formation in the laminar-turbulent flow transition phase (Allen, 1971; Curl, 1974). However, scallops are not representative of the full range of discharges within a conduit because they are typically only formed at high flows.

The head losses associated with friction along a conduit can occur at many different locations and are not always distributed equally over the length of the conduit. A study by Bögli (2012) suggested that 98% of the 2.6 km passage accounted for only 1.3% of the total head loss. This disproportionality is extremely important when considering how a friction factor should be applied over a stretch of conduit. 11% of the head loss was due to change in cross-section, 1.7% for passage bends, 35% for a short, narrow section of the

conduit, and 51% for a section of the conduit that was broken-down. Caves almost always have narrow sections or breakdowns that could heavily skew the friction factor.

2.2 Fluvial Processes

The fluvial system is a continuum that consists of three connected zones linking the uplands to the watershed outlet (Figure 2-3) (Miller, 1990). Zone 1, or the headwaters, is the erosion producing area where streamflow is initiated and incipient sediment motion occurs. Zone 2, or the transfer zone, is the part of the watershed where the fluvial system is the most stable and well-defined with regards to fluvial processes and hydrogeomorphology. The downstream portion is called Zone 3, or the depositional zone, and is near the outlet of the system where aggradation occurs (Chang, 1988).

2.2.1 Sediment Production

Sediment production from soil is a two-phase process including detachment and transport. In the uplands, runoff and rainsplash are the main mechanisms by which soil is detached (Proffitt and Rose, 1991; Morgan, 1995; Toy et al., 2002; Van Dijk et al., 2003). Detached sediment is then transported down gradient towards valleys and streams by overland flow and in gullies. Fluvial erosion is the result of induced shear stresses on stationary soil particles and the bursting and sweeping caused by turbulent ejections (Kaftori et al. 1998; Papanicolaou et al., 2001; Wu and Chou, 2003). The critical shear stress of a particle is a measure of the ability of the soil particle to resist detachment from the soil surface and subsequent entrainment into the fluid column by hydrodynamic shear stresses. Incipient motion occurs when this threshold is overcome (Shields, 1936; Wiberg and Smith, 1987; Papanicolaou and Hilldale, 2002). Soil erosion estimates can be

calculated from well accepted models such as the Revised Universal Soil Loss Equation (RUSLE) and are built into many hydrologic and sediment models.

2.2.2 Deposition and Sedimentation

Eroded sediment that enters the stream channel is conveyed downstream by the energy of the fluid to keep the sediment entrained. Once the carrying capacity of the fluid is exceeded deposition begins to occur (e.g. over-saturation of sediment or hydrograph recession) (Salaheldin et al., 2000). Temporary stored sediment is typically re-suspended at the advent of a subsequent large flow event and later deposited further downstream in the watershed (Walling and Amos, 1999; Smith et al, 2003). This creates a dynamic quasi-equilibrium condition particularly in the transfer zone where erosion rates are nearly equal to depositional and uplift rates. (Cyr and Granger, 2008; Tucker, 2009).

2.2.3 Sediment Transport and Downstream Flux

The transport of sediment in fluvial networks is typically broken down into three distinct size classifications: bedload, suspended load, and wash load. The bedload is the portion of sediment that is transported near the bed of the stream through the action of rolling, sliding, or saltation. The suspended load is made up primarily fine sediment (< 53 micron diameter) that is entrained completely by the flow and is transported at the same speed as the flow. The wash load is made up of the smallest particles in the bed material that are eroded and swept away almost immediately at the onset of hydrologic activity (Woo et al., 1986; Chang, 1988; Evans et al., 2006). There are many methods to estimate the quantity of sediment transported and delivered to the downstream portions of a watershed such as streamflow sampling, reservoir sedimentation surveying, sediment-

delivery method, empirical equations, and simulated-watershed sediment models (Piest et al., 1975).

Sediment from rivers can exhibit controls on both morphologic and biological processes occurring in the stream channel (MacIntyre et al., 1990; Tank et al., 2010; Ford and Fox, 2012). High sediment loads can also negatively affect the ease by which humans use freshwater for recreation and hydration. Sediment loads slow down the ability of water treatment plants to process water, require dredging from reservoirs and dams, and affect the visual aesthetics of recreational waters (Smith et al., 1995; Morris and Fan, 1998; Pflüger et al., 2010). Investigation of sediment loading into subsurface environments and the temporary storage of pirated sediment has been relatively unstudied in the community. This study will create a sediment budget to balance sources and sinks of sediment in coupled surface-subsurface drainage networks.

2.3 Sediment Organic Carbon Processes

The two sources of sediment organic carbon investigated in this study are terrestrial-derived, or allochthonous, organic carbon and autochthonous, in-stream generated carbon. Autochthonous matter is created through photosynthetic production by primary producers in the benthic environment. Allochthonous material is delivered to the stream ecosystem by litterfall from vegetation, streambank erosion, and by entrained soil organic matter in overland flow into the stream. Transported organic carbon consists of dissolved and particulate phases where dissolved organic carbon has a diameter less than 0.45 micrometers. Particulate organic carbon is separated into two different size classes:

fine particulate organic matter (FPOM) and coarse particulate organic matter (CPOM). FPOM has a diameter of 53 micron or less whereas CPOM particles have larger diameters.

Figure 2-4 (Ford and Fox, 2012) shows the possible interactions between the organic, inorganic, particulate, and dissolved constituents of in-stream carbon. Inflow from uplands and tributaries is delivered to the stream where the inorganic portion can undergo precipitation or dissolution depending on the chemical composition of the streamwater. Inorganic carbon that is dissolved within the stream can undergo evasion and be emitted to the atmosphere. Likewise atmospheric carbon can invade the stream channel and become dissolved inorganic carbon. The organic portion of the inflow can be assimilated by macrophytes and aquatic algae to be used in production and carbon generation or it can go through the process of bacterial decomposition which will convert the organic carbon into inorganic carbon. The surface fine grain laminae (SFGL) is the microbially-active boundary between streamwater and deep, legacy sediments. The SFGL is made up of the top layer of recently deposited sediment (up to 1 cm), heterotrophic bacteria, autotrophic algae, fungi, and macrophytes (Droppo and Stone, 1994; Droppo and Amos 2001). Microbial activity within the SFGL is promoted by the biofilm development of extracellular polymeric substances which increase stabilization and shear resistance of the SFGL (Decho, 1990). The importance of the SFGL with respect to karst is manifested in the ability of heterotrophic bacteria to breakdown temporarily-trapped sediment within the karst conduit. There is a lack of research that investigates the level of activity of the SFGL within fluviokarst watersheds.

Dissolved and particulate organic carbon make up 40% of the total flux of carbon in rivers around the world with the inorganic carbon phase dominating flux (Schlesinger

and Melack, 1981; Meybeck, 1982). Of the organic portion, the dissolved phase typically dominates organic carbon exports (Meybeck, 1982; Sharma and Rai, 2004; Aldrian et al., 2008; Zhang et al., 2009; Alvarez-Cobelas et al., 2010) but in some systems the majority of organic carbon exports is in the particulate phase (Howarth et al., 1991; Abril et al., 2000; Worrall et al., 2003; Carey et al., 2005) depending on watershed and stream characteristics. Coarse sized organic matter is often the largest contributor of particulate carbon to the stream system (Wallace et al., 1995; Chadwick et al., 2010). In the Wallace et al. (1995) study, CPOM represented over 86% of the organic inputs to the system, but less than 4% of total organic matter export indicating the ability of in-stream processes to breakdown coarse organic matter into fine and dissolved constituents. Likewise, in an 8th-order stream, FPOM constituted 75 – 98% of the exported organic matter (Minshall et al., 1992).

2.3.1 Source

Particulate organic matter serves as an important energy source for decomposers, a nutrient source for bacteria, and provides physical and biological diversity to the stream (Ward, 1986; Crenshaw et al., 2002; Moore et al., 2004; Aldrige et al., 2009). Separating the source of particulate organic carbon is vital because organic rich sources are more reactive and can be degraded more easily than recalcitrant carbon derived from sedimentary rocks (Ittekkot et al., 1986; Depetris and Kempe, 1993; Stallard, 1998; Gomez et al., 2003). Terrestrial-derived sediment organic carbon originates within surface soils and bank sediments and is transported down gradient during hydrologic events following the physical conservation laws of sediment transport. Soil organic matter (2500 Pg) is the third largest pool of carbon on earth and contains 3.3 times the carbon in the atmospheric

pool (760 Pg) and 4.5 times the carbon in the biotic pool (560 Pg) (Lal, 2004). FPOM can be derived from processing of leaf and litter inputs, woody debris, riparian soil particles, and flocculated dissolved organic matter, and autochthonous plant production. Terrestrial carbon uptake primarily occurs *via* photosynthesis during plant growth. Organic content of terrestrial sources can vary depending on depth and fertility of the eroded soil profile and vegetation type (Jobbágy and Jackson, 2000). Streambank carbon sources typically have a more depleted carbon content due to pre-erosion of upper carbon-rich sediment.

The source of POC to low-order, headwater streams is dominated by soil carbon origin, whereas POC in higher order rivers is primarily associated with algal carbon resulting from phytoplankton production (Masiello and Druffel, 2001; Gomez et al., 2003; Hélie and Hillaire-Marcel, 2006; Gao et al., 2007; Ford and Fox, 2012). In an urban stream in northwestern Oregon, terrestrial-derived soil and leaf litter were the main sources of organic matter which is consistent with the large inputs of riparian litterfall, bank erosion, and mass wasting (Goldman et al., 2014; Keith et al., 2014; Sobieszczyk et al., 2014).

2.3.2 *Generation*

Organic biofilms are pronounced in lowland watersheds where deposition of fine sediments allow for microbial communities to develop (Walling et al., 2006). Allochthonous organic material delivered from upstream can be deposited and enriched by in-stream producers. Low-order streams are characterized by fast velocities and relatively low water residence times. As a result, autochthonous benthic production is favored over phytoplankton production that is more commonly found in rivers with lower gradients (Naiman et al., 2001; Allan and Castillo, 2007).

The most common type of primary producers found in headwater and low-order streams are periphyton (e.g., benthic algae, bacteria, and associated organic material). Periphyton growth occurs on any benthic surface receiving light such as stones (epilithon), sediment (epipelon), and even on other plants (epiphyton) (Allan and Castillo, 2007). Periphyton communities are attached to surfaces by a mucilaginous secretion that resists the shear force enacted by water and enables production and growth (Biggs et al., 1998; Dodds and Biggs, 2002). The growth of macrophyte communities also displays a feedback to water flow in small lowland streams by modifying velocity gradients and turbulence (Sand-Jensen and Pedersen, 1999). As algal material ages and experiences limited nutrient or sun exposure it can be eroded and delivered downstream as part of the detrital carbon pool (Naiman et al., 2001).

2.3.3 Decomposition

Heterotrophic decomposition is the biological process by which carbon is converted from an organic state into an inorganic state. During the decomposition process carbon dioxide is released as well as energy, water, and plant nutrients (i.e. mineralization). The rate of decomposition is mainly a function of the type of soil organism, the physical environment, and the quality of organic matter (Brussaard, 1994). In fluvial systems, leaf litter and coarse algae are labile carbon sources for macroinvertebrate and heterotrophic communities with faster decomposition rates than that of soil organic carbon (Short et al., 1980; Minshall et al., 1983; Sinsabaugh et al., 1994; Webster et al., 1999; Alvarez and Guerrero, 2000; Jackson and Vollaire, 2007; Rier et al., 2007; Yoshimura et al., 2008). FPOM pools are considered more recalcitrant than CPOM pools due to utilization of the glucose components of CPOM during breakdown to FPOM (Yoshimura et al., 2008). Rowe et al.,

(1996) showed a connection between water chemistry and decomposition rates of litter in a karstified watershed due to the high influence of the underlying limestone bedrock on buffering acidic deposition due to high pH levels. Modeling the effects of the transport-limited, phreatic karst conduit on carbon decomposition and re-mobilization is an area that requires further investigation.

2.4 Sediment Transport Studies in Karst

While recent research works towards an understanding of sediments in karst environments, much more study is needed to provide a conceptual model of fluvial sediment functioning in these systems (White, 2002; Bai et al., 2013). Sediment transported to phreatic conduits occurs during stormflow when rainfall activated surface water tributaries carry high sediment loads and provide quickflow via swallets to the subterranean karst. The fluid energy threshold of the phreatic conduits offers the potential to trap pirated sediment through deposition. Hydrologic events resulting in increased turbidity in karst systems are characterized as either primary or secondary (Lacroix et al., 2000; Pronk et al., 2006). A primary turbidity peak occurs synchronously with event peaks, but secondary turbidity peaks are delayed appearing days (or weeks) after the initial peak. The secondary peaks are a result of delayed water that has infiltrated through the karst fracture and macropore network. Pronk et al. (2008) also found two turbidity peaks where one coincides with increasing flow rate and remobilization of the conduit bed and the other matches the particle transfer of sediment from the soil. The two turbidity peaks can be investigated using particle size distributions and, it has been shown that the second peak has a relative increase in finer particles.

Research in the transport of fine sediments in karst has focused upon the ability of karst networks to convey sediment under various ground saturation and moisture conditions (Herman et al., 2008), entrain and transport sediment by intensity of flows (Dogwiler and Wicks, 2004), store and discharge sediment in watersheds with changing land use (Hart and Schurger, 2005), and transport contaminants based on organic carbon content and specific surface area (Mahler et al., 1999). Dogwiler and Wicks (2004) found that baseflow was not enough to mobilize sediment and that the median diameter particles began to mobilize at 50% less than bankfull. During bankfull discharge conditions, 50-85% of the substrate can be transported. The sediment size (>1 cm) used in the Dogwiler and Wicks research was relatively large compared to that of this study. The recurrence interval for a bed-reforming event was every 2.4 months as viewed from a karst window. Investigation of bed changes in phreatic conduits has been lacking due to the high costs, heavy field work and instrumentation, and time required. This study will look at how the SFGL changes in a perpetually submerged karst conduit.

2.5 Sediment Organic Carbon Studies in Karst

Bacteria and other microbes in subsurface karst environments rely primarily on transported sediment organic carbon for their energy (Danovaro et al. 2001; Humphreys, 2006). The lack of any sunlight in these areas means no primary production is possible and carbon can only be decomposed and not generated. The microorganism food cycle is largely driven by the percolation of primarily-produced POC or DOC which makes its way downward through the cracks, fractures, and matrix of the aquifer (Chapelle, 2001). Some karst systems can produce energy from within the karst basin via chemoautotrophs that fix inorganic carbon by using hydrogen sulfide as an energy source (Sarbu et al., 1996).

However, the large majority of karst systems do not have a method of carbon production (Simon et al., 2007).

Simon and Benfield (2001) found that most coarse particulate organic matter in caves is broken down by physical or biological action in as little as tens of meters. The SFGL layer of the cave bed has also been found to be an important food and organic carbon source in cave streams due to the existence of microbial films and bacterial communities (Simon et al., 2003; Farnleitner et al., 2005). Particulate organic carbon and dissolved organic carbon can enter the subsurface karst environment either by point sources (e.g., swallets) or by distributed flow (e.g., epikarst). POC is effectively filtered by soil and bedrock so it primarily enters through sinking streams and large openings (Gibert, 1986).

Figure 2-5 conceptualizes some of the pathways and transformations that organic carbon can undergo while in a fluviokarst watershed. The carbon is initially generated by primary production in agricultural fields and by urban soils easily susceptible to erosion. Once the SOC is delivered to the primary surface channel there is the possibility that the SOC will be pirated from the surface to the subsurface via swallets. Due to the decreased sediment transport capacity of the subsurface conduit a net deposition occurs which allows heterotrophic bacteria to consume the fresh, labile organic carbon. The depleted organic carbon can then be re-suspended and brought back to the surface either by estavelles (karst features that can act as sources or sinks to the subsurface) or springs. Few studies have investigated the effect of upwelling on sediment and carbon estimates in fluviokarst watersheds.

Given the considerable global extent of karst topography, its role on potentially modifying the fate and transport of sediment organic carbon within the fluvial system is of interest. Specifically, the commonly reported phreatic nature of many karst conduits and drainages (Atkinson, 1977; Bonacci and Magdanlenic 1993; Fleury et al., 2007; Bakalowicz et al., 2008; Fleury et al., 2013) offer the potential to temporarily trap terrestrial-derived sediment organic carbon in the subterranean environment.

2.6 Water, Sediment, and SOC Source, Fate, and Transport in Karst

2.6.1 Flow and Storage of Water in Karst

The conceptual model for karst hydrology has experienced tremendous development and change over the past 50 years. Early conceptual models focused on the variety of geologic settings and how they influence groundwater flow patterns in karst (Shuster and White, 1971). Smart and Hobbs (1986) and Ray et al. (1994) also added the components of recharge and storage to the karst aquifer classification scheme with the latter determining combined risk factors for groundwater sensitivity in Kentucky. More recent work has focused on conceptualizing the role of the epikarst to the overall karst system (Klimchouk, 2000; Aquilina et al. 2006). There exists three basic conceptual models: the physically-based models that require a hydrological basin grid and deep understanding of the system, empirical models (black-box models) that do not require info on structure or hydrodynamic parameters, and reservoir models that are based on simple relationships such as the linear law (Tritz et al., 2011). However as researchers (Jeannin, 2001; Jukić and Denić-Jukić, 2009) have shown, many karst systems have flow and sediment processes that are strongly non-linear.

Ashton (1966) was one of the first to suggest a method by which storage in a subsurface conduit that feeds a spring can be estimated. The method described by Ashton uses the natural flood pulses within the conduit-spring system as a tracer. Within a conduit, the flood pulse of the contributing recharge is felt almost instantly since the conduit water is being displaced, however, the flood water takes a finite time until it can reach the spring. Typically the flood water reaching the spring can be noticed by a decrease in the hardness of the spring water since the recharge has not had sufficient time to interact and exchange with the underground rock and soil formations.

Another method for estimating the storage within a karst aquifer that is drained by a phreatic conduit is through the use of a residence time for tracer injections. A mean residence time is calculated using the method of moments from the integral of the tracer concentrations and spring discharges over the time period of observation. Multiplying the mean tracer residence time by the spring discharge yields a conduit volume (Sauter, 1992; Field and Nash, 1997). This conduit volume can then be used to estimate average cross-sectional area for the cave by dividing the volume by the sinuous length. There are also several different methods of quantifying and parameterizing the discharge and other properties of the system. Another method for calculating discharge is through the use of a Flo-Mate® digital current meter and top-setting rods (Reed et al., 2010).

2.6.2 Dye Tracing

Dye tracing can be both quantitative and qualitative. Qualitative dye tracing gives insight into subsurface flow paths and source-sink connectivity. Dye tracing can be particularly helpful because of the inability of researchers to explore most karst environments of interest. Karst hydrogeologic dye tracing has been performed for over 100

years (Matson and Palmer, 1909; White, 2002). Dye tracing is performed by injecting a substance into a known inflow and then monitoring the recovery of the substance at several suspected outflows. Fluorescent dyes have become the primary method of dye tracing due to their ease of use and cost (Smart and Laidlaw, 1977). Underground flow maps which aide in contaminant tracking can be created by mapping the connectivity of various karst sinks and springs (Benischke et al., 2007).

The other form of dye tracing is quantitative dye tracing which is used to estimate spring or conduit discharge. A dye or other substance is injected at an inlet and the flow rate and concentration of that substance is recorded. The concentration of the substance is then monitored at a second location and the mass conservation principle is applied to find the discharge at the second point. Researchers in Kentucky developed travel time maps to estimate how long it would take for a contaminant to reach drinking water sources depending on the distance of the contamination spill or leak (Paylor and Currens, 2004). More advanced dye tracing techniques can estimate the dispersivity, retardation and degradation, and conduit-matrix interactions in karst aquifers (Massei et al., 2006; Geyer et al., 2007; Goldscheider et al., 2008). By looking at the width of tracer breakthrough curves and fluid velocity, researchers were able to determine that dispersion is caused by small scale turbulent eddies and that retardation is a consequence of changes in conduit geometry (Hauns et al., 2001).

2.6.3 Mapping of Karst Features

Surface karst features typically have to be identified through field surveying although more recently geographic information system (GIS) tools have incorporated analysis tools that aid in identifying features based on topographic maps and other high

quality aerial photography. GIS tools allow users to identify distribution of sinkholes and other karst features (Doerfliger et al., 1999; Bruno et al., 2008; Anchuela et al., 2013).

2.6.4 Laboratory Studies

Dye tracing gives some insight into the interconnectivity of karst features, but as a result of the extreme complexity of karst coupled with the reality that most karst features cannot be navigated, fundamental processes in karst environments will have to be simulated in scaled laboratory experiments. Some work has been done in laboratory-scale branch models (Peterson, 2002) and colonization by aerobic bacteria in karst, which can affect organic carbon (Personné et al., 2004); however, scale karst laboratory experiments are a very untouched aspect in karst knowledge.

2.6.5 Hydrograph Separation

The application of hydrograph separation to karst aquifers is a well-recognized method for gaining insight into the functioning of a karst aquifer by using as few parameters as possible (Dreiss, 1989; Long, 2009). It is a method that has been used on surface streams to separate baseflow and stormflow. Using hydrograph separation, the effective precipitation is the input signal that creates a response at the outlet of the watershed in the form of discharge. The two distinct conceptual flow types in karst hydrology are quickflow and diffuse flow. Adding additional data such as tracer and runoff data allows for creating a more complete picture of karst hydrodynamics (Weiler et al., 2003). Concepts of porous media aquifers and hydrograph separation such as transmissivity and specific yield have also been applied to karst aquifers (Baedke and Krothe, 2001) although due to the heterogeneity of karst it is difficult to identify spatial variability of these parameters.

2.6.6 Isotope Analysis

Many researchers have used tracers in karst ranging from finding flow paths to fingerprinting sediment to characterizing surface water and groundwater interactions (Lee and Krothe, 2001; Einsiedl, 2005). Sediment samples go through extensive isotope analysis and then are discretized based on the signatures of samples from different sources. Isotope analysis has been an extremely useful tool for the discretization of sediment and rainwater sources both in surface channels as well as karst springs (Gibert, 1986; Perrin et al., 2003). Flow rate through a spring has been previously calculated using environmental isotope tracers such as tritium (^3H) and stable isotopes (^{18}O and/or ^2H) (Maloszewski et al., 2002). Emblanch et al. (2003) found contrasting information from using the ^{18}O and ^{13}C tracers and concluded that the ^{13}C of dissolved inorganic carbon is better suited to find the total contribution of the unsaturated zone whereas the ^{18}O signature gives information as to age of the water being discharged.

2.6.7 Numerical Modeling

Numerical modeling is an important tool for investigating water resources in porous media aquifers, however numerical modeling has not had the same level of success when it comes to extremely heterogeneous aquifers such as karst; the application of such models to karst would not accurately simulate the direction or rate of water flow on local scales (Scanlon et al., 2003). Karst aquifers behave as coupled porous-media/pipe-flow systems and pipe-flow models can be successfully applied to karst (Thraikill, 1974; Jeannin, 2001). Pipe-flow models and storm drainage models are widely used in civil engineering, especially in areas such as storm water management (Schlüter, 1999; Lam and Horvath, 2000; Campbell and Sullivan, 2002). However, the application of these programs in karst can run into problems because of the unmapped areas of the conduit.

Although making assumptions is essentially a requirement for many karst systems, changes of length and diameter of karst conduits can lead to statistically significant differences when using models (Peterson and Wicks, 2006). Researchers have created a fully integrated discrete-continuum modeling for coupling conduit flow, channel flow, overland flow, and matrix flow in karst systems (de Rooij et al., 2013), but they have only focused on flow characteristics and have not delved into the surface-subsurface interaction, suspension, and deposition of sediments in karst watersheds. Researchers have also shown that in many karst systems flow and sediment processes are strongly non-linear and must be modeled with more sophisticated techniques (Herman et al., 2008; Jukić and Denić-Jukić, 2009).

Table 2-1: Table of Discharges and Catchment Areas for Karst Springs

Spring	Q min (m ³ s ⁻¹)	Q max (m ³ s ⁻¹)	Q mean (m ³ s ⁻¹)	Area (km ²)	Q mean /Area	Source
Dumanli, Turkey	25	>100	50	2800	0.02	Goldscheider and Drew, 2007
Matali, Papua New Guinea	20	>240	90	350	0.26	
Vaucluse, France	4.5	200	29	2100	0.01	
Tisu, China	4	545	38	1004	0.04	
Timavo, Italy	9	130	17.4	980	0.02	
Trebisnjica, Herzegovina	2	>300	80	1144	0.07	
Ombla, Croatia	2.3	154	33.8	600	0.06	
Ljubljana, Slovenia	4.3	132	39	1100	0.04	
Buna, Herzegovina	2.5	123	23.7	112	0.21	
Bunica, Herzegovina	0.7	207	20.2	512	0.04	
Chingshui, China	4	390	33	1040	0.03	
Silver, U.S.	15	36.5	23.3	1900	0.01	
Frio, Mexico	6	515	28	>1000	0.03	
Coy, Mexico	13	200	24	>1000	0.02	
Sinjac (Piva), Yugoslavia	1.4	154	21	505	0.04	
Grab-Ruda, Croatia	2	105	20	283	0.07	
Rijecina, Croatia	1.2	80	12.4	330	0.04	
Karuc, Yugoslavia	1.9	>50	7	120	0.06	
Gregava, Herzegovina	0.5	59	17.5	396	0.04	
Waikoropupu, New Zealand	5.3	21	15	450	0.03	
Maligne, Canada	1	45	13.5	730	0.02	
Perucac, Yugoslavia	0.4	9	1.2	67	0.02	

Table 2-1 Continued

Spring	Q min (m ³ s ⁻¹)	Q max (m ³ s ⁻¹)	Q mean (m ³ s ⁻¹)	Area (km ²)	Q mean /Area	Source
Mlava, Yugoslavia	0.7	17	1.7	120	0.01	Goldscheider and Drew, 2007
Jadro, Croatia	3.9	70.1	10.0	250	0.04	Bonacci, 2001
Zrnovnica, Croatia	0.4	16.7	1.9	50	0.04	
Areuse, Switzerland	<1	>30	4.6	128	0.04	Kiraly, 1998
Anjar- Chamsine, Lebanon	-	-	2.6	250	0.01	Bakalowicz, 2004
Zarka, Syria	-	-	13	2000	0.01	
Afka, Lebanon	-	-	4	150	0.03	
Maramec Spring, MO, USA	-	22	4.4	795	0.01	Wicks and Hokes, 2000
Buffalo Spring, KY, USA	-	-	0.5	25	0.02	Meiman and Ryan, 1999
Engen, Germany	-	-	8.5	36	0.24	Goldscheider, 2005
Sv Ivan Spring, Croatia	0.1	2.2	0.9	74	0.01	Bonacci and Magdalenic, 1993
Jinci, China	0	2.05	1.1	2430	<0.01	Guo et al., 2005
Areuse Spring, Malm, Switzerland	0.3	51	4.9	130	0.04	Eisenlohr et al., 1997
Serriere Spring, Malm, Switzerland	0.2	11	2.5	88	0.03	
Schneealpe Karst, Vienna, Austria	0.1	2.3	0.5	23	0.02	Maloszewski et al., 2002
Milandre, Switzerland	0	1.6	0.1	13	0.01	Fleury et al., 2007
Barton Springs, Texas, USA	-	-	1.6	330	<0.01	Scanlon et al., 2003
Royal Spring, KY, USA	0	5.0	0.6	65	0.01	This Study

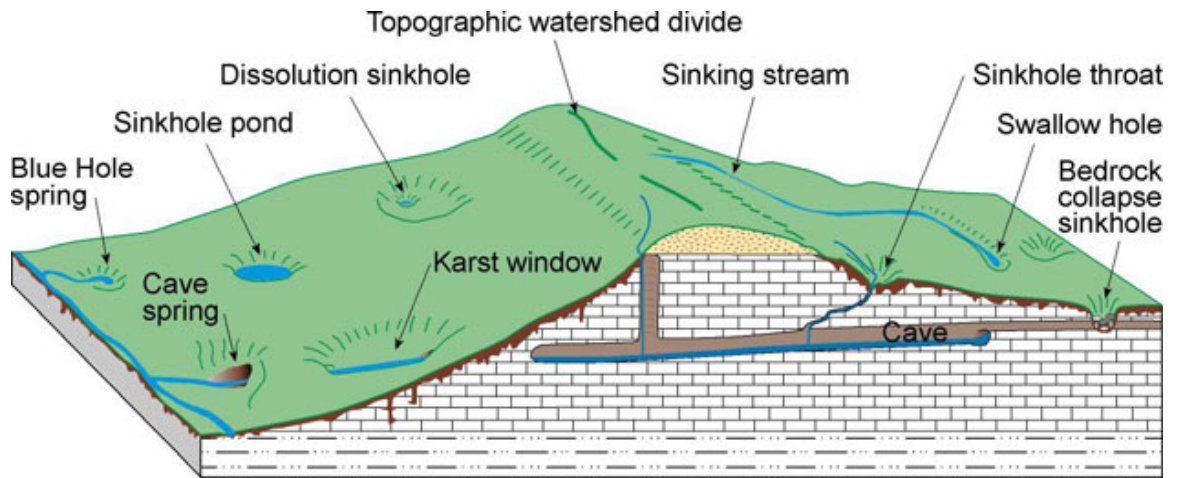


Figure 2-1: Common Karst Topographical Features (KGS, 2002)

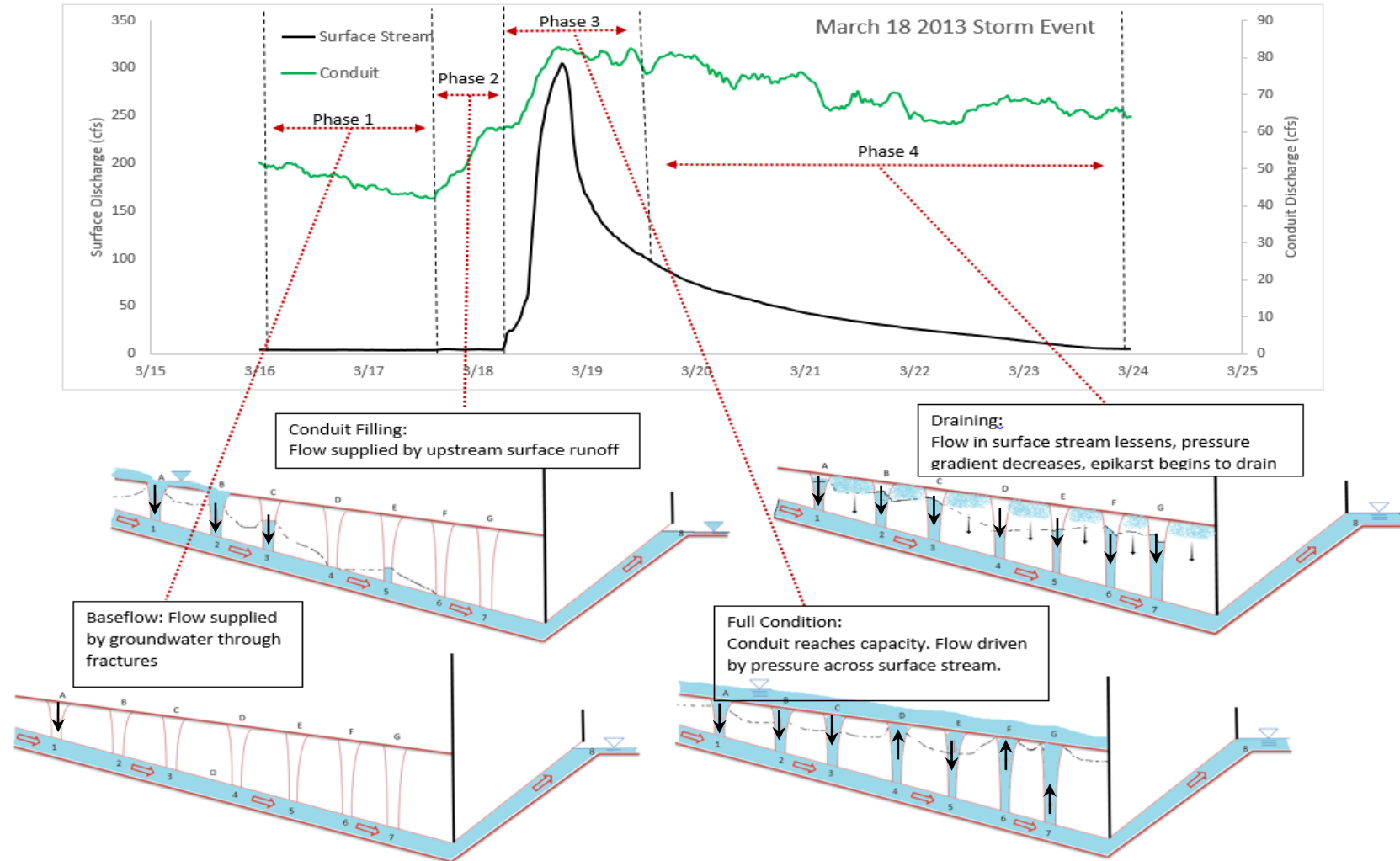


Figure 2-2: Conceptual Model of Surface-Subsurface Hydraulics Using an Observed Hydrograph

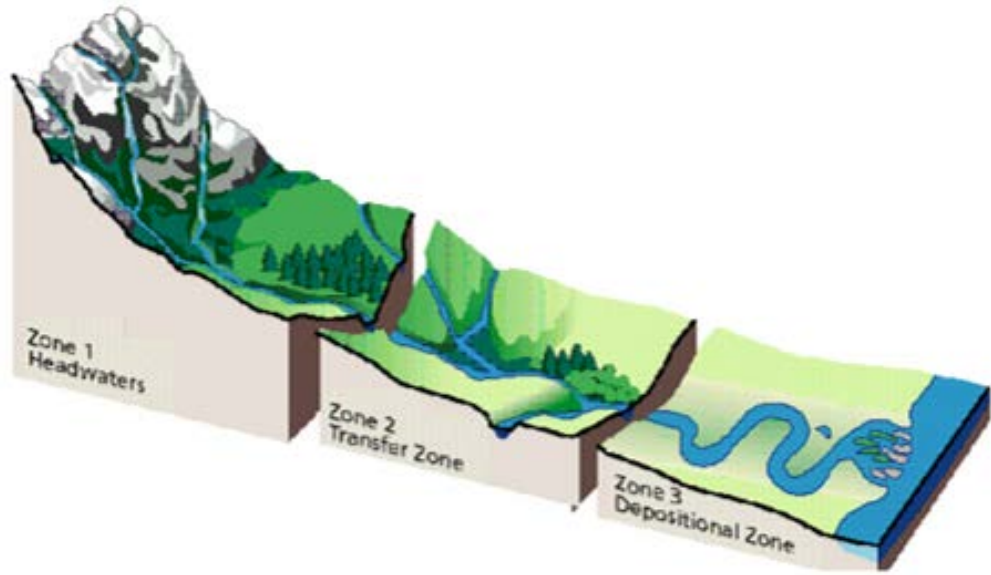


Figure 2-3: The Fluvial System (Miller, 1990)

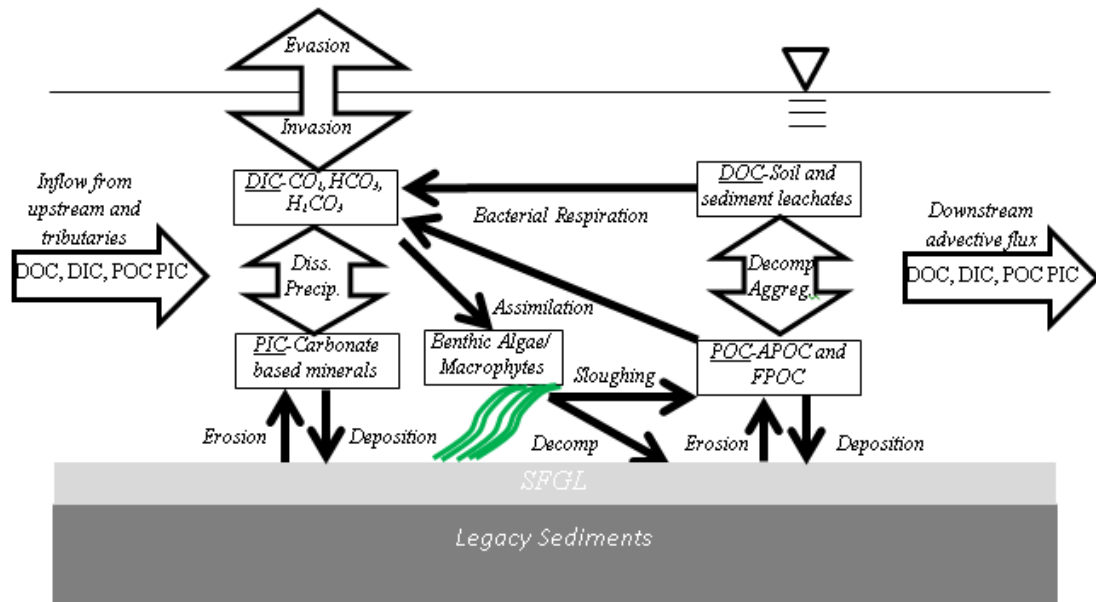


Figure 2-4: In-stream sediment carbon physical and biogeochemical processes including advective flux in and out of the stream reach, dissolution, precipitation, erosion, deposition, invasion, evasion, assimilation, sloughing, decomposition, aggregation, and bacterial respiration. (Ford and Fox, 2012)

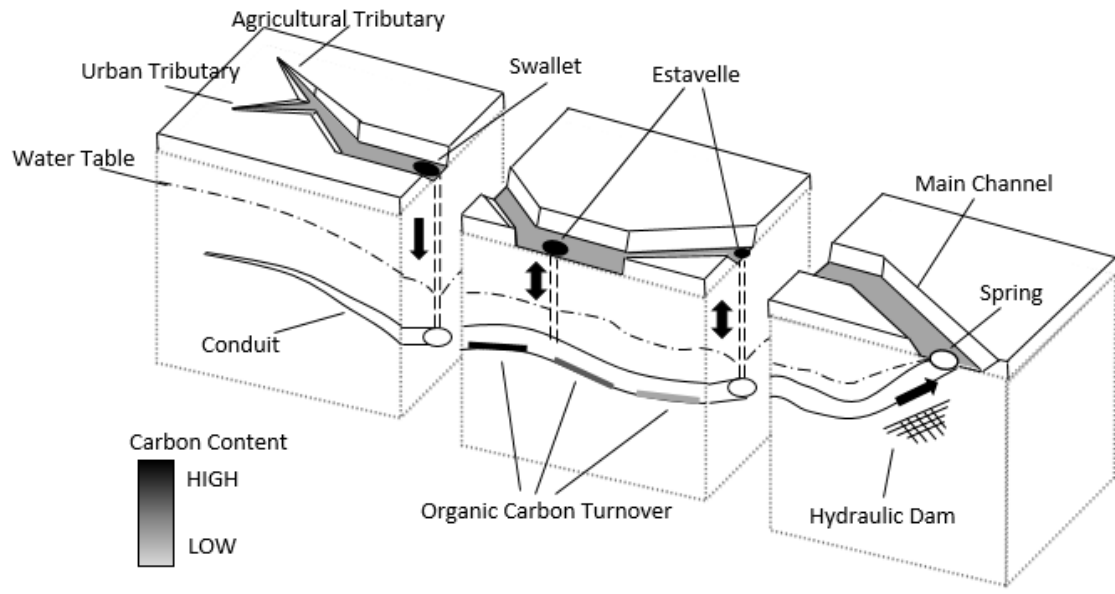


Figure 2-5: Conceptual Model of SOC Transport in Fluviokarst

Chapter 3 Study Site

The Cane Run Watershed (96 km²) is a mixed-use, fluviokarst watershed located in the Bluegrass Region of central Kentucky in close proximity to the University of Kentucky and the city of Lexington. The Cane Run Creek watershed is a coupled surface water and karst drainage network (Figure 3-1). Urban and agriculturally impacted tributaries to Cane Run Creek drain the uplands (see “Urban Trib” and “Ag Trib” Figure 3-1). The underlying karst groundwater basin, termed “Royal Spring”, surfaces in Georgetown, Kentucky where it serves as a drinking water source for the city. Royal Spring has the largest base flow discharge of any spring in the Inner Bluegrass (Currens et al., 2015). A primary conduit conveys water through the karst aquifer and is monitored at the “Groundwater Station” (Figure 3-1). For this research study, the investigated portion of the Cane Run Watershed is the area upstream of the intersection between the main stem of the Cane Run Creek and the Royal Spring Groundwater Basin boundary (labeled as “Surface Outflow” in Figure 3-1). This portion of the coupled surface-subsurface network has a drainage area of 58 km². The investigated portion is a mixed-use watershed that is 40.5% urban and 59.5% agricultural in use (Figure 3-2).

The coupled surface sub-surface watershed was chosen as a testbed for investigating fate and transport of sediment organic carbon in fluviokarst watersheds due to (i) the mature topographical nature of karst in the Bluegrass Region characterized by high flow and contaminant transport rates; (ii) the high connectivity between the surface stream channel and subsurface karst conduits; (iii) the extensive database of knowledge and data collected by previous researchers (e.g., the KGS and the University of Kentucky College of Agriculture); (iv) the karst groundwater emerging at the primary springhead is

used as a municipal water source by the City of Georgetown; and (v) on-going data collection and research efforts such as nutrient sampling and physical modeling being performed in the watershed.

3.1 Physiogeographic Setting

The topography of the Cane Run Watershed is similar to that of other areas in the Bluegrass Region which are characterized by a temperate climate, gently undulating hills, and lowlands. The headwaters of the stream begin near downtown Lexington, Kentucky. The Inner Bluegrass Region is known for its horses and many horse farms are located within the watershed. One such horse facility is the Kentucky Horse Park which is located near the point where the surface stream and subsurface conduit diverge in their flow paths (labeled as Groundwater Station on 3-1). The stream gradient of Cane Run is mild and averages 2.34 m per km over the course of the main channel. The region is well vegetated with grass and trees; riparian zones exist around the stream throughout most of the watershed. The soil in the watershed ranges from fairly level to strongly sloping silt loam and silty clay loam (USDA, 1993). The area is comprised of deep, well-drained series of soils (e.g., Maury, McAfee, and Lowell) that are formed from weathered phosphatic limestone (USDA, 1993). These soil series are characterized by moderate low to moderately rapid permeability (USDA, 1993).

Tributaries draining smaller, less-karstified sub-catchments provide recharge to the main stem of Cane Run Creek. Urban tributaries are largely rainfall activated and agricultural tributaries are intermittent to perennial. The subsurface conduit drains the watershed year round, while the main stem of Cane Run Creek tends to contain no flow over nine months of the year during low and moderate hydrologic events. Connectivity

between Cane Run Creek and the karst subsurface occurs via a series of swallets and estavelles. Fifty seven karst holes have been mapped in and around the stream corridor (Paylor and Currens, 2004). The portion of the Cane Run Creek downstream of the Surface Outflow maintains flow at the surface nearly year round. Both the subsurface conduit and Cane Run Creek are active in the winter when soil moisture conditions are high and rainfall activity is prolonged.

3.2 Geology

Over 50 percent of Kentucky is underlain by rock that could eventually develop karst terrain (Currens and Paylor, 2009). The high percentage of limestone in Kentucky has also allowed for the generation of many different kinds of karstic features ranging from small fractures to the world's longest cave, Mammoth Cave. The underlying bedrock in the Cane Run Creek Watershed is composed of Lexington Limestone of the Middle Ordovician period (Cressman and Peterson, 1986). The Lexington Limestone member is approximately 95 meters thick. The strata creating the subsurface aquifer is highly complex with micrograined argillaceous carbonate facies interbedded primarily within limestone (Cressman, 1967). The rock structures in the region are a result of a tectonic stress-field which initiated a pattern of en echelon minor faults and joints directing from the southeast towards the northwest (Drahovzal et al., 1992; Drahovzal and Noger, 1995). Karst conduits have formed along these structures and many of these conduits cross through catchment boundaries created by surface geomorphology (Taylor, 1992). Near the Groundwater Station, a minor syncline is created with an azimuth from southeast to northwest, and a minor normal fault trending northwest is also located near this area (Cressman, 1967).

The fast response porosity of the Cane Run karst system consists of a series of vertical shafts and anastomosis conduits that converge to a main subsurface conduit that transports and stores water. Dissolution of near-surface limestone has formed the existing karst holes and sinking features within the stream channel that pirate flow during low to moderate hydrologic conditions. The primary conduit is believed to be formed along the normal fault and generally follows the path of the surface stream until divergence near the Groundwater Station. The conduit is phreatic and the primary spring head is approximately 7 meters above the conduit low point.

3.3 Human Disturbances

The Royal Spring karst aquifer has been used as a water source since its discovery in the late 18th century. The water recovered from the spring and aquifer has been used for distilleries, grist mills, and as a raw municipal water supply for the City of Georgetown. More recently, the aquifer has been pumped for agricultural purposes such as hydrating cattle and horses and irrigating crops. During dry periods, the primary springhead runs dry due to over-pumping of aquifer water resulting in the lowering of the groundwater table.

The urbanization of Lexington, the second largest city in Kentucky, has introduced many potential contamination sources (e.g., lawn fertilizer, septic tanks, chemical waste) into the watershed. In 2006, the U.S. Environmental Protection Agency filed a lawsuit against the Lexington-Fayette Urban County Government for not complying with the urban stormwater runoff regulations of the Clean Water Act (Martin, 2009). The historic increase in impervious areas in the headwaters of the watershed reduces baseflow and, coupled with flow pirating from karst features, hinders aquatic habitats. Transportation routes such as I-75 and I-64 cut through the center of the coupled drainage network and are prominent

sources of contamination. Anthropogenic agricultural and urban practices cause harmful algal blooms, transport of deleterious metals, and proliferation of fine sediment, which in turn severely impedes the ability of the Georgetown water treatment plant to safely provide drinking water to the local population.

3.4 Historic Study of System

Pre-knowledge of the Cane Run system was provided through much study of the system primarily by the Kentucky Geological Survey (KGS) over the past four decades (Cressman, 1973; Thraikill, 1985; Taylor, 1992, Clepper, 2011) and more recently in peer reviewed journal papers (Jewell et al., 2004; Palanisamy and Workman, 2014; Sawyer et al., 2015) . The groundwater basin of Royal Spring was first mapped in the 1980's using dye traces injected into swallets and then monitored at different locations in order to map connectivity of karst features (Spangler et al., 1982; Taylor, 1992). Paylor and Currens (2004) used quantitative dye tracing techniques in the basin to determine travel times for a variety of hydrologic conditions. Qualitative dye traces were also performed to check for connectivity of different swallets to the main conduit. A more refined groundwater basin was created using the accumulation of many tracer studies (Figure 3-3).

Thraikill and Gouzie (1984) estimated linear velocity, channel geometry, and conveyance in the groundwater basin using travel time of dye slugs and discharges obtained by dye dilution. Thraikill and Gouzie also believed that some flow was bypassing the primary spring through overflow routes. In later research, Thraikill et al. (1991) concluded that the subsurface conduit had a shallow flow of a few centimeters that should be considered an 'equivalent depth' and that the significant flow in the aquifer is in a thin, high porosity zone beneath the water table.

Tripathi (2009) employed electrical resistivity and self-potential techniques at multiple locations within the Royal Spring karst basin in order to locate the main trunk conduit that fed into the primary springhead. In 2010, the KGS measured electrical resistivity profiles over eight kilometers of the surface using a dipole-dipole electrode configuration method. This method works by using the difference in the low resistivity of water in the conduit to the high resistivity of water in the fracture matrix component of the limestone to map potential surfaces and high conveyance areas. Potentiometric surfaces were also plotted as more and more monitoring wells were installed in the basin. In total, the KGS drilled 44 wells in search of the primary conduit using the electrical resistivity profiles to determine drilling location. Four wells drilled by the KGS either directly intersected the main conduit or are hydraulically connected to the conduit (identified by “Groundwater Station” in Figure 3-1). These wells were instrumented with water quality sondes, pressure transducers, an automatic sampler, and a velocimeter.

Down-hole video imaging of the system was performed by the KGS in order to obtain more information about conduit geometry. Doppler sonar instruments were used to estimate distance to the wall from one of the wells that directly intersected the conduit. This instrument was also used to verify readings by the Marsh-McBirney® 201-D velocimeter. Early estimates by both visual inspection, quantitative dye traces, and Doppler sonar results have narrowed down the general shape of the conduit which represents a shallow, wide rectangular channel with an averaged measured height of 0.9 m and an average width of 6.2 m.

In 1998, the Cane Run Watershed was identified as an impaired waterway by the Kentucky Division of Water. The University of Kentucky’s College of Agriculture, Food,

and Environment developed a watershed based plan in order to remediate deficiencies caused by point and nonpoint source pollution (UKAg, 2011). Conclusions of the research were that the overall watershed is in bad ecological health and that major problems are bacteria, nutrient pollutants, and stream bank erosion. The single biggest problem identified in the watershed was the coupling of the surface and subsurface drainage network which inhibited aquatic species in streams due to flow pirating by the karst geomorphology.

3.5 Water Processes, Source, and Mechanics

Streams in the Cane Run Creek are primarily activated by rainfall events. This results in the primary channel of the watershed running dry for a majority of the year when prolonged rainfall is absent. Runoff in the headwaters is poorly infiltrated due to the high percentage of impervious areas and is delivered to the stream channel soon after rainfall is initiated. The majority of the downstream portion of the watershed is agriculturally impacted and provides more sustained flow, during events, to the main channel through tributaries and surface runoff.

During hydrologic events, runoff enters the streambed and is captured by the many swallets and estavelles located along the stream profile. Streamflow is maintained on the surface only after the subsurface karst aquifer is filled. This occurs during moderate to high hydrologic activity that exceed karst aquifer capacity. Once the karst aquifer is at “capacity”, streamflow will overtop the karst features in the streambed and allow for downstream water conveyance on the surface. Streamflow continues to be exchanged between the surfaces and subsurface, but in a more complex manner which is governed by the energy difference between different swallets along the conduit.

The flow in the subsurface portion of the Cane Run Creek Watershed is primarily through a wide, rectangular conduit 20 meters below the ground surface. There are several anastomosing conduits that flank and interact with the main, central conduit. The karst conduit is generally aligned with the surface channel of Cane Run Creek, however, the two flow paths eventually diverge with Cane Run Creek leading into the North Elkhorn and the Royal Spring conduit leading to Georgetown.

3.6 Sediment Transport Sources and Processes

Sediment in the watershed is derived from the various agricultural and urban land uses. In-stream sediment transport processes are heavily influenced by the short-lived hydrologic events and infrequent sustained streamflow. Sediment is delivered from the uplands, transported downstream, and stored in the watershed during active periods. The lack of erosion controls and sufficient runoff have negatively impacted stream bank stability leading to erosion of stream bank sediments. Urbanization of the upstream portion of the watershed is believed to be a large source of sediment erosion and in-stream storage. Sediment is also introduced into the main stream corridor due to livestock and equine grazing in the cattle and horse farms in the watershed.

As with the streamflow, the suspended sediment in the stream is also diverted and re-routed to the subsurface karst aquifer during low to moderate flows. This sediment is then deposited in the subsurface due to a decrease in the transport carrying capacity of the fluid. This decrease is a result of a downstream hydraulic control (i.e. the water surface at the primary springhead). Sediment deposited in the subsurface can be either re-introduced to the surface through estavelle action or carried down-gradient towards Royal Spring.

In addition to mapping flow connectivity, both point samples and continuous water quality data were collected from a monitoring well accessing the karst conduit. The monitoring well is adjacent an existing large farm well used to access the same karst water for irrigation. Fine sediment is well recognized to transport contaminants down-gradient in watersheds. The karst aquifer repeatedly has fecal coliform counts exceeding 10,000 c/100 mL of water that are highly correlated with total suspended solids concentration of karst water (Currens et al., 2015). Such occurrences of high fecal and sediment loads in the karst were most frequent during or after storm events. Water and sediment transported within the karst conduit could potentially be unsafe although natural bacteria are known for breaking down contaminants given enough time.

3.7 Carbon Mechanisms and Transport

Carbon is introduced to the stream primarily through runoff carrying eroded soil from the banks and uplands as well as fine detrital material. Autotrophic carbon production is low in the watershed due to poor aquatic habitats resulting from the intermittent streamflow due to the karst hydro-geomorphology. Organic enrichment from urban runoff and storm sewers is also a concern along the entire length of the channel. Carbon-rich sediments from the surface have the potential to be diverted to the subsurface conduit where heterotrophic bacteria decomposition is pronounced. Depleted sediment then could resurface to the stream corridor, remain in storage, or be flushed out to the main spring. One unknown that will be investigated in this study is the transformation of carbon during temporary fate in the subterranean karst corridor.

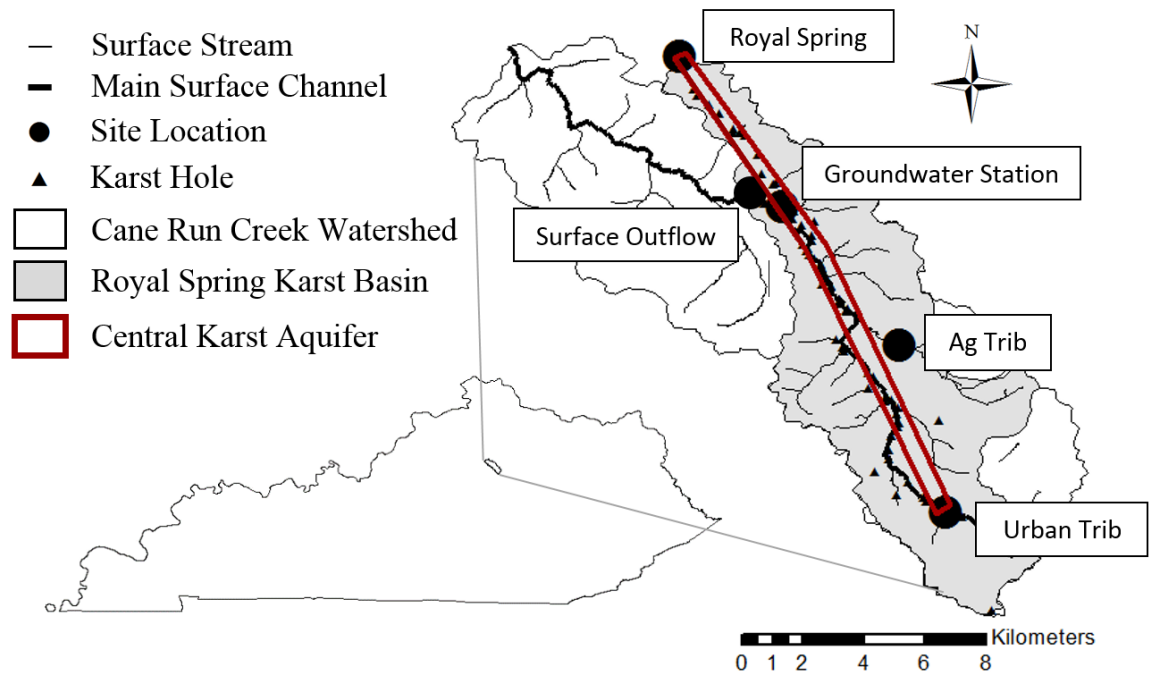


Figure 3-1: Location Map of Cane Run Watershed and Royal Spring Basin

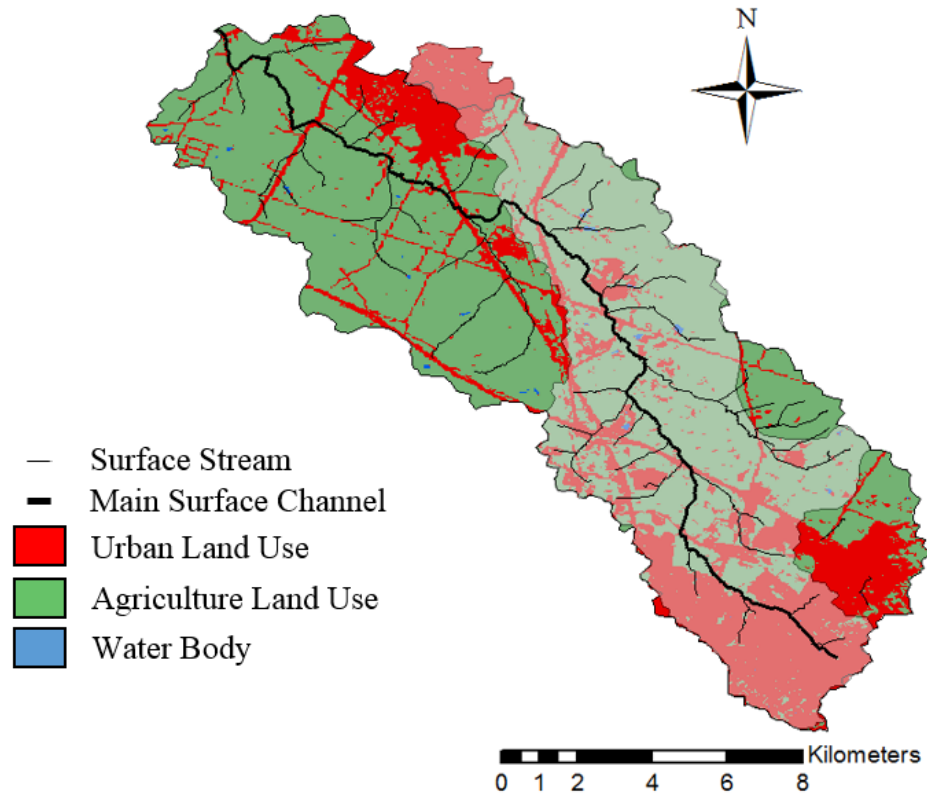


Figure 3-2: Cane Run Creek Land Use Map

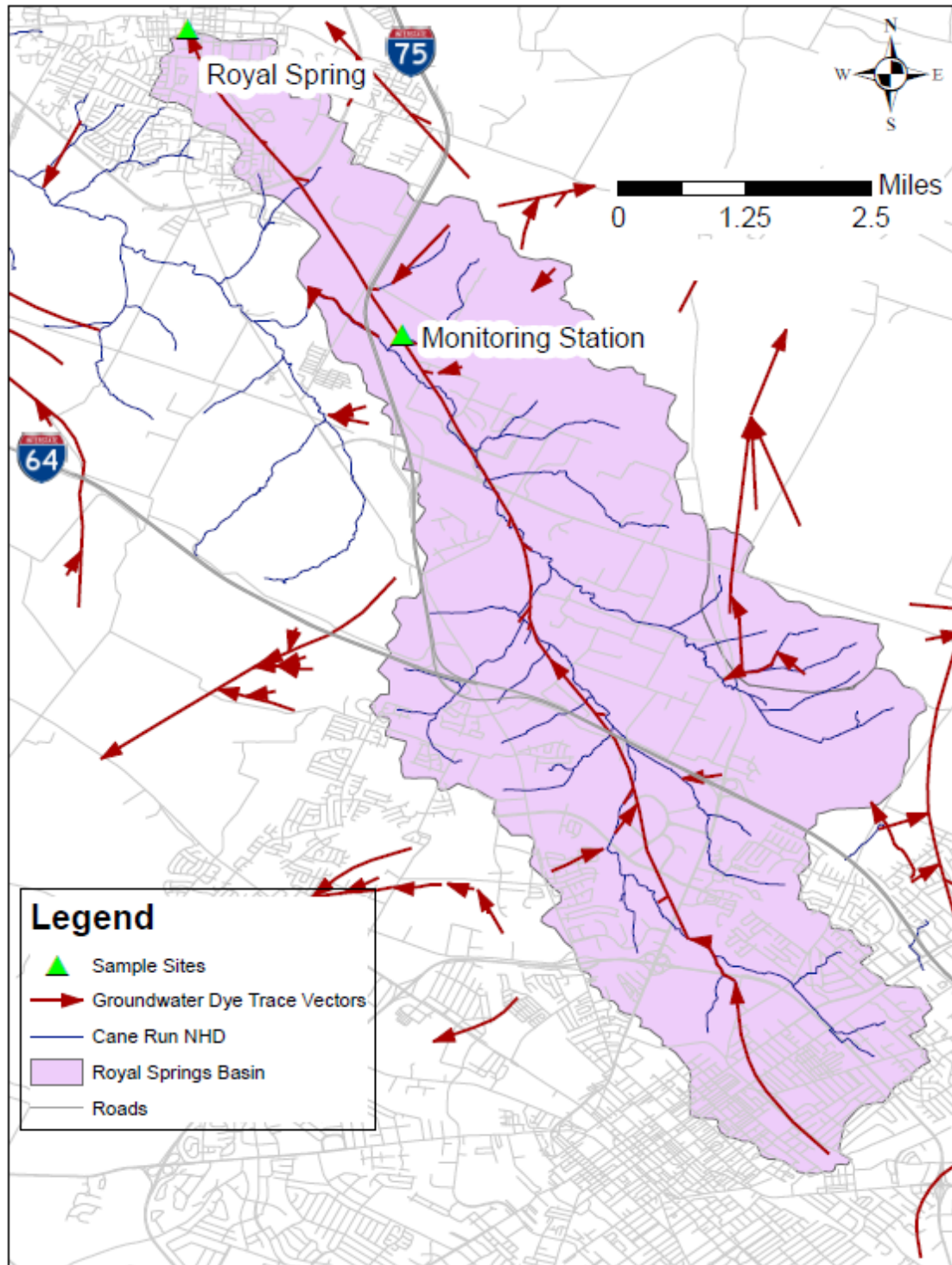


Figure 3-3: Qualitative Dye Traces in Royal Spring (adapted from Lee, 2012)

Chapter 4 Methodology

Modeling the sediment transport capabilities and carbon transformations in a coupled surface-subsurface karst drainage network was performed using a coupled model framework including hydrologic, hydraulic, and biological processes. The model addresses physical erosion and deposition in the conduit as well as decomposition of sediment organic carbon temporarily trapped in the subsurface. Figure 4-1 shows the modeling outline used in this study. The major inputs to the sediment transport model are the sediment fluxes pirated from surface stream tributaries, the flow rate in each cell of the conduit, and the hydraulic and hydrologic inputs for the surface and subsurface. Inputs to the sediment transport model were collected through field investigation and laboratory analysis. The major inputs to the carbon model were the contributions of different source carbon pools, litter and algae decomposition rates, and fixed percent algae in the sediment organic carbon. Carbon inputs were collected through isotopic and elemental lab analysis. Investigated hydraulic and biochemical parameters were adjusted to optimize model results. Other parameters such as critical shear stresses and decomposition rates were based off of results published in peer-reviewed literature. Calibration and validation was performed using statistics (e.g., Nash-Sutcliffe Efficiency) to evaluate model results against results obtained from measured data.

4.1 Water Data

4.1.1 Stream Gages

Inputs and outputs to the Cane Run Creek and the associated karst drainage network were measured using continuous flow monitoring. Therefore, in-situ pressure transducers were installed at the Surface Outflow, Urban Trib, and Ag Trib locations (Figure 3-1) and

collected stage every 10 minutes. The two inflowing tributaries were representative of the urban and agriculture catchments that make up the Cane Run Creek Watershed, but did not have sinkholes upstream of the sampling site. Surface water outflow for the drainage area was measured at the location where surface water pathways and subsurface flow paths begin to diverge. Flow velocity measurements taken by the United States Geological Survey (USGS) at different stage heights were used to develop stage-discharge relationships.

The two primary flow gages set up in the urban and agriculture streams were removed for periods of time for calibration and cleaning leaving gaps in the continuous data records that were filled using other operational gages as surrogates. The three gages used to fill in missing data for tributary inflow are the Cane Run Creek Surface Overflow Station (CRCK) which is located a few hundred meters from the Groundwater Station and is operated by the Kentucky Geological Survey; the Cane Run at Berea Road (USGS 03288200) station which was decommissioned halfway through the investigation period in June 2012; and the Cane Run at Citation Boulevard (USGS 03288180) station which replaced the Berea Road station. Hydrologic relationships between the gages were created and are shown in Table 4-1 to optimize which surrogate gage would perform the best when data at the original stations were not available. The relationships between the gages performed as expected with sites closer spatially to one another acting as better proxies than those further away.

4.1.2 Observation Wells

Several observation wells were drilled within the watershed in order to monitor the piezometric head, subsurface flow, and sediment transport processes. The location of

where the wells were to be drilled was determined using surface geophysical techniques (Tripathi, 2009). Researchers applied an electrical resistivity technique (ER) to 972 m of the surface by measuring ER profiles using a SuperSting™ R8/IP instrument with dipole-dipole electrode configuration at 2 – 3 m spacing. Self-potential (SP) measurements were taken along the ER lines by using one stationary reference electrode and another roving electrode. The ER technique used the difference in resistivity between water and limestone bedrock to locate conduits. The SP technique measures the natural electrical potential caused by the electrokinetic or streaming potential of fluid flow through subsurface media. Subsequent drilling of over 44 six inch diameter wells established the elevation of the conduit to be 20 m below the ground surface. Many of the original 44 wells entirely missed the conduit and some were instrumented with depth gages to monitor groundwater levels in the surrounding karst aquifer. Three wells directly intersected the conduit and one well just barely missed the wall of the conduit, but was believed to be in hydraulic communication with the conduit (i.e., head in the conduit is similar to that of the well).

Telog® Water Level Recorders (model 2109) were placed in six of the wells and measured spatial variability of the piezometric surface. One of the wells directly intersecting the conduit was instrumented with a Marsh-McBirney® 201-D velocimeter to measure average conduit velocity. A YSI® 6920v2 turbidity probe was installed into one of the wells for continuous water quality and sediment monitoring and measures pH, temperature, conductivity, dissolved oxygen percentage, and turbidity. A Teledyne ISCO® 6712 Water Sampler was used to collect suspended sediment samples every 30 minutes throughout hydrologic events as well as during baseflow. Afterwards, a Total Suspended Solids (TSS) analysis was performed to determine sediment concentration for each sample.

A relationship between turbidity readings and TSS concentrations was developed by taking many TSS samples and fitting them with the turbidity probe data (Figure 4-2).

Flow through the subsurface conduit at the Groundwater Station was measured by a Marsh-McBirney® 201-D continuous velocity recording device. The Marsh-McBirney® 201-D magnetic water flow-meter is a robust sonde that measures instantaneous velocity. The instrument has a relatively small profile which makes it less susceptible to being damaged by debris. If the instrument does become damaged it is relatively inexpensive to repair or replace. The velocimeter was placed at 8/10ths of the maximum height of the conduit to collect the depth average velocity within the conduit. The range of this instrument at the Groundwater Station was found to be between 0.01 and 0.48 m s⁻¹. A Campbell Scientific® CR200 data logger was used to record the analog velocity signal at 10 minute intervals starting in October 2011 and continuing to October 2013.

Due to the abundance of data over the two year time period, there is a reliable estimation of the discharge within the conduit for much of the time period. However, the Marsh-McBirney® Velocimeter was in need of maintenance quite often and there are gaps of missing velocity data within the conduit. The velocimeter was impacted by lightning strikes, contact with debris, and animals chewing through the wiring. A spring gage (USGS 03288110) was used as a surrogate during time periods when the conduit instrumentation was out of order.

4.1.3 Dye Traces

The Kentucky Geological Survey used quantitative dye tracing to estimate the instantaneous discharge and establish a stage-discharge relationship for the conduit. All dye traces were injected at a location known as “Eclipse Road karst window” located about

955 m upstream from the Groundwater Station, including sinuosity. Water was filled in a container and then the dye tracer was mixed with water which was later injected into the karst window. The concept of a dye trace is based on conservation of mass in that the dye injected at one location should be recoverable at another location along the path of the flow assuming the tracer is conservative (White, 2002) as

$$C_I/Q_I = C_R/Q_R, \quad (5)$$

where, C_I and Q_I are the initial concentration (mg L^{-1}) and inflow rate at the Eclipse Road karst window ($\text{m}^3 \text{s}^{-1}$), respectively, C_R (mg L^{-1}) is the concentration of the recovered dye tracer, and Q_R is the unknown variable solved in the equation which represents the discharge ($\text{m}^3 \text{s}^{-1}$) at the location of dye recovery.

Rhodamine WT and fluorescein were the two dye tracers injected into the karst window. These tracers are commonly used in karst environments due to low adsorptive tendency, strong fluorescence, chemical stability, and benign character in benthic environments (Smart and Laidlaw, 1977; Wilson et al., 1986). Downstream concentration of the tracers was measured by collecting water samples every 10 minutes using an ISCO® sampler. Tracer analysis was done with a Cary Eclipse Varian® fluorescence spectrophotometer. The arrival time of the center of mass of the fluorescein was used to estimate the velocity of the discharge. The concentration of the Rhodamine WT was used to calculate the rate of the discharge. In turn, the cross-sectional area of the conduit was estimate by simply dividing the flow rate measured by the Rhodamine WT with the velocity measured by the Marsh-McBirney®. This technique of dye tracing proved useful

to corroborate the readings and estimations of both velocity and cross-sectional area obtained from other methods.

4.2 Sediment Data

4.2.1 Total Suspended Solids Pumps and Samplers

Sediment concentration measurements of water from the conduit and surface streams were measured using water samples collected with Teledyne ISCO® 6712 automated pump samplers. Automated samplers were programmed to collect 500 mL samples at 30 or 60 minute intervals. Grab samples were also collected from the surface streams. Samples were returned to the lab and processed with Whatman filters which retain sediment larger than 0.45 microns. The Whatman filters were rinsed with de-ionized organic free water and dried in an oven at 105°C to remove all water prior to analysis (USEPA, 1999). The volume of water in the sample bottles was noted and the samples were run through the filters to retain the sediment. The filters were then dried again and weighed to find the sample mass.

Due to the intense field and laboratory work required for collecting and analyzing TSS, it is not practically feasible to continuously sample using a pump sampler. One solution to monitoring suspended solids in the water column continuously is by using a turbidity probe. In this study we used several YSI® 6920v2 turbidity probes at the inlets and outlets to the drainage network. Turbidity is a measure of how much the suspended material in water decreases the passage of light through the water (McLusky, 1971). Sediment in the water column attenuates sunlight preventing it from penetrating deeper into the stream. A turbidity probe works by measuring the amount of transmitted light in

the water column. The amount of transmitted light decreases with increasing suspended solid concentrations. A surrogate relationship between TSS and turbidity was used to allow for low-cost and continuous sampling. Figure 4-2 shows the relationship between TSS and turbidity at the conduit Groundwater Station.

During the two year investigation period, the turbidity probes would often be damaged by debris in large flow events, electrical short circuiting, and by animals chewing through the probe cables. The probes were also often removed for data collection, recalibration, and cleaning. To fill in the time periods where turbidity data were missing from the YSI® sondes, several relationships were developed between flow and total suspended solids for each site as

$$C_{ss} = C_{int} \left(P_{urban}(1.3) + P_{ag}(0.75) \right) [E(1 - e^{-aQ_i})] + D, \quad (6)$$

where, C_{int} is an integration coefficient, Q_i is the flow rate for the tributary ($m^3 s^{-1}$), P_{urban} and P_{ag} are the land area fraction for urban and agricultural areas, respectively, and E , a , and D are empirical coefficients for curve fitting. These relationships allow for an estimate of the suspended solids when no other data were available and were developed from Russo and Fox (2012) and Coulter et al. (2004). The relationships between turbidity and flow are listed in Table 4-2.

4.2.2 Sediment Flux

The method used for estimating suspended-sediment discharge in this study is termed Einstein's Approach (1950) which integrates the velocity and concentration profiles over the flow depth as

$$q_{ss} = \int_a^D C u dz, \quad (7)$$

where, q_{ss} is sediment discharge per unit width ($\text{kg s}^{-1}\text{m}^{-1}$), a is the lower limit where suspension begins (m), D is the flow depth (m), C is the sediment concentration (mg L^{-1}), u is velocity (m s^{-1}), and z is in the direction perpendicular to the bed (m).

The concentration profiles of the surface streams and subsurface conduit were parameterized using a reference concentration, C_a , at the depth of the ISCO® sampler inlet. The concentration equation (Rouse, 1937) has the form

$$\frac{C}{C_a} = \left(\frac{D-z}{z} - \frac{a}{D-a} \right)^{z_*}, \quad (8)$$

where, z_* is the Rouse Number. Higher Rouse Numbers have an exponentially decaying sediment concentration profile heavily skewed towards the bed due to high particle sizes or low slopes whereas low Rouse Numbers approach a near-uniform concentration profile and are more typical for fine sediment. The Rouse Number is formulated as

$$z_* = \frac{w_s}{\kappa U_*}, \quad (9)$$

where, w_s is the settling velocity of the sediment (m s^{-1}), κ is the von Karman constant (approximately 0.4 for clear fluids), and U_* is the friction, or shear, velocity (m s^{-1}) which, in open channel flow, is estimated (Chang, 1998 p. 41) as

$$U_* = \sqrt{gRS}, \quad (10)$$

where, g is the acceleration due to gravity (m s^{-2}), R is the hydraulic radius (m), and S is the energy slope (m m^{-1}). For pipes or conduits, the shear velocity is estimated (Allen et al., 2007) as

$$U_* = \sqrt{\frac{f \cdot U_{avg}^2}{8}}, \quad (11)$$

where, f is the Darcy friction factor, and U_{avg} is the average flow velocity (m s^{-1}).

The velocity profile for surface streams was slightly modified from the log-law equation for hydraulically rough surfaces (Chang, 1988 p. 46). Due to the protrusion of roughness elements through into the fully turbulent zone, the effects of fluid viscosity are not felt by the fluid and instead the shear stress, density, and roughness height dominate the velocity profile. A scaling factor, C , is also introduced to fit the integrated velocity profiles (flow rates) with field measurements in the following equation for velocity as

$$u = \frac{U_*}{C} \times \left(\frac{1}{k} \ln \left(\frac{z}{k_s} \right) + 8.5 \right), \quad (12)$$

where, k_s is the equivalent mean diameter of sand grains (m). Figure 4-3 shows a sample velocity profile and concentration profile for one of the surface tributaries to the system.

The velocity profile for the karst conduit was estimated using the one-seventh power-law velocity profile for turbulent flow (De Chant, 2005) as shown in the following equation as

$$u = U_{max} \left(1 - \frac{r}{R} \right)^{\frac{1}{n}}, \quad (13)$$

where, U_{max} is the centerline, maximum velocity in the conduit ($m s^{-1}$), r is the distance (m) from the centerline of the conduit to the wall of the conduit constrained by 0 and R , the radius (m), and n is the exponent for the power-law which increases with increasing Reynolds number, but is commonly assumed as 7 for fully turbulent flow. Figure 4-4 shows a sample velocity profile and concentration profile for the conduit.

Equation (7) is used together with channel geometry and equations (8) and (12), and we arrive at the final equation for sediment discharge ($kg s^{-1}$) for streams:

$$Q_{ss} = q_{ss} \cdot B = B \int_a^D C_a \left(\frac{D-z}{z} \frac{a}{D-a} \right)^{z_*} \cdot \frac{U_*}{C} \cdot \left[\frac{1}{k} \ln \left(\frac{z}{k_s} \right) + 8.5 \right] dz, \quad (14)$$

and for the conduit referring back to equation (7) together with (8) and (13):

$$Q_{ss} = q_{ss} \cdot B = B \int_a^D C_a \left(\frac{D-z}{z} \frac{a}{D-a} \right)^{z_*} \cdot U_{max} \left(1 - \frac{r}{R} \right)^{\frac{1}{n}} dz. \quad (15)$$

4.2.3 Particle Size Distribution

The Urban Trib, Ag Trib, Groundwater Station, and Surface Outflow locations were sampled and analyzed for the particle size distributions of the sediment. Suspended sediment samples were collected from the two inflow tributaries to the system as well as the surface and subsurface outflows (see Figure 3-1). Samples collected in the field were returned to the laboratory where the fine fraction of the sediment was wet-sieved from the bulk sample. Afterwards a subsample of the fine portion was run through a LISST-Portable|XR particle size analyzer. The LISST particle size analyzer works by using laser light scattering or laser diffraction. De-ionized water constantly recirculates the sediment sample within the mixing chamber where the instrument measures the angular variation in intensity of light scattered as a laser beam is passed through the sample. The LISST particle

size analyzer measures sediment particles between 0.34 - 500 μm and outputs D_{10} , D_{16} , D_{50} , D_{60} , D_{84} , and D_{90} readings. The particle size distributions of sediment from different locations in the watershed can be seen in Figure 4-5.

4.3 Carbon Data

4.3.1 Source Sampling

The carbon sources to the coupled surface-subsurface drainage network were separated as two allochthonous sources (soil and litter) and one autochthonous source (algae). In this study, the transported POC of inflowing tributaries was measured in a stream impacted by urban development and one dominated by agricultural land use. The data collected and analyzed from these trap samples were used to calibrate the carbon flux portion of the model. The tributaries (Urban Trib and Ag Trib) to the system were sampled on a predominantly bi-weekly sampling routine for a period of almost two years (09/2011-07/2013).

The method to collect these samples is described by Phillips et al. (2000) and includes installing *in situ* sediment trap samplers to collect time-integrated samples. The trap samplers can be seen in Figure 4-6. The sampler works by accelerating the fluid and sediment through the small opening nozzle and then suddenly expanding into a larger cross-sectional area which slows the velocity of the fluid inside of the trap considerably. The decrease in velocity allows for the particles to settle to the bottom of the trap where they are recovered when the sampler is pulled from the stream. Water exits through a small diameter hole at the end of the sampler. The sampler does preferentially collect coarser sediment due to the smaller particles remaining suspended for a long enough duration to

allow for passing through the trap, however the sampler does a sufficient job of providing representative, integrated total carbon during the sampling period (Phillips et al., 2000; Ford and Fox, 2012).

Table 4-3 shows the source contribution of the soil, litter, and algae pools. The soil carbon pool was the highest source of carbon to the Cane Run Watershed. The other allochthonous source was litter detritus which is derived from trees and riparian vegetation. Litter represents the second largest contributor of organic carbon to the Cane Run Watershed. Autochthonous or algal carbon originates from primary production of instream benthic organisms. The percent of algal carbon contributing to the downstream carbon flux was modeled as an input because of the intermittent nature of the surface streams which do not sustain water year round and provide conventional growth for instream producers. Urban streams were assumed to not have any primary production due to the quick pirating of flow by the subsurface karst.

4.3.2 Outlet Sampling

Outlets (Surface Outflow, Groundwater Station, and Royal Spring) were also instrumented with sediment trap samplers. The surface stream outlet was instrumented similarly to the tributaries. Due to the phreatic conduit at the Groundwater Station being sixty feet below the ground surface and that constant pump-sampling would be costly and time-intensive, an integrated trap sampler was installed downstream of the conduit where it re-surfaces as Royal Spring (see Figure 3-1). There were believed to be no significant additional carbon sources contributing to the conduit from the Groundwater Station to Royal Spring due to the diverging pathways of the surface channel and subsurface conduit. Additionally, the hydraulics and flow of the two sites are comparable and allow for the

extension of analysis from the conduit at the Groundwater Station to the conduit outlet (i.e., Royal Spring). Maximum weekly flows between the two sites showed a near 1:1 relationship indicating that the ability of the conduit to transport sediment in the final third of the conduit (Figure 4-7). The duration of sampling for the surface outlet was two years (2011-2013) while the subsurface pathway was sampled for one year (2012-2013).

4.3.3 Lab Analysis

The sediment trap samplers were installed at inlets and outlets to the system in order to collect time-integrated samples. The traps were routinely brought back to the lab, the sediment separated from the trap into a bucket, cleaned, and then re-installed in the field. Samples brought back to the lab went through a biogeochemical analysis process consisting of centrifugation, freezing, freeze drying, consolidating and weighing, wet sieving, and isotope ratio mass spectrometry. The first step in the process involves allowing the sediment within a 19 L bucket to settle to the bottom by placing the bucket in a refrigerator for 48 hours. Refrigeration of the sample to approximately 1.6°C promoted settling of the sediment. Afterwards, most of the water in the bucket was decanted using a siphon right up until the moment that the settled sediment was disturbed. The remaining sediment slurry was dispensed into 750 mL bottles and placed into a centrifuge. The 750 mL bottles were decanted and centrifuged until there was 100 mL or less of water remaining in the sample. The bottles were then placed in a freezer overnight until the sample was completely frozen. Afterwards the samples were placed into a Thermo Electron Corporation® Modulyo-D freeze dryer where pressure and temperature were reduced down to 3.0 mbar and -40°C, respectively. The process of sublimation converted the ice in the sediment sample into

water vapor. Once completely removed of moisture, the dry mass of the sediment was recorded.

Depending on the overall sample size, a subsample of either the entire sample, 0.5 g, 1.0 g, or 2.0 g was separated from the bulk sample. The subsample was wet-sieved through a 53 μm sieve to separate the fine and coarse sediment within the sample. Due to the samples having had water added to them again, the same process of centrifuging, decanting, and freeze drying was repeated for the fine sediment subsample. Once completely dry, the mass of the remaining fine fraction of the sediment was measured. The coarse fraction of the sediment was discarded.

The samples were prepared for elemental analysis by first being ground up into a fine powder using a Sigma-Aldrich Wig-L-Bug® grinder/mixer. The powdered sediment samples were weighed into silver capsules and acidified with 6% sulfurous acid to remove any inorganic carbonate phases in the sample (Verardo et al., 1990). Finally, samples were analyzed in a Costech® 4010 elemental analyzer coupled to a Finnigan Isotope Mass Spectrometer which estimated percent carbon and the carbon isotopic ratio of $\text{C}^{13}/\text{C}^{12}$ within the sample versus that of the elemental standard used, acetanilide.

4.4 Numerical Modeling

The numerical modeling framework for the coupled surface-subsurface model is shown in Figure 4-8. The inputs to the model consisted of surface and subsurface hydrologic, hydraulic, and isotopic data and parameters. Sediment processes simulated within the model are in-stream erosion, temporary sediment storage, SFGL and deep-bed mixing, sediment flux and conduit bed depth evolution. Additionally, sediment pirated

from surface streams into the subsurface by swallets and other karst features was modeled as a function of sediment concentration in surface streams and conduit flow rate. Carbon processes performed within the model were source discretization, multiple carbon pool partitioning, SOC decomposition, suspended and bed carbon mixing, and carbon dioxide efflux estimation. To achieve the stated goals in section 1.3, a coupled surface-subsurface fluviokarst model was developed to link fluvial processes in the uplands with subsurface transformation and conveyance processes. The model is data-driven and was calibrated by data obtained from two years of sample collection and monitoring. Data collected included suspended sediment concentrations for sediment model calibration and organic carbon samples for carbon model calibration. Parameters were estimated through a 70/30 calibration/validation time period.

4.4.1 Water Budget and Hydrologic Model

Using a control volume approach that included upscaling the tributary catchments to the system as inflows and incorporating downstream surface and subsurface pathways as outflows, a change in storage was modeled for the system (Figure 4-9). The change in storage $\left(\frac{dS}{dt}\right)$ calculations are data-driven by using equation (16) and inputting the recorded inflows and outflows to the system at each time step:

$$\frac{dS}{dt} = [\Sigma Q_{IN} - \Sigma Q_{OUT}]_{CV} = Q_{IN_{AG}} + Q_{IN_{URBAN}} - Q_{OUT_{CONDUIT}} - Q_{OUT_{STREAM}}, \quad (16)$$

where, $Q_{IN_{AG}}$ is the upscaled flow in from agricultural streams ($m^3 s^{-1}$), $Q_{IN_{URBAN}}$ is the upscaled flow in from urban streams ($m^3 s^{-1}$), $Q_{OUT_{CONDUIT}}$ is the outflow from the conduit ($m^3 s^{-1}$), and $Q_{OUT_{STREAM}}$ is the outflow from the surface stream ($m^3 s^{-1}$).

4.4.2 Hydraulic Model

The transport of sediment in the subsurface is driven by shear forces exerted from the conveyance of fluid within the conduit. Therefore, a hydraulic model is needed to predict fluid shear stress and transport capacity. Energy losses in the subsurface conduit were investigated with a pipe flow modelling approach using the Darcy friction factor to represent flow resistance. Due to the heterogeneous nature of karst conduits, identifying individual discontinuities and point losses (i.e., minor losses) involves additional assumptions and over-specification of unknowns within the system. Thus, head losses in the model were assumed to be major losses manifested by the roughness of the conduit wall.

The friction factor was estimated by solving the Energy Equation for a segment of the conduit, as

$$\frac{p_1}{\gamma} + z_1 + \frac{v_1^2}{2g} - f \frac{V_{avg}^2 L}{2g D} = \frac{p_2}{\gamma} + z_2 + \frac{v_2^2}{2g}, \quad (17)$$

where, p is the pressure (N m^{-2}), γ is the specific weight of the fluid (N m^{-3}), z is the elevation (m), v is the velocity of the fluid (m s^{-1}), g is the acceleration due to gravity (m s^{-2}), f is the Darcy friction factor, L is the length of the conduit including sinuosity (m), V_{avg}^2 is the average velocity of the fluid at a given cross-section (m s^{-1}), and D is the average equivalent diameter of the conduit (m). The subscripts 1 and 2 represent the Groundwater Station and Royal Spring, respectively.

The karst cave is a complex system which exhibits vast heterogeneity; the roughness, tortuosity, and turbulence are extremely variable along most reaches of the conduit and often times it is extremely difficult to get a single, representative friction factor

for the entire conduit. However, the median of the modeled results from equation (17) was used in the sediment transport model due to it being near the 1st quartile, the mean, and the 3rd quartile of the dataset. Equation (17) was solved for low and high velocities (0.02 – 0.39 m s⁻¹) to arrive at a friction factor that captures the effects of a range of flow conditions. Other karst study locations such as Jordtulla, Norway (Lauritzen et al. 1985) and Holloch, Switzerland (Jeannin and Marechal, 1995) have friction factor values ranging from 0.12 to 104, respectively. Figure 4-10 shows the relationship between friction factor and conduit velocity.

A mass balance approach was applied to model the sediment transport within the conduit. The model framework was adapted from the work by Russo and Fox (2012) on surface streams in the Inner Bluegrass Region with similar suspended sediment, physical, biological, and chemical properties. The length of each cell in the conduit was selected in order to satisfy the Courant-Friedrichs-Lewy condition in which the spatial scales and timescales are on the same order of magnitude as the downstream transmission of information (Islam and Chaudhry, 1997). For each cell, j , in the conduit, the suspended sediment at each time step, SS_i , was given as

$$SS_i = SS_{i-1} + E_{sfgl_i} + E_{bed_i} - D_i + P_S Q_{ss\,pirated_i} \Delta t + Q_{ss_i}^{j-1} \Delta t - Q_{ssOUT_i} \Delta t, \quad (18)$$

where, SS_{i-1} is the mass of suspended sediment from the previous time step (kg), E_{sfgl_i} is the mass of SFGL eroded from the conduit during the time step (kg), E_{bed_i} is the mass of bed material eroded from the conduit during the time step (kg), D_i is the mass of sediment deposited to the conduit (kg), P_S is the density of swallets connecting the surface to the subsurface in a given reach (unitless), $Q_{ss\,pirated_i}$ is the sediment flow rate of pirated

sediment into the conduit cell (kg s^{-1}), Q_{SSi}^{j-1} is the suspended sediment flow rate into a given cell from the cell directly upstream (kg s^{-1}), Q_{SSOUT_i} is the suspended sediment flow rate out of the conduit reach at the time step (kg s^{-1}), and Δt is the time step length (s). The sediment outflow during a time step was calculated as

$$Q_{SSOUT_i} = \frac{SS_i}{V_i} Q_i, \quad (19)$$

where, V_i is equal to the volume of water in the conduit at a cell (m^3), and Q_i is the flow rate of the conduit at a given cell ($\text{m}^3 \text{s}^{-1}$). Finally, equation (19) can be rewritten as

$$SS_i = SS_{i-1} + E_{sfgl_i} + E_{bed_i} - D_i + P_S Q_{SS \text{ pirated}_i} \Delta t + Q_{SSi}^{j-1} \Delta t - \frac{SS_i}{V_i} Q_i \Delta t, \quad (20)$$

and rearranging the above equation to solve for suspended sediment yields the solution as

$$SS_i = \frac{SS_{i-1} + E_{sfgl_i} + E_{bed_i} - D_i + P_S Q_{SS \text{ pirated}_i} \Delta t + Q_{SSi}^{j-1} \Delta t}{1 + \left(\frac{Q_i \Delta t}{V_i}\right)}. \quad (21)$$

The mass flux of sediment pirated from the main surface channel into a given cell in the subsurface model was modeled as a function of the flow rate in the conduit and the average TSS of urban and agricultural streams. Sediment pirated from the surface was modeled as:

$$Q_{SS \text{ pirated}_i} = Q_i \cdot C_{SS}, \quad (22)$$

where, Q_i is the water flow rate in the subsurface conduit ($\text{m}^3 \text{s}^{-1}$), and C_{SS} is the average concentration of suspended solids in surface streams (mg L^{-1}). It was assumed that when water was present in the surface channel and sediment as being conveyed, an equivalent amount of surface water displaces the water discharged by the conduit at each time step.

The pirated sediment is then distributed throughout the cells in the subsurface conduit system that are connected to the surface. Table 4-4 shows the spatial density of the swallets (i.e., the number of swallets in a given reach divided by the total number of swallets in the entire watershed) on the surface as they are aligned with cells in the subsurface conduit. It was also assumed that flow rate was pirated proportionally to swallet density to maintain conservation of mass (e.g. a swallet density of 0.09 at one conduit cell would receive 9% of total pirated surface flow and sediment). Cells 1 through 10 are physically connected to the surface and take in sediment and flow while cells 11 through 16 act simply as conveyors of conduit sediment (Figure 4-11).

The model assumes that erosion and deposition are mutually exclusive processes within the model (i.e., if erosion occurs in a time step then no deposition can occur within that same time step and vice versa). The mechanism by which the SFGL and bed material of the conduit are eroded was through shear stress induced by the movement of fluid modeled as

$$\tau_o = \frac{f \rho_{water} V_{avg}^2}{8}, \quad (23)$$

where, τ_o is shear stress of the fluid at the conduit wall ($N\ m^{-2}$) and ρ_{water} is the density of the fluid ($kg\ m^{-3}$).

Erosion of the SFGL layer was only possible if the transport capacity of the fluid to carry energy was greater than the amount of sediment already in suspension. Likewise, material was deposited from suspension when the amount of material exceeds the energy of the fluid to keep the sediment entrained. The transport capacity (kg) was modeled as

$$T_{c_i} = C_{tc}(\tau_{o_i})^{1.5} L\Delta t, \quad (24)$$

where, C_{tc} is the transport calibration coefficient ($m^{1/2}s^2 kg^{-1/2}$), τ_{o_i} is the shear stress of the fluid at the sediment boundary ($N m^{-2}$), and L is the length of the conduit reach (m). The transport calibration coefficient was used to differentiate between high and low flow regimes in the conduit. A boundary flow rate was chosen to separate low flow and high flow transport coefficients. The transport coefficients are unique to each watershed and as a result were calibrated to sediment yield data (Russo and Fox, 2012). High and low transport coefficients reflect the change in sediment transport behavior between baseflow and hydrologic events.

The conduit bed was modeled as a composition of two layers of material: the SFGL and the deep bed sediment. The SFGL is typically the most easily erodible sediment while deep bed sediment is only accessed when the SFGL is entirely depleted. The amount of deep bed sediment that can be eroded is a function of critical shear stress and also the residual transport carrying capacity. As some of the SFGL is entrained into the water column, it reduces the remaining transport energy for additional sediment to be entrained (Chang, 1998). The residual transport carrying capacity (kg) of the fluid to erode the first source of sediment from the bed was modeled as

$$T_{res_i} = T_{c_i} - SS_{i-1}, \quad (25)$$

A residual transport capacity is also calculated for sediment sources deeper than the SFGL. For additional bed sources the residual bed carrying capacity (kg) was modeled as:

$$T_{res_i}^{bed} = T_{res_i} - E_{sfgl_i}, \quad (26)$$

The availability of the sediment sources within the conduit to be eroded was limited either by shear, transport capacity, or by supply (Russo and Fox, 2012). The source was considered shear limited when its critical shear stress is greater than that of the shear stress enacted by the fluid and incipient motion does not occur. The source was considered transport capacity limited if the energy of the water to entrain sediment is surpassed. Finally, supply limited sources were those that had been exhausted (i.e., the supply of the source was 0 kg) and are bypassed for other sources. Erosion of the SFGL was modeled using

$$E_{sfgl_i} = \min \left[\left(a_{sfgl} (\tau_{oi} - \tau_{crsfgl})^{b_{sfgl}} SA_{sfgl} \Delta t \right), (T_{res_i}), (S_{sfgl_i}) \right], \quad (27)$$

where, a_{sfgl} is the erodibility of the SFGL source ($\text{kg Pa}^{-1} \text{m}^{-2} \text{s}^{-1}$), τ_{crsfgl} is the critical shear stress of the SFGL source (N m^{-2}), b_{sfgl} is an exponent for SFGL erosion (unitless), SA_{sfgl} is the surface area of the SFGL source (m^2), and S_{sfgl_i} is the supply of the SFGL source (kg). Erosion of the bed material was modeled in a similar manner

$$E_{bed_i} = \min \left[\left(a_{bed} (\tau_{oi} - \tau_{crbed})^{b_{bed}} SA_{bed} \Delta t \right), (T_{res_i}^{bed}), (S_{bed_i}) \right], \quad (28)$$

where, a_{bed} is the erodibility of the bed source ($\text{kg Pa}^{-1} \text{m}^{-2} \text{s}^{-1}$), τ_{crbed} is the critical shear stress of the bed source (N m^{-2}), b_{bed} is an exponent for bed erosion (unitless), SA_{bed} is the surface area of the bed source (m^2), $T_{res_i}^{bed}$ is the residual transport capacity for the bed source (kg), and S_{bed_i} is the supply of the bed source (kg).

Supply of the SFGL and bed sources were modeled using a mass balance approach as

$$S_{sfgl_i} = \min[S_{sfgl_{i-1}} - E_{sfgl_i} + D_i - DEC_{soil_i} - DEC_{litter_i} - DEC_{algae_i}, S_{sfgl_{max}}], \quad (29)$$

where, $S_{sfgl_{i-1}}$ is the supply of SFGL from the previous time step (kg), D_{sfgl_i} is the amount of SFGL deposited out of suspension in the time step (kg), DEC_{soil_i} , DEC_{litter_i} , DEC_{algae_i} are the amounts of organic carbon decomposed to into dissolved carbon from soil, litter, and algae sources, respectively (kg), $S_{sfgl_{max}}$ is the maximum allowable supply of SFGL (kg). The SFGL was assumed to be the top biologically active layer of the conduit sediment that is limited to a maximum depth of 5 mm. The maximum SFGL for any cell was calculated as

$$S_{sfgl_{max}} = d_{sfgl_{max}} \rho_{sfgl} SA, \quad (30)$$

where, $d_{sfgl_{max}}$ is the maximum depth the SFGL can reach before being assimilated into the deeper bed (m) and ρ_{sfgl} is the density of the SFGL material (kg m⁻³).

The supply of SFGL allowed for microbial activity and the transformation of organic carbon into inorganic carbon. All suspended sediment that was deposited to the conduit was assumed to be assimilated into the SFGL layer first. Once the SFGL layer was at a maximum depth, the SFGL sediment at the SFGL/bed interface assimilated into the deep bed sediment. Supply of the bed was modeled in a similar manner as

$$S_{bed_i} = S_{bed_{i-1}} - E_{bed_i} + A_{sfgl_i}, \quad (31)$$

where, $S_{bed_{i-1}}$ is the supply of bed sediment in the previous time step (kg) and A_{sfgl_i} is the amount of SFGL sediment assimilated into the deep bed (kg) which was modeled as

$$A_{sfgl_i} = S_{sfgl_i} - S_{sfgl_{max}}, \quad (32)$$

SFGL sediment is only assimilated into the deeper bed if the maximum supply of SFGL sediment was exceeded due to deposition of suspended sediments.

The depth of the SFGL was also continuously monitored throughout the model as

$$d_{sfgl_i} = \min \left[\frac{S_{sfgl_i}}{\rho_{sfglSA}}, \frac{S_{sfgl_{max}}}{\rho_{sfglSA}} \right], \quad (33)$$

where, ρ_{sfgl} is the density of the surface fine grained laminae material (kg m^{-3}). The bed depth was modeled as

$$d_{bed_i} = \frac{S_{bed_i}}{\rho_{bedSA}}, \quad (34)$$

Deposition was modeled at each time step if the transport carrying capacity was exceeded by the suspended sediment load. The suspended sediment was deposited first into the SFGL and modeled as

$$D_i = \frac{\omega_s \Delta t}{k_p H} (SS_{i-1} - T_{c_i}), \quad (35)$$

where, D_i is the mass of sediment deposited in the time step (kg), ω_s is the settling velocity of the entrained particles (m s^{-1}), k_p is the deposition coefficient based on the Rouse concentration profile, H is the height of the conduit (m), and T_{c_i} is the transport carrying capacity of the fluid (kg).

4.4.3 Carbon Model

Carbon in the subsurface karst system was derived from surface sources such as terrestrial and autochthonous carbon. Sources of carbon to the subsurface include soil organic carbon, algal or autochthonous carbon, and allochthonous leaf litter. Allocating the

contribution of carbon from various locations in the watershed was performed by using a least squares method (Davis and Fox, 2008). The tracer used in this study was the $\delta^{13}C$ isotopic signature of collected sediment due to the fact that $\delta^{13}C$ has been found to discriminate sources in this region (Ford and Fox, 2014). The carbon pool sources are soil organic carbon, litter detritus carbon, and autochthonous algal carbon. The un-mixing was modeled as a conservation of mass using equations

$$z^T = \sum_k (x_k^T \times P_k), \quad (36)$$

and

$$\sum_k P_k = 1, \quad (37)$$

where, z is the tracer data from the sampled soil, x is the tracer data of the source, T is represents the tracer being used, k indicates the carbon pool source, P is the fraction of carbon originate from a particular source. The matrix formed by equations (36) and (37) was overdetermined if two tracers were used and can be solved efficiently using the above framework. However, in this study only one tracer was used to solve equations (36) and (37). The source fraction of algae, P_{algae} , was treated as an input for the system parameterized by percent algae distributions in the literature (Ford et al., 2015). Urban fed streams in the system do not provide a benthic ecosystem for a duration long enough to sustain autochthonous plant growth. In-field observations along urban tributaries of the watershed verified this assumption. Therefore, urban streams in the watershed were modeled as having only two sources: soil organic carbon and allochthonous leaf litter.

The carbon model budgeted three separate pools of organic carbon: the suspended sediment organic carbon (SS_{SOC_i}) was comprised of soil organic carbon (SS_{soil_i}), litter detritus carbon (SS_{litter_i}), and autochthonous algal carbon (SS_{algae_i})

$$SS_{SOC_i} = SS_{soil_i} + SS_{litter_i} + SS_{algae_i}, \quad (38)$$

The bed SOC was budgeted with the same approach as

$$S_{SOC_i} = S_{soil_i} + S_{litter_i} + S_{algae_i}, \quad (39)$$

where, S_{soil_i} is the supply of soil carbon in the bed (kg), S_{litter_i} is the supply of litter carbon in the bed (kg), and S_{algae_i} is the supply of algal carbon in the bed (kg).

The carbon content of suspended and bed sediments was calculated throughout the model using a mass balance and decomposition routine. During the temporary storage of sediment in the SFGL, the microbial community works to transform terrestrial and autochthonous derived carbon (Webster et al., 1999; Alvarez and Guerrero, 2000; Jackson and Vollaire, 2007). Suspended sediment organic carbon (SOC) (SS_{SOC_i}), and all three pools, in the system were modeled at the same intervals and locations as sediment using

$$SS_{SOC_i} = SS_{SOC_{i-1}} + E_{SOC_i} - D_{SOC_i} + P_S Q_{ss\ pirated_i} SOC\%_{pirated} \Delta t + Q_{SOC_i}^{j-1} \Delta t - Q_{SOC\ OUT_i} \Delta t + X_{BED \rightarrow SS} - X_{SS \rightarrow BED}, \quad (40)$$

where, $SS_{SOC_{i-1}}$ is the mass of SOC from the previous time step (kg), E_{SOC_i} is the mass of SOC eroded from the conduit during the time step (kg), D_{SOC_i} is the mass of SOC deposited to the conduit (kg), P_S is the density of swallets connecting the surface to the subsurface in a given reach (unitless), $Q_{ss\ pirated_i}$ is the sediment flow rate of pirated sediment into the

conduit cell (kg s^{-1}), $\text{SOC}\%_{\text{pirated}}$ is the organic content of the pirated sediment ($\text{gC}/100\text{gSed}$, calculated), $Q_{\text{SOC}_i}^{j-1}$ is the SOC flow rate into a given cell from the cell directly upstream (kg s^{-1}), $Q_{\text{SOC OUT}_i}$ is the SOC flow rate out of the conduit reach at the time step (kg s^{-1}), Δt is the time step length (s), $X_{\text{BED} \rightarrow \text{SS}}$ is the mass of bed SOC exchanged with the suspended SOC (kg), and $X_{\text{SS} \rightarrow \text{BED}}$ is the mass of suspended SOC exchanged with bed SOC (kg).

Rearranging equation (40) using the same approach as equation (21) to solve for suspended SOC:

$$SS_{\text{SOC}_i} = \frac{SS_{\text{SOC}_{i-1}} + E_{\text{SOC}_i} - D_{\text{SOC}_i} + P_S Q_{\text{ss pirated}_i} \text{SOC}\%_{\text{pirated}} \Delta t + Q_{\text{SOC}_i}^{j-1} \Delta t + X_{\text{BED} \rightarrow \text{SS}} - X_{\text{SS} \rightarrow \text{BED}}}{1 + \left(\frac{Q_i \Delta t}{V_i} \right)} \quad (41)$$

Sediment organic carbon flux was then calculated as

$$Q_{\text{SOC OUT}_i} = \frac{SS_{\text{SOC}_i}}{V_i} Q_i, \quad (42)$$

The supply of bed sediment organic carbon (S_{SOC_i}) (kg) within the surface fine grain laminae was modeled using a mass balance approach

$$S_{\text{SOC}_i} = S_{\text{SOC}_{i-1}} - E_{\text{SOC}_i} + D_{\text{SOC}_i} - \text{DEC}_{\text{SOC}_i} - X_{\text{BED} \rightarrow \text{SS}} + X_{\text{SS} \rightarrow \text{BED}}, \quad (43)$$

where, $S_{\text{SOC}_{i-1}}$ is the supply of organic carbon from the previous time step (kg), E_{SOC_i} is the mass of eroded carbon attached to eroded SFGL (kg), D_{SOC_i} is the mass of organic carbon deposited out of suspension (kg), and $\text{DEC}_{\text{SOC}_i}$ is the decomposition of organic carbon through microbial respiration from the supply of the bed (kg).

The suspended and bed soil, litter, and algae pools are modeled using equations (41) and (43) for each specific source. Likewise, with erosion, deposition, and fluxes, the percentages and quantities of soil, litter, and algae were budgeted and conserved using the same equations as for the sediment organic carbon. Percentages of organic carbon in the suspended ($OC_{SS}\%$) sediment and bed ($OC_{bed}\%$) were modeled as

$$OC_{SS}\% = \frac{SS_{SOC_i}}{SS_i}, \quad (44)$$

and

$$OC_{bed}\% = \frac{S_{SOC_i}}{S_{sfgl_i}}, \quad (45)$$

The amount of eroded SOC was modeled as

$$E_{SOC_i} = OC_{bed}\% \times E_{sfgl_i}, \quad (46)$$

The amount of deposited SOC was modeled as

$$D_{SOC_i} = OC_{SS}\% \times D_i, \quad (47)$$

The carbon quality of the pirated sediment varied both with source and also with flow intensity and these variations were incorporated within the model. Urban sources in the Cane Run watershed had higher carbon contents than agriculture sources potentially due to storm sewer leaks and failures. Storm intensity had a net decreasing effect on carbon density of sediment due to eroding deeper, recalcitrant sediment from the surface sources. The urban sediment in the watershed had a distinct drop of carbon content when flows in the surface channel exceeded $10 \text{ m}^3 \text{ s}^{-1}$. The SOC percentage of pirated sediment was calculated as

$$SOC\%_{\text{pirated}} = \begin{cases} SOC_{\text{urban}_{\text{low}Q}} * P_{\text{urban}} + SOC_{\text{ag}} * P_{\text{ag}}, & \text{if } Q < 10 \text{ m}^3 \text{ s}^{-1} \\ SOC_{\text{urban}_{\text{high}Q}} * P_{\text{urban}} + SOC_{\text{ag}} * P_{\text{ag}}, & \text{if } Q > 10 \text{ m}^3 \text{ s}^{-1} \end{cases} \quad (48)$$

where, SOC_{urban} is the carbon content from collected urban samples (gC/100gSed), SOC_{ag} is the carbon content from collected agriculture samples (gC/100gSed), P_{urban} is the percentage of land use associated with urban activities, P_{ag} is the percentage of land use associated with agricultural practices, and Q is the stream flow rate ($\text{m}^3 \text{ s}^{-1}$). Percentages of urban and agriculture land use can be found in Table 4-4.

In this study we introduce the concept of suspended and bed sediment mixing with a net-zero effect on erosion-deposition dynamics. The mixing, or exchange, between the suspended and bed sediment incorporates the idea that sediment is continuously mixing as a result of deposition, erosion, and turbulence in the conduit. Although this mixing does not have any effect on the net erosion or deposition, it does affect the carbon content of the material suspended and the material on the bed. The mass of sediment exchanged in a time step (X_i) was modeled by

$$X_i = e_x \cdot SS_i, \quad (49)$$

where, e_x is the exchange rate between the surface and subsurface. Within this exchanged sediment, a portion will be organic carbon. The amount of organic material exchanged to the bed from the suspended sediment was calculated as

$$X_{SS \rightarrow BED} = X_i \cdot OC_{SS}\%, \quad (50)$$

where, $OC_{SS}\%$ is the organic carbon content of the suspended sediment (gC/100gSed). A mass of bed sediment will be swapped with an equal mass of suspended sediment, but with

varying carbon densities. The amount of organic material exchanged from the bed to the suspended sediment was modeled as

$$X_{BED \rightarrow SS} = X_i \cdot OC_{BED} \%, \quad (51)$$

where, $OC_{BED} \%$ is the organic carbon content of the bed sediment (gC/100gSed).

The transformation of the three carbon pools was modeled using a zero-order decomposition function

$$DEC_{SOC_i} = k_{soil} \frac{S_{soil_i}}{S_{sfgl_i}} + k_{litter} \frac{S_{litter_i}}{S_{sfgl_i}} + k_{algae} \frac{S_{algae_i}}{S_{sfgl_i}}, \quad (52)$$

where, k_{soil} is the soil decomposition rate (d^{-1}), S_{soil_i} is the supply of soil organic carbon in the SFGL (kg), S_{sfgl_i} is the supply of the SFGL (kg), k_{litter} is the litter decomposition rate (d^{-1}), S_{litter_i} is the supply of litter organic carbon in the SFGL (kg), k_{algae} is the algae decomposition rate (d^{-1}), and S_{algae_i} is the supply of algal carbon in the SFGL (kg).

4.4.4 Model Inputs and Parameterization

The sediment transport and carbon model was applied to the Cane Run karst system. Turbidity and flow data were collected at 10-15 minute intervals and sediment organic carbon data were collected on a bi-weekly sampling routine. Inputs and parameters are literature derived or specified based on field observations. A list of model inputs and parameters is shown in Table 4-5. Figure 4-11 displays the layout of conduit cells, pirated sediment, and flow within the model. The sediment model for the coupled drainage network was modeled with the Groundwater Station (Cell 10) as the outlet due to the divergence of the surface and subsurface flow and sediment pathways. The carbon model was extended to Royal Spring (Cell 16) because of the feasibility of sample collection and

the inclusion of the entire subsurface karst conduit. There were no suspected additional sediment or carbon sources from the Groundwater Station to Royal Spring which allowed for extension of the model (Figure 4-11).

Conduit bathymetry inputs were estimated using the existing measurements from the karst system. Bathymetry at the Groundwater Station was known from use of multiple qualitative tracer, Doppler sonar, and video techniques. The geometry at other cells was estimated based on model results that showed a net dynamic equilibrium with respect to erosion and deposition (Table 4-3). Frictional losses in the conduit were modeled using a Darcy-Weisbach friction factor calculated from the Energy Equation. Sediment particle size was estimated from collected distributions of sediment from inflowing tributaries. Sediment organic carbon values of the tributaries and outlets were measured using in situ trap samplers (Phillips et al., 2000). The percent algae in the agricultural streams was modeled using a distribution from a nearby agriculturally dominated watershed (Ford et al., 2015). The $\delta^{13}C$ signatures of the soil organic carbon, algal carbon, and litter carbon were identified using published literature by Fox et al. (2010), Ford et al. (2015), and Acton et al. (2013), respectively.

Parameters used for sediment and carbon model calibration were initially based on published literature results and adjusted to reflect the hydro-biogeochemical dynamics of the coupled surface-subsurface watershed. Several tributaries are present in the Cane Run system, and new field measurements as well as literature-reported measurements for the Lexington area were used to produce an empirical model of sediment influx from the tributaries (Coulter et al., 2004; Russo and Fox, 2012). The maximum supply of the SFGL was estimated by assuming that the neutrally buoyant mixture has a bulk density of 1000

kg m⁻³ and that the SFGL reaches a maximum depth of 5 mm (Droppo and Stone, 1994; Stone and Droppo, 1994; Droppo and Amos, 2001). The surface area of the SFGL within the conduit was assumed to blanket the entire bed. The settling velocity of the fine sediment was estimated by solving Stoke's Law iteratively and using the fall velocity of quartz spheres in water nomograph by Rouse (1937). Transport capacity coefficients are empirical and were adjusted as part of the calibration process (Dou, 1974; Ahmadi et al., 2006; Yan et al., 2008; Guy et al., 2009; Madej et al., 2009). Excess shear was parameterized using existing theory for a one-dimensional simplification and relevant empirical literature. The exponent in the erosion equation, b , was assumed to be 1 for all fluvial erosion sources, which agrees with the concept of erosion being a shear driven process and agrees with the assumption of a number of other studies (Hanson and Simon, 2001; Sanford and Maa, 2001; Wynn et al., 2008; Simon et al., 2009). Erodibility and critical shear stress for these equations, a and τ_{cr} , was parameterized uniquely for each erosion source based on literature reported values and equations (Droppo and Amos, 2001; Hanson and Simon, 2001; Sanford and Maa, 2001; Simon and Thomas, 2002; Russo and Fox, 2012). Decomposition rates for fine litter detritus and algae were parameterized based on results from literature (Webster et al., 1999; Six and Jastrow, 2002; Ford and Fox, 2012). The decomposition rate of the soil organic carbon was calibrated based on field samples, lab analysis, and model results. The exchange rate was calibrated as necessary to fit modeled results to collected organic carbon data.

4.4.5 Calibration and Validation

Sediment model calibration and validation was performed by comparing collected suspended sediment data with simulated model results (Figure 4-1). Calibration parameters

for the sediment model included the transport capacity coefficients for low ($C_{t_{low}}$) and high ($C_{t_{high}}$) flows. Modeled and observed sediment fluxes in the conduit at the Groundwater Station were used as the basis for calibrating the transport coefficients. Parameters were estimated initially by values in the literature and then optimized to fit collected sediment concentration (TSS) and flow data. Statistical methods were also applied to calibrate model results with field observations including the coefficient of determination (R^2) and the Nash-Sutcliffe efficiency (Nash and Sutcliffe, 1970). The statistics were applied to the measured vs modeled sediment fluxes at the prescribed model time step rather than time-integrated sediment yields providing for a more robust analysis of model performance. The sediment model calibration time period spanned 7 months (10/2011 – 05/2012) and the sediment model validation time period spanned 3 months (02/2013 – 05/2013).

Sediment organic carbon model calibration and validation was performed by comparing collected SOC data with model carbon results (Figure 4-1). Calibration parameters for the carbon model included the decomposition rate of soil organic carbon (k_{soil}) and the sediment exchange rate (e_x). The carbon model was calibrated so that the mean of the modeled SOC results matched the mean of the collected SOC samples from Royal Spring. The carbon model calibration time period spanned 5 months (12/2012 – 04/2013) and included 12 time-integrated SOC samples. The sediment model validation time period spanned 3 ½ months (04/2013 – 08/2013) and included 6 time-integrated SOC samples.

For surface flow and sediment models, Donigan (2000) has recommended guidelines for calibration of the Nash-Sutcliffe efficiency; however, this model was applied

to a subsurface karst sediment transport model and the guidelines by Donigian were used as a general benchmark for model performance. The guidelines in Moriasi et al. (2007) state that Nash-Sutcliffe efficiency values between 0.0 and 1.0 are generally viewed as acceptable levels of performance. ASCE (1993) suggests the use of the Nash-Sutcliffe coefficient and it has become widely used in the field allowing for comparison of values between research studies. The Nash-Sutcliffe coefficient (E_{NS}) was calculated as follows

$$E_{NS} = 1 - \frac{\sum_{i=1}^n (Q_{data_i} - Q_{model_i})^2}{\sum_{i=1}^n (Q_{data_i} - \bar{Q}_{data})^2}, \quad (53)$$

Q_{model_i} is the modeled sediment discharge (kg s^{-1}), Q_{data_i} is the observed sediment discharge from data (kg s^{-1}), and \bar{Q}_{data} is the average observed sediment discharge (kg s^{-1}). E_{NS} compares the variance between the observed values and the modeled values in the numerator and the variance between the observed values and the average observed value of the dataset in the denominator. Nash-Sutcliffe values closer to an efficiency of 1 indicate a near-perfect match of modeled to observed data. An efficiency of 0 indicates that a model is as accurate as the average observed value with regards to predicting future values. Efficiencies less than one indicate that a model is less accurate than using the average observed value as a prediction tool.

4.4.6 Sensitivity and Uncertainty Analysis

Model sensitivity was performed for a number of model parameters such as the transport coefficients, settling depth coefficient, exchange rate, decomposition rates, and source critical shear stresses. Initial conditions for the model's calibration parameters were based on values found in the literature (Table 4-5). These parameters were then varied individually through a range of values and the effects on net erosion-deposition, sediment

yield, and carbon content were monitored to see which parameters had the greatest effect on results and in turn were the most sensitive. Parameters were varied from their minimum value in literature, their median value in literature, and their maximum value in literature. The relative change on the results was also investigated.

A number of parameters and inputs possessed statistical variability and uncertainty that was incorporated into the model. After a sufficient number of field data were collected, probability density functions were fit to observed statistical distributions. Applying uncertainty allowed the model to incorporate the natural variability of many inputs and parameters as well as more accurately representing the stochastic nature of some physical and biogeochemical processes. Descriptive statistics such as mean and standard deviation, were estimated using data collected from the field and literature-based results. For example, the $\delta^{13}C$ isotopic ratio for the algal source would be modeled as

$$D(X_{alg}) \rightarrow N(\mu_{alg}, \sigma_{alg}^2), \quad (54)$$

where, X_{alg} is the distribution of the mean, μ_{alg} is the mean of the source population, and σ_{alg}^2 is the variance of the source population. The mean and standard deviations of the carbon and isotopic signature inputs to the model are shown in Table 4-6. The two tributary sources locations, Urban Trib and Ag Trib, were subdivided into three separate carbon pools: soil, litter, and algae. Each carbon pool had its own mean and standard deviation for the $\delta^{13}C$ signature based off of reported values in the literature (Fox et al., 2010; Acton et al., 2013; Ford et al., 2015). The isotopic signature and organic content of the bulk samples from Urban Trib and Ag Trib were collected from field and lab methods.

Randomization of carbon source inputs was performed using Monte-Carlo simulations. Sediment source fingerprinting was applied by taking sediment from the outlet of a system and estimating the contribution of each source to the total amount at the outlet. 10,000 realizations were performed for each of the eight different fixed percent algae (P_{algae}) values (0, 5, 10, 15, 17.81, 20, 30, and 40%). Each realization was independent of the prior and the inputs to the model were randomly selected from their respective distributions. The use of an uncertainty analysis also allowed error bounds to be placed on results.

4.4.7 High Performance Computing

Simulation of the coupled sediment and carbon model over the two year investigation period required extensive computational resources. Numerical modeling and statistical analysis was performed using the University of Kentucky's Lipscomb High Performance Computing Cluster. The cluster is rated at over 140 teraflops including all CPUs and GPUs. The system allows for batch scripting and the allocation of individual processors to serial jobs for solving several realizations of the model concurrently thus reducing computation time. In this study, 10,000 total realizations of the model were performed over 16 different processing cores which reduced the computational time by hundreds of hours.

Table 4-1: Flow rate relationships between stream gages in Cane Run Watershed

Site Relationship*	Equation	R ²
Berea Road → Lexmark	$Q_{LEX} = 0.28 \cdot Q_{BER} + 2.72$	0.78
Berea Road → Spindletop	$Q_{SPIN} = 0.26 \cdot Q_{BER} - 1.10$	0.94
Berea Road → Lisle Road	$Q_{LISLE} = 0.62 \cdot Q_{BER} + 2.50$	0.89
Citation Blvd → Lexmark	$Q_{LEX} = 0.72 \cdot Q_{CIT} + 0.79$	0.91
Citation Blvd → Spindletop	$Q_{SPIN} = 0.33 \cdot Q_{CIT} - 0.75$	0.69
Citation Blvd → Lisle Road	$Q_{LISLE} = 1.12 \cdot Q_{CIT} - 0.65$	0.73

*Lexmark is “Urban Trib”, Spindletop is “Ag Trib”, Lisle Road is “Surface Outflow”, Citation Blvd and Berea Road are other stream gages along the main Cane Run Creek channel used to fill in missing data at Urban Trib, Ag Trib, and Surface Outflow.

Table 4-2: Relationships between sediment concentration, C_{SS} , and stream flow rate, Q

Site	Equation	R ²
Urban Trib	$C_{SS} = 73.7(0.8(1.3) + 0.2(0.75))[37,495(1 - e^{-1.9 \times 10^{-5}Q})] - 4.2$	0.48
Ag Trib	$C_{SS} = 0.5(0.2(1.3) + 0.8(0.75))[275(1 - e^{-0.75Q})] + 21.1$	0.55

Table 4-3: Conduit Bathymetry, Q_{ss} Inflow, and Land Use Information for Model Cells

Cell*	Height (m)	Width (m)	Surface Area (m ²)	Swallet Density (%)	Urban Land-use (%)	Ag Land-use (%)
1	0.833	5.754	5754	9	80	20
2	0.840	5.805	5805	6	80	20
3	0.848	5.857	5857	11	70	30
4	0.855	5.909	5909	10	60	40
5	0.863	5.961	5961	7	50	50
6	0.870	6.013	6013	6	40	60
7	0.878	6.065	6065	10	30	70
8	0.900	6.220	6220	14	20	80
9	0.900	6.220	6220	12	10	90
10	0.900	6.220	6220	15	0	100
11	0.900	6.220	6220	No surface sediment diverted to the conduit in Cells 11 – 16		
12	0.900	6.220	6220			
13	0.900	6.220	6220			
14	0.900	6.220	6220			
15	0.900	6.220	6220			
16	0.900	6.220	6220			

*Refers to the spatial cell within the conduit as seen on Figure 4-11.

Table 4-4: Un-mixing Results for Means of Data Inputs using Carbon Stable Isotope

URBAN		
	Fraction (%)	$\delta^{13}C$ (‰)
Soil	48.4	-25.0
Litter	51.6	-27.6
Algae	0.0	-37.7
AGRICULTURAL		
	Fraction (%)	$\delta^{13}C$ (‰)
Soil	72.7	-25.0
Algae	17.8	-37.7
Litter	9.5	-27.6

Table 4-5: Inputs and parameter values for sediment transport model

Symbol	Description	Value	Unit
L	Channel length	1×10^4	m
D	Equivalent diameter of conduit	2.13	m
Δt	Temporal step	3600	s
f	Darcy friction factor	0.422	unitless
k_p	Settling depth coefficient	0.5	unitless
$Q_{boundary}$	Boundary between low and high flows	1	$m^3 s^{-1}$
d_{sfgl}	Initial depth of SFGL sediment in the conduit	0.003	m
$d_{sfgl_{max}}$	Maximum depth of SFGL sediment	0.005	m
S_{bed}	Initial supply of bed sediments in the conduit	5.4×10^{-6}	kg
ρ_{water}	Density of fluid	1×10^3	$kg m^{-3}$
ρ_{sfgl}	Bulk density of SFGL sediments	1×10^3	$kg m^{-3}$
ρ_{bed}	Bulk density of bed sediments	1.5×10^3	$kg m^{-3}$
ω_s	Mean settling velocity of suspended material	8×10^{-5}	$m s^{-1}$
$C_{tc_{low}}$	Transport capacity coefficient for low flows	2.28×10^{-5}	$m^{1/2} \cdot s^2 kg^{-1/2}$
$C_{tc_{high}}$	Transport capacity coefficient for high flows	1.77×10^{-6}	$m^{1/2} \cdot s^2 kg^{-1/2}$
SS_0	Initial suspended sediment	0	kg
$\tau_{cr_{sfgl}}$	Critical shear of the SFGL source	0.05	Pa
$\tau_{cr_{bed}}$	Critical shear of the bed source	1	Pa
b_{sfgl}	Erodibility exponent of the SFGL source	1	unitless
b_{bed}	Erodibility exponent of the bed source	1	unitless
a_{sfgl}	Erodibility of the SFGL source	8.94×10^{-4}	$kg Pa^{-1} m^{-2} s^{-1}$
a_{bed}	Erodibility of the bed source	2.12×10^{-4}	$kg Pa^{-1} m^{-2} s^{-1}$
$SOC_{urban_{low}}$	Carbon content of urban sediment (low flows)	5.83	gC/100gSed
$SOC_{urban_{high}}$	Carbon content of urban sediment (high flows)	4.37	gC/100gSed
SOC_{ag}	Carbon content of agriculture sediment	3.83	gC/100gSed
e_x	Exchange rate for sediment mixing	0.025	unitless
k_{soil}	Decomposition rate of soil carbon	-1.0×10^{-4}	d^{-1}
k_{litter}	Decomposition rate of litter carbon	-1.3×10^{-3}	d^{-1}
k_{algae}	Decomposition rate of algal carbon	-1.3×10^{-3}	d^{-1}

Table 4-6: Carbon and $\delta^{13}C$ Uncertainty Analysis Inputs

Sampling Site		$\delta^{13}C$ (‰)	SOC (%)
Lexmark (Urban Trib)	Mean	-26.36	5.70
	Std Dev	0.67	1.07
Spindletop (Ag Trib)	Mean	-27.51	3.83
	Std Dev	0.44	0.26
Conduit (Groundwater Station)	Mean	-26.61	3.35
	Std Dev	0.86	0.60
Carbon Pool		$\delta^{13}C$	
Soil	Mean	-25.00	
	Std Dev	0.64	
Litter	Mean	-27.63	
	Std Dev	0.54	
Algae	Mean	-37.71	
	Std Dev	5.51	
Percent Algae, P_{algae}			
0, 5, 10, 15, 20, 30, 40			

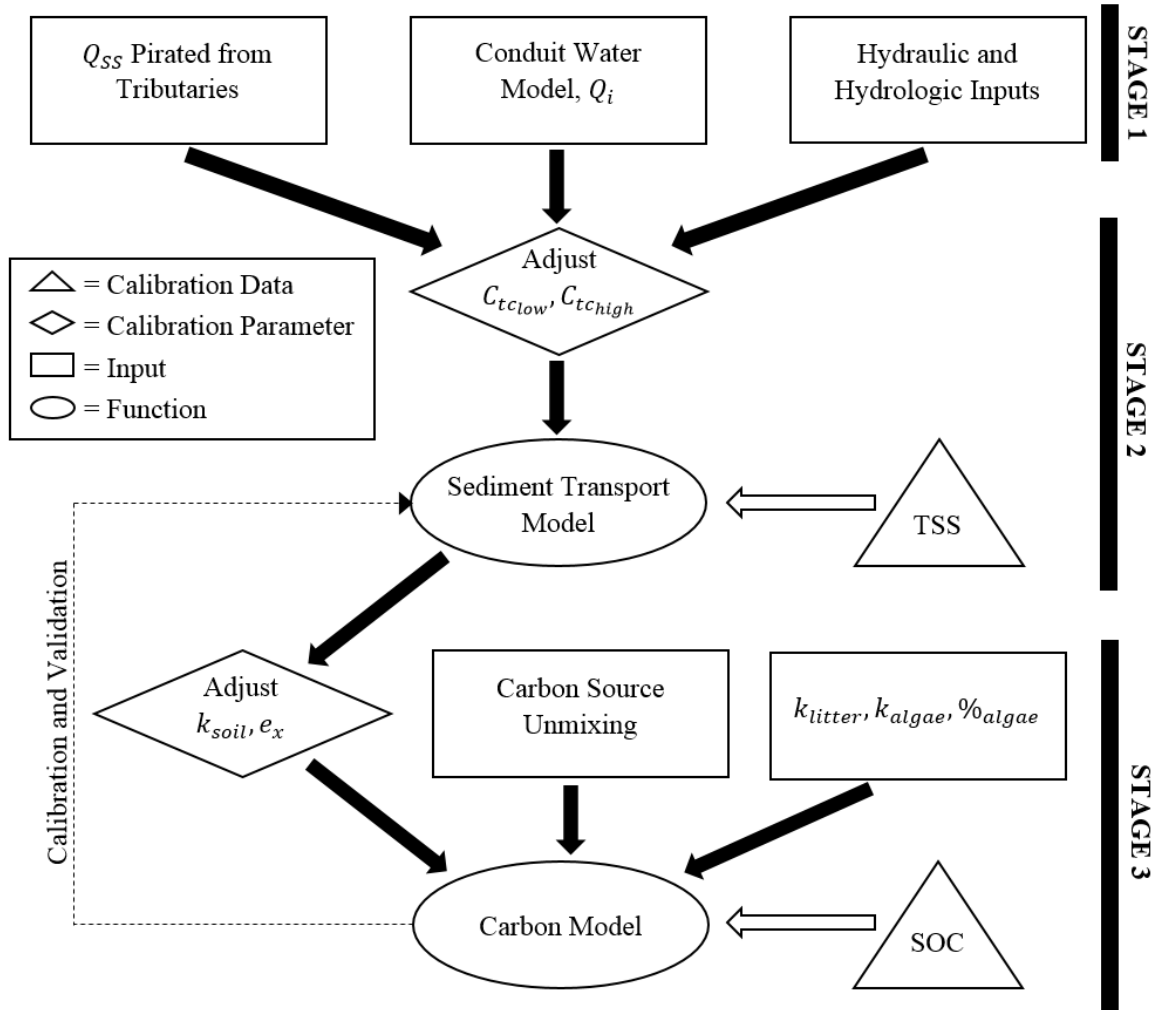


Figure 4-1: Fluviokarst Sediment and Carbon Transport Calibration Method. STAGE 1: model preparation. Sediment pirated from tributaries (Q_{SS}), conduit flow rate (Q_i), and hydraulic and hydrologic inputs were supplied to the Sediment Transport Model. STAGE 2: sediment calibration. Transport coefficients (C_{tc}) are adjusted so that model results reflect TSS data. STAGE 3: carbon calibration. Sediment transport model results, carbon source unmixing, decomposition rates (k), and percent algae ($\%_{algae}$) were used as inputs to the Carbon Model which was calibrated by adjusting the soil decomposition rate (k_{soil}) and sediment exchange rate (e_x) to reflect SOC data.

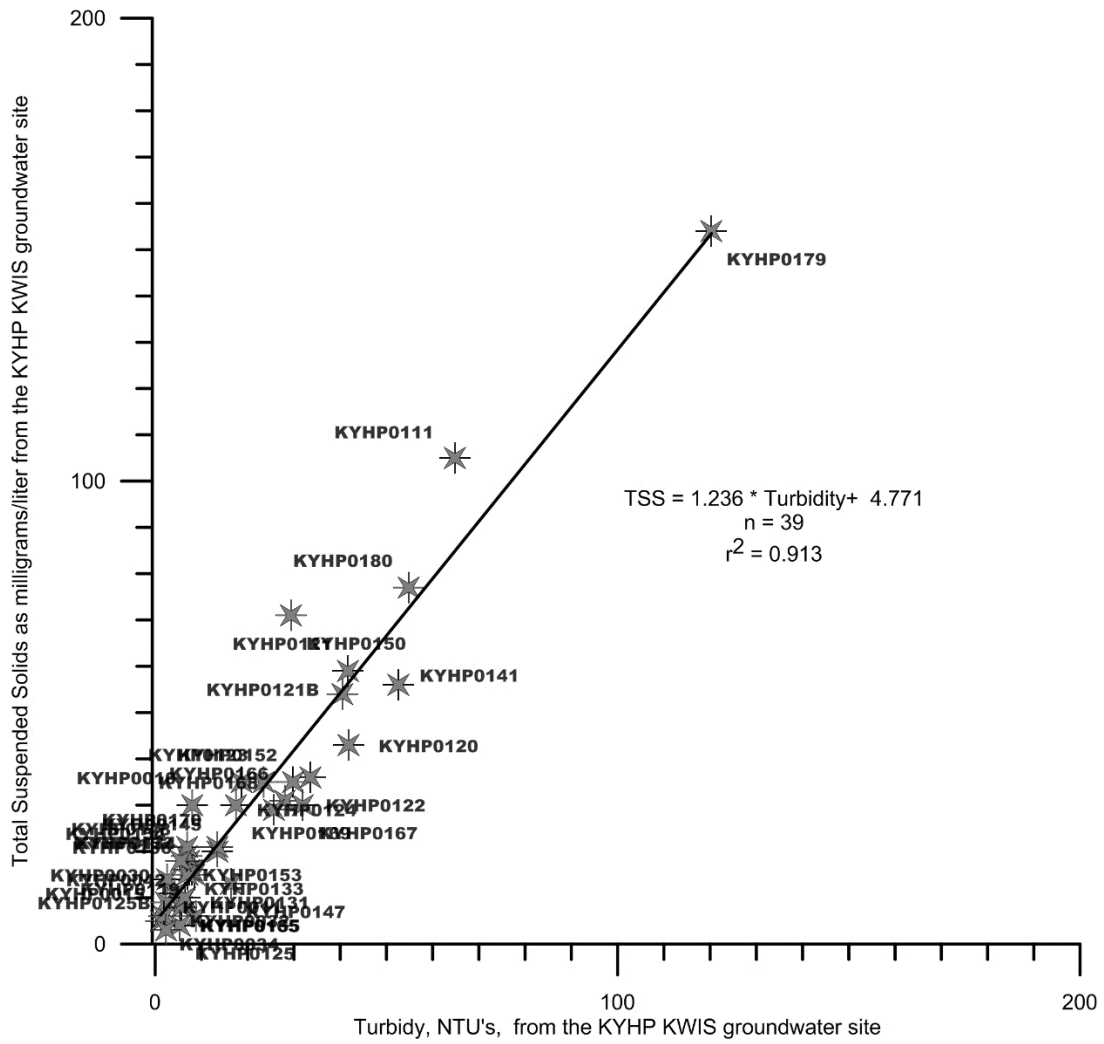


Figure 4-2: TSS vs Turbidity Relationship for Groundwater Station Samples

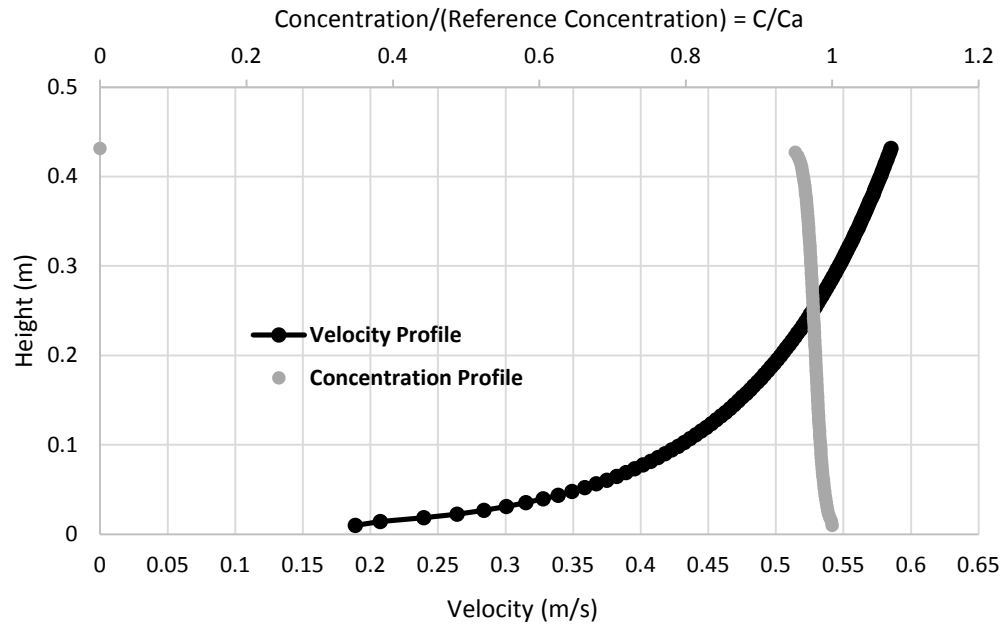


Figure 4-3: Velocity and Concentration Profiles in Surface Streams

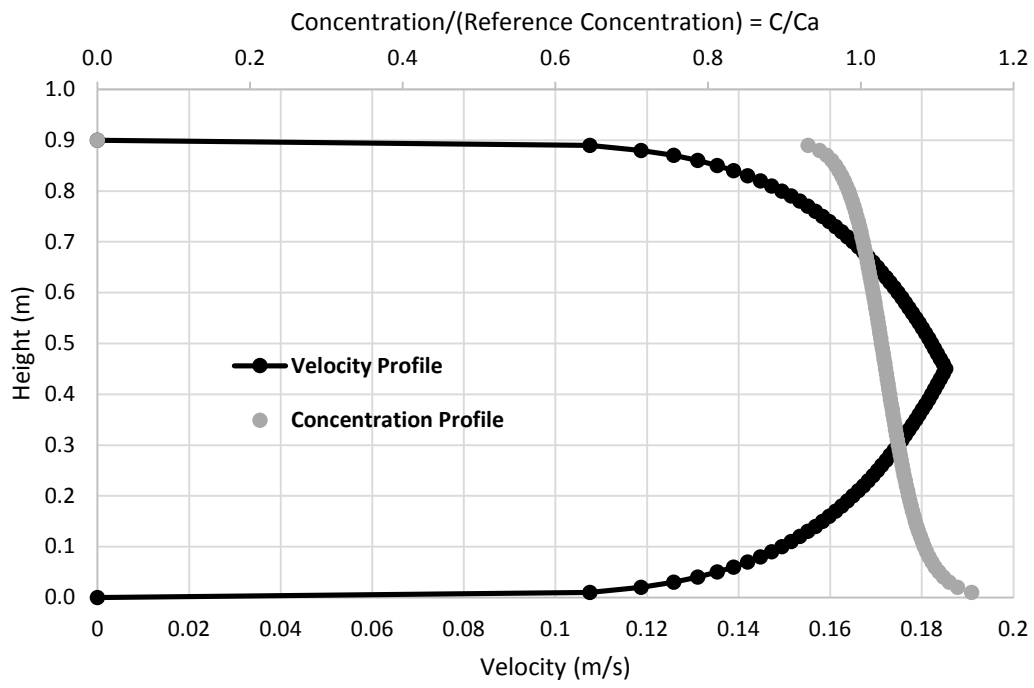


Figure 4-4: Velocity and Concentration Profiles in Karst Conduit

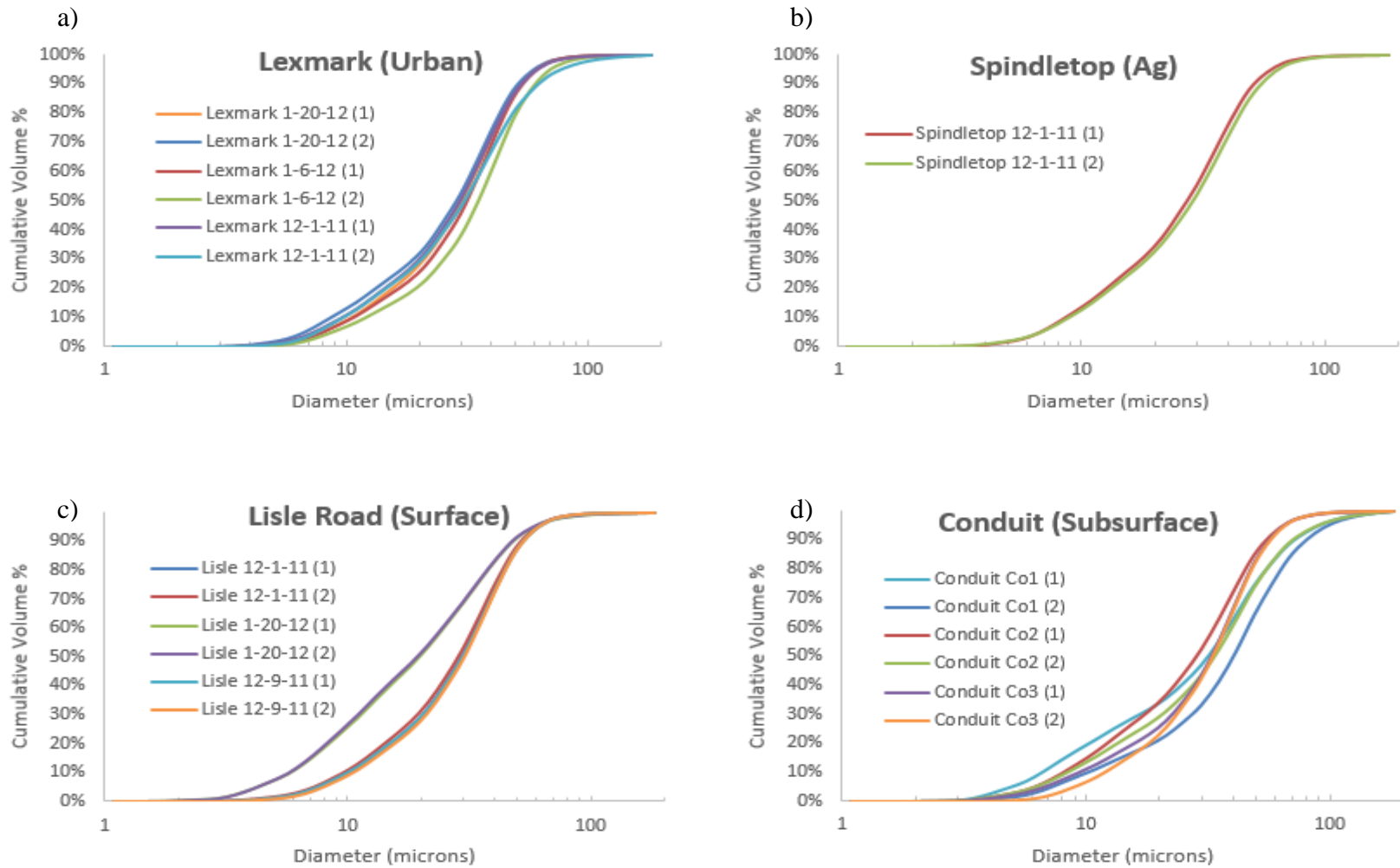


Figure 4-5: Particle Size Distributions a) urban tributary, b) agriculture tributary, c) surface outflow, d) subsurface outflow. (1) and (2) indicates multiple samples taken on same date.

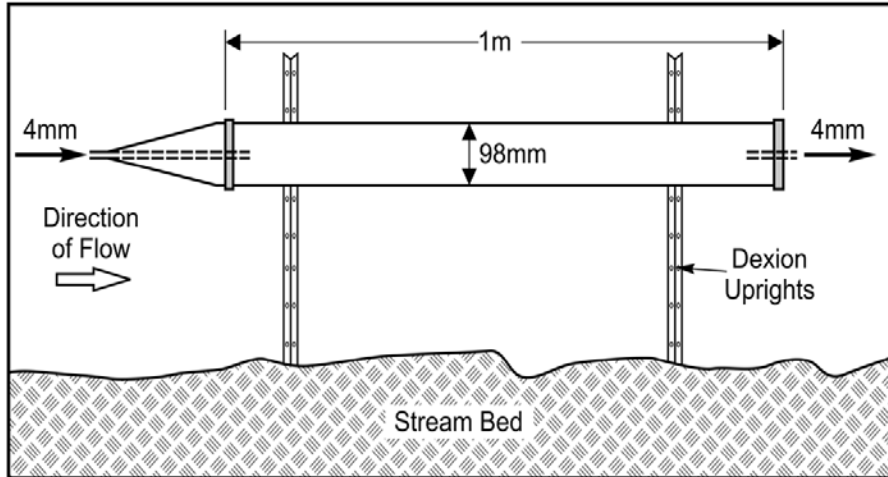


Figure 4-6: Sediment Trap Sampler (Phillips et al., 2000)

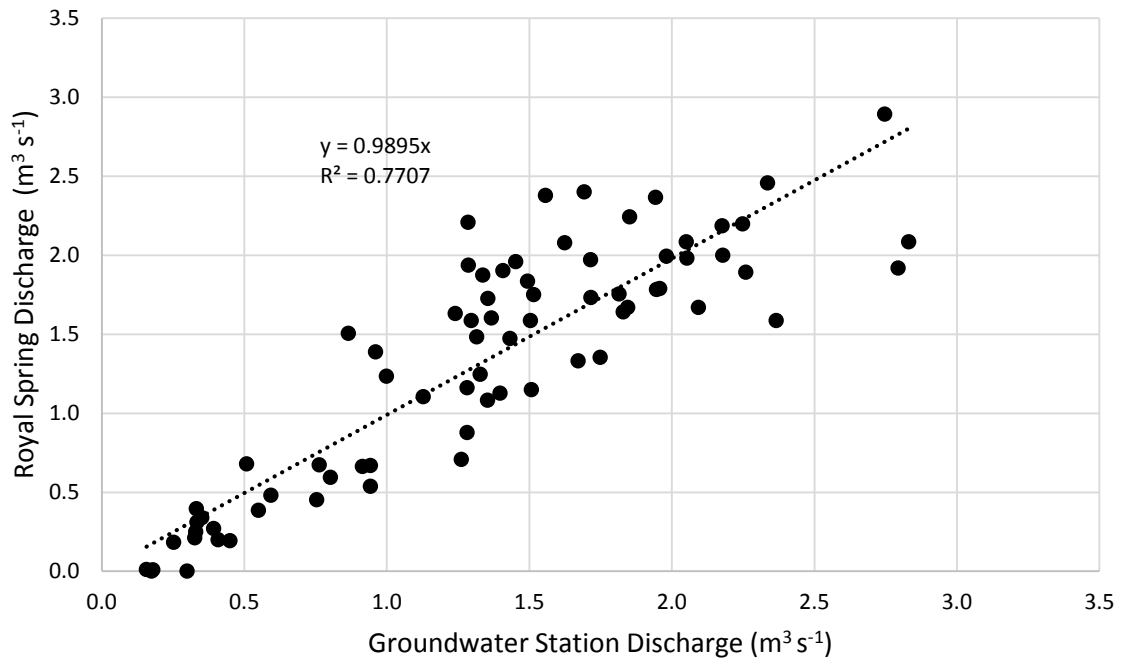


Figure 4-7: Weekly Max Flows Royal Spring vs Conduit (Groundwater Station)

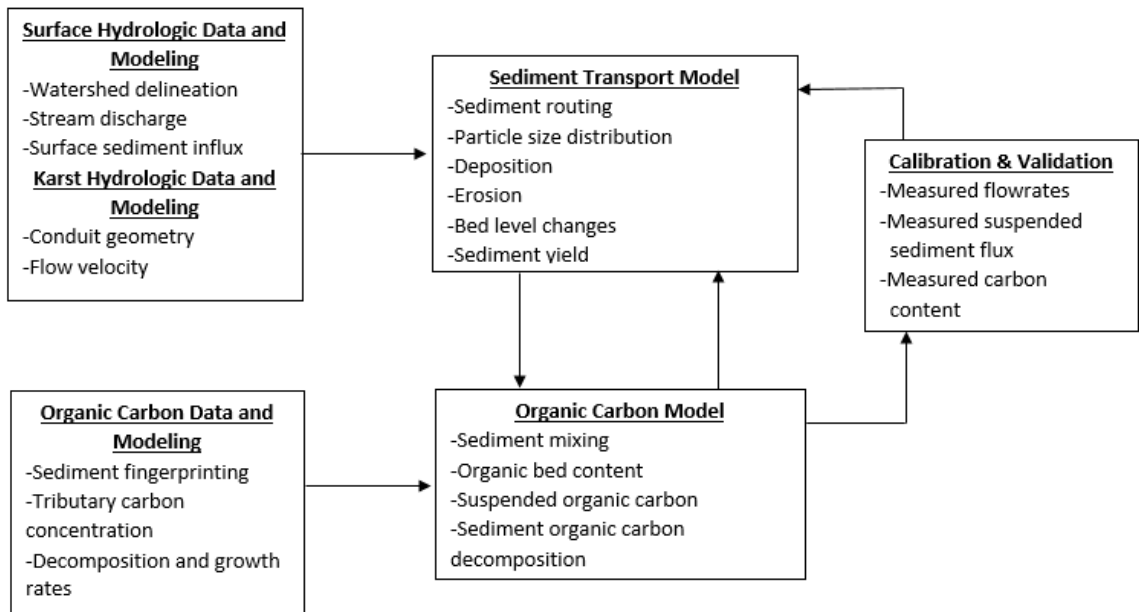


Figure 4-8: Modeling Framework for Coupled Surface-Subsurface Model

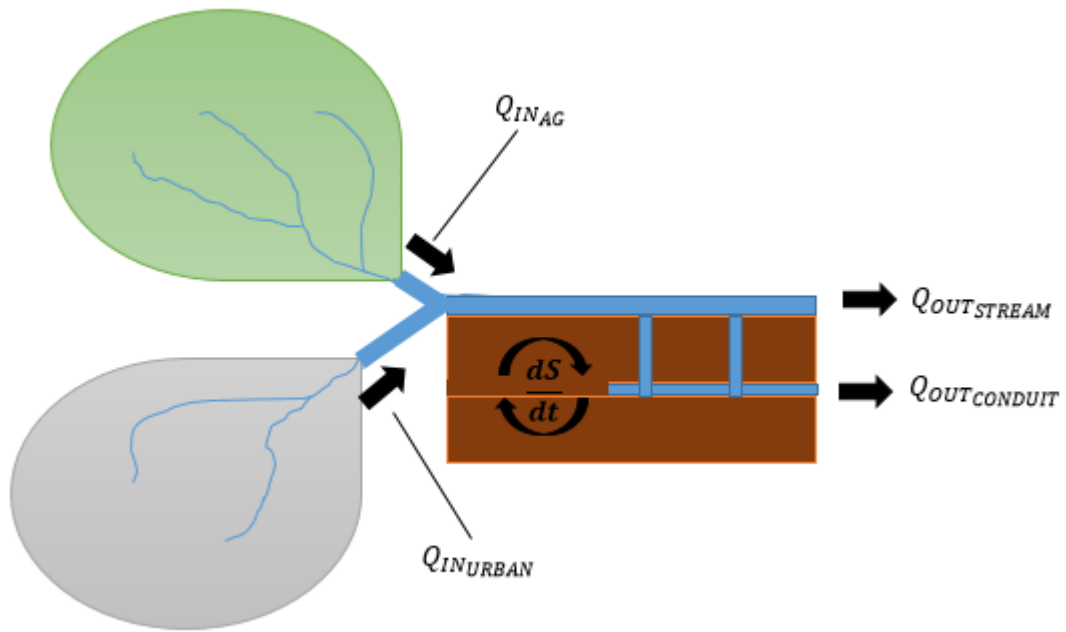


Figure 4-9: Conceptual Water Budget for Coupled Drainage Network

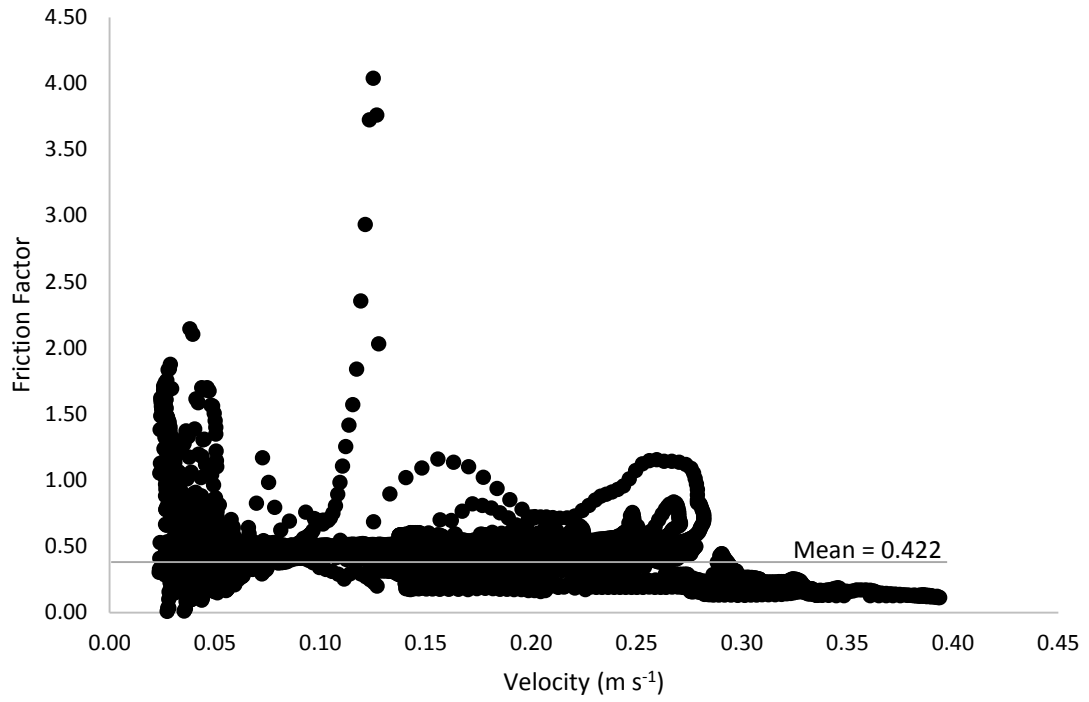


Figure 4-10: Friction Factor vs Conduit Velocity

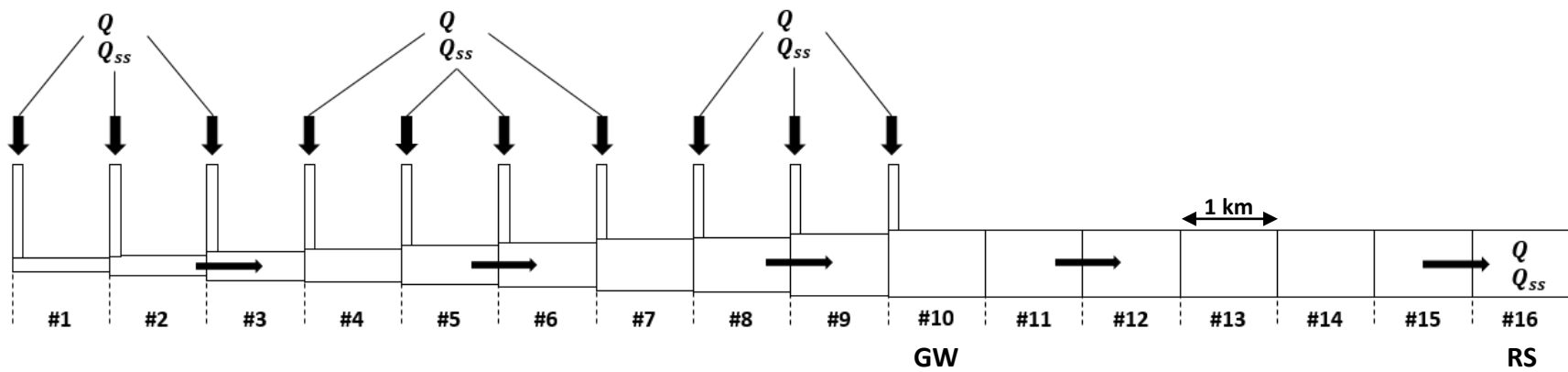


Figure 4-11: Flow and Sediment into Subsurface Conduit Conceptualization (GW = Groundwater Station, RS = Royal Spring).

66

Conduit geometry increases from Cell 1 – 10 then remains constant from Cell 10 – 16.

Chapter 5 Results

5.1 Model Evaluation

5.1.1 Water

Water flow rates within the coupled surface-subsurface drainage network were monitored over a two year period at inflow and outflow locations (see Fig 3-1). The difference between the upscaled inflows from the tributaries and the outflows from the surface channel and subsurface conduit over the model period was 4.48%. The data-driven results of water flowrates show that the upscaled inflows to the system nearly equal the surface and subsurface outflows supports the choice of the streams selected as representative tributaries. In addition, the data results reinforce the idea that Royal Spring is a mature hydro-geomorphologic system dominated by low storage, high transmissivity conduits. Mature karst systems are characterized by well-developed conduit networks that transport flow at speeds that are orders of magnitude greater than porous media flow or fracture matrix flow (Clemens et al., 1997; Waltham and Fookes, 2003).

5.1.2 Sediment

The results of the sediment transport model for the calibration and validation periods are shown in Figure 5-1. The model tended to underestimate the initial sediment peak during hydrologic events. Baseflow conditions were reflected well in the model suggesting that the low flow transport capacity coefficient represented the sediment transport dynamics in the conduit adequately. The fit for the validation time period is closer than that of the calibration period as the Nash-Sutcliffe efficiency for the calibration and validation periods is 0.45 and 0.62, respectively. The coefficient of determination for the calibration and validation periods is 0.50 and 0.54, respectively. The R^2 and Nash-

Sutcliffe efficiencies for calibration and validation perform satisfactorily when compared to other literature particularly when considering that most calibration is done on daily and monthly time steps (Moriassi et al., 2007). For the current study, the time step used was one hour. Yuan et al. (2001) showed that statistical evaluation values perform worse as time steps are shortened.

A sensitivity analysis was performed on the sediment transport model to evaluate how model parameters effect the sediment yield out of the watershed. Figure 5-2 shows a graph of parameter sensitivity and change in sediment yield. Table 5-1 gives exact values of minimum, optimal, and maximum parameter values as well as percent change in sediment yield with the corresponding value used in the calculation. The minimum and maximum values are literature derived and the optimal values are those calibrated to the model. The transport coefficients and the settling depth coefficient were the sensitive parameters in this study. The sensitivity of transport coefficients has been recognized in other fine sediment models (Russo and Fox, 2012).

5.1.3 Sediment Organic Carbon

As mentioned in the methods, calibration of the sediment carbon model was performed through adjustment of decomposition and sediment exchange rates. Calibrated model results showed that the decomposition rate of soil was one order of magnitude smaller than that of the algal and litter carbon pools ($k_{soil} = 0.0001 \text{ d}^{-1}$) (Table 5-2), but very near the maximum end of soil decomposition rates published in other studies (Alvarez and Guerrero, 2000; Ford and Fox, 2012). Calibrated model results show that the amount of sediment in suspension within the conduit that is exchanged with bed sediment at any given time step is 2.5%. The effect of this carbon exchange was realized through the

variation in exported carbon flux by altering the carbon density of suspended sediments without changing the mass of sediment discharged.

Figure 5-3 shows calibration and validation results of the sediment carbon model and the measured sediment carbon results at the subsurface conduit springhead. The time series shows that all but one of the collected samples falls within range of the modeled results. The means of the modeled and measured data were used as a calibration goal due to the high variability and uncertainty related to carbon data. The mean sediment carbon density of the measured data for the calibration period was 3.36%. The results for the modeled sediment carbon mean were 3.36%. The range of SOC measured values was [2.45%, 4.15%] whereas the range of the modeled values was [2.88%, 3.77%]. For the validation period the measured mean of the sediment carbon data was 3.31% and the modeled mean was 3.65%. The range of SOC measured values during the validation period was [2.21%, 4.10%] whereas the range of the modeled values was [3.42%, 4.03%]. Results show that the sediment carbon data bounds the model results well suggesting confidence that the mean behavior of the physical and biological processes in the karst conduit are represented by the model. For a number of occurrences, the sediment carbon model under predicts the range of variability exhibited by the sediment carbon data results (see Fig 5-3) reflecting the mean representation of erosion and decomposition in the model (e.g., constant rates over grid cells that are approximately one kilometer in length). For example, it is realized that fluvial sediment carbon data can be highly variable (Ford et al., 2015) reflecting episodic transport of eroded sediment (Fox and Papanicolaou, 2008) and the spatial variability of decomposition hot spots in fluvial systems (Battin et al., 2003). Nevertheless, the fact that the data range is on the same order as the model results adds

confidence to the results and highlights that the model is able to reflect the mixing of new sediment carbon transported to the subsurface and resuspended sediment carbon that was temporarily stored in the bed.

Table 5-2 and Figure 5-4 display the parameter sensitivity and change in average suspended sediment organic carbon content. The minimum and maximum parameter values are literature derived, when applicable, and the optimal values are those calibrated to the model. The carbon model was not overly sensitive to any of the five parameters tested. The most sensitive parameters were the litter decomposition rate and the exchange rate. The litter decomposition rate showed sensitivity because of the high contribution of litter carbon to the system and the relatively high rate of decomposition of litter compared to the other large carbon source, soil. The sensitivity in the exchange rate was manifested in the overall carbon content of the conduit bed being increased with an increase in exchange rate. In this manner, a more thorough mixing of suspended and bed sediment occurs which has the result of dampening the “flush” effect of incoming surface sediment being immediately discharged through the conduit without adequate mixing. The low variability in the organic content of suspended sediment within the conduit was a result of two processes: 1) similar decomposition rates for autochthonous and litter carbon and 2) the soil organic carbon contribution remaining relatively stable regardless of percent algae in agricultural streams

5.1.4 Sensitivity of P_{algae}

During the sensitivity analysis of the sediment carbon sub-model, the model input P_{algae} was also varied due to our lack of certainty with respect to this input and due to the fact that adjustment of P_{algae} in turn impacted the isotope un-mixing analysis for tributary

sources. Table 5-3 provides the Monte Carlo simulation results for the carbon un-mixing process at seven fixed algae percentages. Litter and algae percent contributions in the agricultural network are inversely proportional with percent litter carbon decreasing with rising percent algae. Soil carbon percent has a non-linear relationship with percent algae when considering agriculture sources. Figure 5-5 also displays how the percent of algae in transported sediment carbon affects source contribution from the three carbon pools. The variation in the urban soil and litter source contributions can be explained by the fact that the random draw for the $\delta^{13}C$ signature of algae can potentially make the solution matrix non-converging thus requiring another draw that would slightly change the modeled mean and standard deviation from their respective sources. However, in urban soil, this difference was less than 5% over a 40% range of percent algae.

Table 5-4 provides the uncertainty results for the sediment carbon samples collected during the validation and calibration time periods. The modeled results show very little variation in the carbon content of suspended sediment. The low variability is attributed to the surface sediment thoroughly mixing with conduit bed sediment before discharging at the springhead.

5.2 Temporal and Spatial Distributions of Water, Sediment, and Sediment Carbon

5.2.1 Water

Figure 5-6a and 5-6b displays the water inflows into the fluvial system from both the urban tributary and the agricultural tributary. The urban tributary has greater peaks and was generally much more active throughout the two year period. The peak flow for the urban tributary during the monitoring period was $25 \text{ m}^3 \text{ s}^{-1}$ in July 2013. The urban tributary

was more active due to the high percentage of impervious areas contributing runoff from downtown Lexington. The agriculture tributary had relatively low flows attributed to reduced runoff primarily due to the infiltration of rainfall into the soil and epikarst.

The surface and subsurface outflows from the system are shown in Figure 5-6c and 5-6d. The surface stream outlet of the drainage network had a similar behavior to that of the tributaries in that it was activated primarily during hydrologic events and had relatively short-lived hydrographs due to karst features pirating streamflow. Peak stormflow in the surface streams during large hydrologic events can often times be orders of magnitude greater than baseflow, which is consistent with surface stream hydrology (Gupta, 2008, p. 349). The contrasting data from the phreatic karst conduit shows that there was sustained, year round flow at the conduit. Peak flows in the conduit are much more limited in their extremes and the variability of flow in the conduit was low relative to the surface streams. Flow rate in the surface stream was highly variable and ranges from 0 to $25 \text{ m}^3 \text{ s}^{-1}$ while flow in the conduit never exceeds $3 \text{ m}^3 \text{ s}^{-1}$. These results are due to a subsurface hydraulic dam near the primary springhead that constrains the maximum water conveyance of the conduit. The primary springhead allowing flow out of the conduit is 6.5 meters above the minimum conduit elevation. Well stage data from the subsurface conduit and surrounding karst aquifer shows that during very low flow conditions (conduit velocity ≈ 0) the conduit remains entirely phreatic (see Figure 5-7). The mean conduit velocity was $0.124 (\pm 0.110) \text{ m s}^{-1}$.

5.2.2 Sediment

Figure 5-8 provides the suspended sediment discharge for the urban and agricultural tributaries feeding into the fluviokarst network. Sediment flux in urban streams was almost

always greater than the corresponding flux in agricultural tributaries. The prevalence of impermeable surfaces near heavily-urbanized Lexington, KY results attributes to the observed high flows and erosion rates (Hollis, 1975; Konrad, 2003). High infiltration rates and vegetative cover provided protection for agricultural sediment and in turn reduce erosion and sediment flux (El-Swaify, 1994).

Figure 5-9 shows the modeled suspended sediment flux out of the system by the subsurface karst conduit. Results from the collected sediment data in the conduit are in contrast with that of the surface streams. The peak sediment discharge within the conduit was 0.21 kg s^{-1} , two orders of magnitude smaller than the urban surface tributary sediment discharge of 29.73 kg s^{-1} . Unlike sediment concentration peaks in surface streams, which are caused by the perturbation of undisturbed sediment and occur prior to the peak of the storm flow hydrograph (Bača, 2008), data results show that turbidity spikes in the subsurface are maintained for longer durations and last through the peak of a hydrologic event. Sustained sediment concentration results in high yields of sediment and is attributed to both the perturbation of latent conduit bed sediment and the introduction of pirated surface sediment. Additionally, during baseflow conditions when the surface channel runs dry, water in the subsurface conduit continues to erode conduit bed material and export sediment from the coupled drainage network.

The spatial evolution of the conduit bed is shown in Figure 5-10. Bed depths were modeled throughout the entire longitudinal extent of the conduit and four locations are presented in the figure to show the changing dynamics of the subsurface. Cells 4, 8, and 12 were responsive to individual storm events with significant deposition or erosion occurring depending on factors such as cell geometry, flow rate, and suspended sediment influx. Cell

16 (the conduit outlet) is located at the outlet of the conveyor belt portion of the conduit and shows little variability in bed depth indicating that storm-derived surface sediment is trapped in the subsurface and gradually exported.

5.2.3 Sediment Organic Carbon

Sediment carbon yield at the springhead tends to be fairly constant in part due to the phreatic nature of the karst conduit which provides continuous flow for most of the two year period allowing for erosion and transport processes to occur in the subsurface (Figure 5-11). The shape of the sediment organic carbon flux very closely resembles that of the suspended sediment discharge and contains peaks during storms and subsequent smaller loads during baseflow.

Urban and agriculture tributary data averaged $4.77 (\pm 1.24)$ gC 100g^{-1} sediment while the downstream subsurface conduit averaged $3.35 (\pm 0.53)$ gC 100g^{-1} sediment. Modeling results show that the average carbon content of suspended sediments exported out of the subsurface karst network, over the two year period, was $3.32 (\pm 0.43)$ gC 100g^{-1} . The carbon density differences are worthy of note given that temporary storage of sediment in the drainage network results in a decrease in sediment stored carbon. The inflow and outflow differences in the carbon data and model results are attributed to the decomposition process. Sediment organic carbon becomes temporarily trapped in the subsurface due to the limited transport capabilities of the karst conduit. During this temporary fate, it is plausible that heterotrophic bacteria oxidize the organic carbon associated with fine sediment and respire carbon dioxide (CO_2). During transport within the phreatic conduit, data results show that nearly 30% of the sediment organic carbon was lost while modeling results during the same time period show a loss of 27%.

A further inspection of the suspended and bed organic carbon contents shows the dynamics and biologic processes in the subsurface conduit. Figure 5-12 shows the changes in organic carbon in the suspended and bed sediment at the Groundwater Station. Initially carbon rich sediment was pirated from the surface and injected into the subsurface conduit causing a rise in carbon content of the suspended sediment within the conduit. After deposition and mixing the suspended sediment percentage slowly decreases until it was in near equilibrium with the carbon content of the bed.

Figure 5-13 shows the composition of the Groundwater Station conduit bed with respect to how the fraction of each carbon pool changes with time. Soil organic carbon dominates the location due to the slow decomposition rate of the recalcitrant carbon and also because of the large soil source from both urban and agricultural lands. Figure 5-14 shows the fractioning of the suspended SOC at Royal Spring between the three carbon sources. The proportions of each source in the suspended sediment slurry can vary greatly, but tend to approach a mean which is representative of the results from the un-mixing process. An 8 month dry period centered in the middle of the investigation period had low carbon yields. However, during this dry period the subsurface conduit was biologically active and turned over organic carbon and maintained a steady flux of CO₂ production (Figure 5-15).

5.3 Long-term Budgets of Water, Sediment, and Sediment Carbon

5.3.1 Water

The water budget for the two year period shows that there was a near-equilibrium in the water mass balance of the system (Figure 5-16). The water budget for the fluviokarst

watershed was closed to within 4.48%. During hydrologic events, the karst aquifer (e.g. the epikarst, matrix, fractures, and conduits) fills up and drains water in a multi-stage process with different conveyance rates ranging from velocities resembling surface channels in conduit flow to slower Darcian groundwater flow in the rock matrix. The phreatic nature of the conduit due to the downstream restriction on the conduit flow dampens the magnitude of the water flowrate that can be conveyed during high flow events. During baseflow conditions, the conduit drains water that has been stored either in the epikarst or the unsaturated zone. The maturity of the karst system and prevalence of secondary and tertiary porosity attributes to the low water storage of the watershed. 76% of the water flowing out of the coupled network was via the karst conduit.

5.3.2 Sediment

Figure 5-17 shows the annual sediment budget for the Cane Run and Royal Springs karst network. Suspended sediment was delivered to the primary surface channel by flow from the many tributaries along Cane Run Creek. Swallets lining the main corridor of the surface channel intercept flow and sediment and divert them to the subsurface. Sediment pirated from the surface was injected into the subsurface where it was either deposited or flushed through the system. Over the entire study period, the net sediment diverted to the subsurface (11.6% of the tributary-produced sediment) was much lower than the net water drained by the conduits (76% of total water outflow). The contrast between the amount of water and sediment exported is a result attributed to two processes: 1) the majority of the tributary-produced sediment remains stored within the surface watershed after conduit reaches capacity flow and swallets are overtopped and 2) the conduit drains flow from the

fracture and matrix network surrounding the conduit which provide large amounts of baseflow with very low sediment concentrations even when the surface streams run dry.

The surface tributaries produce 3,090 t of sediment each year of which 272 t y⁻¹ are exported by the conduit. During the period in this study, there was a net deposition of sediment (299 t y⁻¹) that exceeds the erosion (212 t y⁻¹) which was attributed to a very hydrologically active summer period with high sediment loads that were trapped by the subsurface conduit. However, we speculate that the conduit is in a long-term net-equilibrium due to the fact that erosion and deposition are very similar and fluid energy is fairly consistent in the conduit (see Fig 5-2b). Further evidence of the ability of the karst conduit to limit transport capabilities was evidenced by the observation that sediment deposition in the conduit was very near the amount of sediment diverted from the surface.

5.3.3 *Sediment Organic Carbon*

A carbon budget was performed for the coupled surface-subsurface network to estimate changes and transformations of carbon during temporary fate and transport within the fluviokarst system. Figure 5-18 shows the yearly carbon budget for the Cane Run and Royal Springs karst network. Of the total amount of SOC introduced to the surface system from tributaries, 10.4% was pirated into the subsurface conduit by swallets and other karst features. The surface tributaries produce 157.3 tC y⁻¹ of which 16.9 tC y⁻¹ was pirated by the subsurface. Once introduced into the karst environment the phreatic nature of the conduit acts to temporarily trap the pirated sediment. The highly active exchange between the high quality tributary carbon and the depleted conduit bed carbon was shown when comparing the mass of SOC pirated with the quantity of SOC deposited to the conduit bed, 16.3 tC y⁻¹ and 16.9 tC y⁻¹, respectively. The deposition of SOC being larger than the influx

of SOC suggests that most of the fresh carbon was mixed temporarily with the subsurface sediment and decomposition and transformation occurs prior to the SOC being eroded and transported out of the system. The amount of organic carbon exchanged between the conduit and the water column during net-zero erosion/deposition indicates that suspended sediment with greater carbon densities are more readily assimilated into the subsurface than otherwise expected. Modeling results also show that an average of $0.05 \text{ tC y}^{-1} \text{ km}^{-2}$ was decomposed from the organic state and as a result $0.18 \text{ tCO}_2 \text{ y}^{-1} \text{ km}^{-2}$ was degassed by conduit sediments.

Table 5-1: Sensitivity Analysis Percent Change in Sediment Yield (SY)

Parameter	Units	Min	Optimal	Max	% Change, SY (t)	
					Min	Max
k_p	unitless	0.0001	0.5	0.5	-33	0
$C_{tc_{low}}$	unitless	1.0×10^{-6}	2.3×10^{-6}	5.0×10^{-5}	-54	67
$C_{tc_{high}}$	unitless	1.8×10^{-7}	1.8×10^{-6}	5.0×10^{-6}	-22	45
w_s	$m\ s^{-1}$	4.5×10^{-5}	8.0×10^{-5}	4.5×10^{-4}	15	-30
$\tau_{crit_{sfgl}}$	$N\ m^{-2}$	0.024	0.05	0.8	0	-3
$\tau_{crit_{bed}}$	$N\ m^{-2}$	0.3	1.0	20	0	0
$d_{sfgl_{max}}$	m	0.001	0.005	0.01	-2	0

Table 5-2: Sensitivity Analysis Percent Change in average Suspended Sediment SOC%

Parameter	Units	Min	Optimal	Max	% Change, average SS SOC	
					Min	Max
P_{algae}	unitless	0	0.178	0.4	-3%	-1%
k_{soil}	d^{-1}	-2.6×10^{-5}	-1.0×10^{-4}	-2.3×10^{-4}	1%	-2%
k_{litter}	d^{-1}	-2.3×10^{-4}	-1.3×10^{-3}	-8.0×10^{-3}	9%	-16%
k_{algae}	d^{-1}	-2.3×10^{-4}	-1.3×10^{-3}	-8.0×10^{-3}	2%	-5%
e_x	unitless	0	0.025	0.5	5%	-11%

Table 5-3: Carbon Source Contribution for Fixed Algae Percent using Monte Carlo Simulation (n = 10,000)

Fixed Algae (%)	Urban (%)		Agriculture (%)		
	Soil	Litter	Soil	Litter	Algae
0.0	52.0	48.0	21.7	78.3	0.0
5.0	49.9	50.1	31.6	63.4	5.0
10.0	48.9	51.1	43.2	46.8	10.0
15.0	47.7	52.3	49.0	36.0	15.0
20.0	46.5	53.5	49.0	31.0	20.0
30.0	46.3	53.7	42.7	27.3	30.0
40.0	47.1	52.9	35.5	24.5	40.0

Table 5-4: Carbon Model Calibration and Validation Uncertainty using Monte Carlo Simulation (n = 10,000)

Algae (%)	Calibration		Validation	
	Mean SOC (%)	StDev (%)	Mean SOC (%)	StDev (%)
0.00	3.27	0.01	3.56	0.01
5.00	3.30	0.01	3.59	0.01
10.00	3.34	0.01	3.63	0.01
15.00	3.35	0.01	3.64	0.01
17.81	3.35	0.01	3.65	0.01
20.00	3.35	0.01	3.64	0.01
30.00	3.33	0.01	3.62	0.01
40.00	3.31	0.01	3.60	0.01

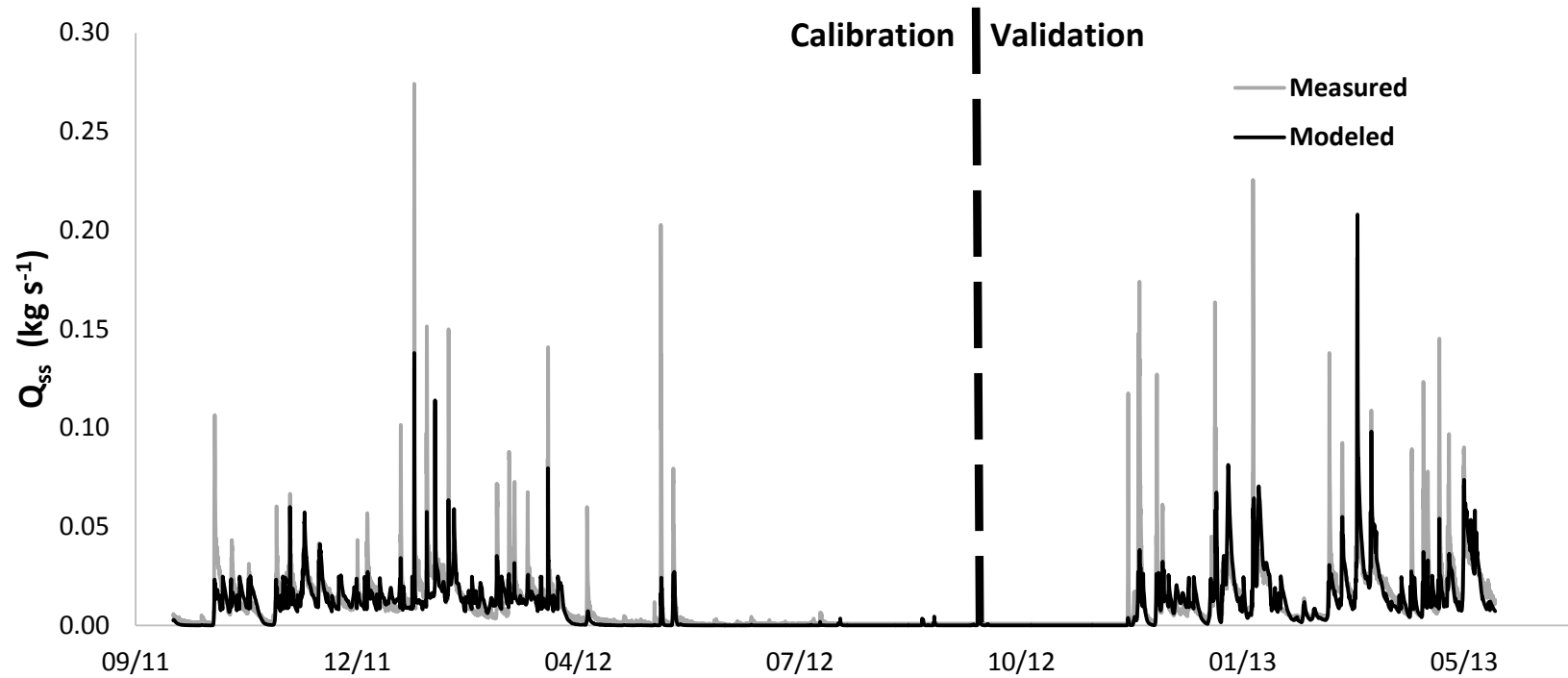


Figure 5-1: Suspended Sediment Discharge (Groundwater Station) Model Calibration and Validation

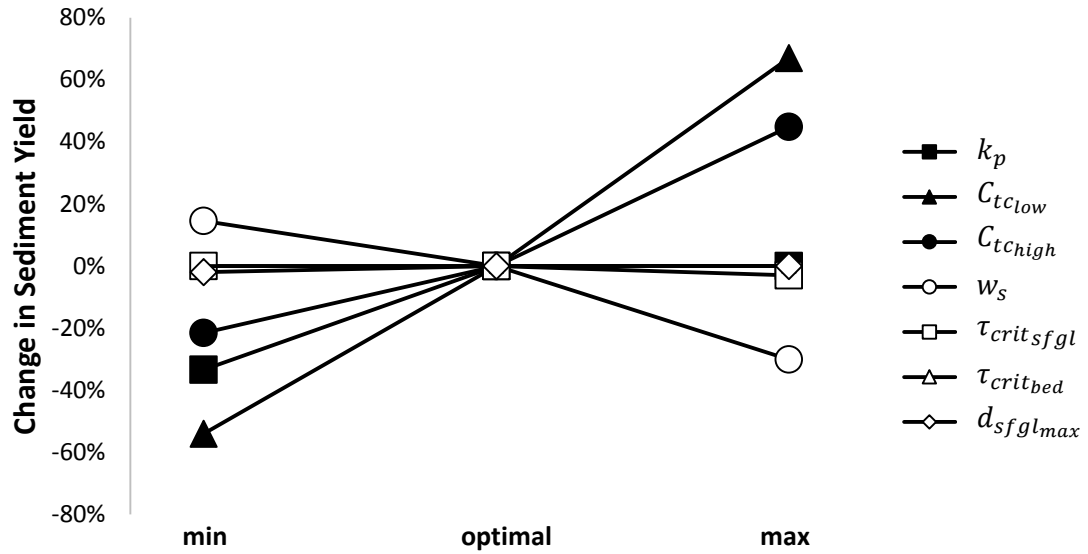


Figure 5-2: Sensitivity Analysis for Sediment Model

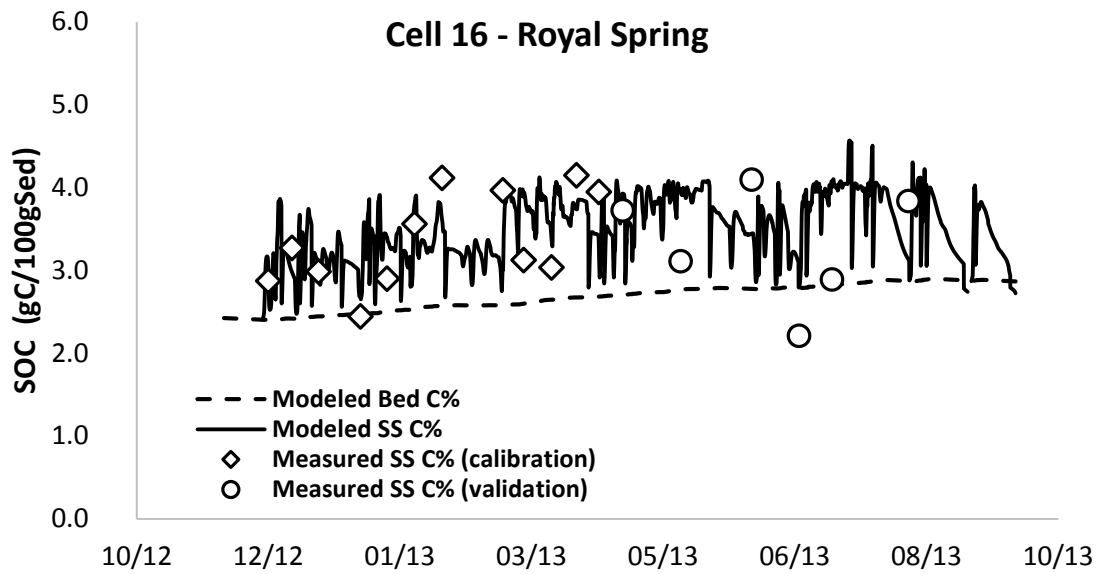


Figure 5-3: Calibration and Validation of Carbon Model. Model results are for the springhead in comparison with the sediment carbon trap measurements also collected at the springhead.

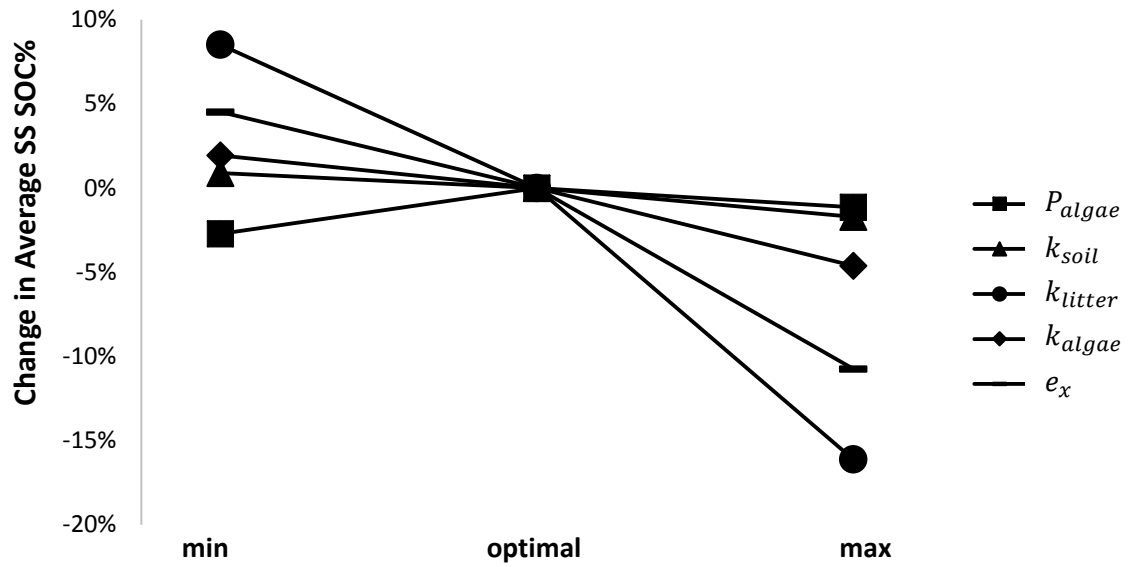


Figure 5-4: Sensitivity Analysis for Carbon Model

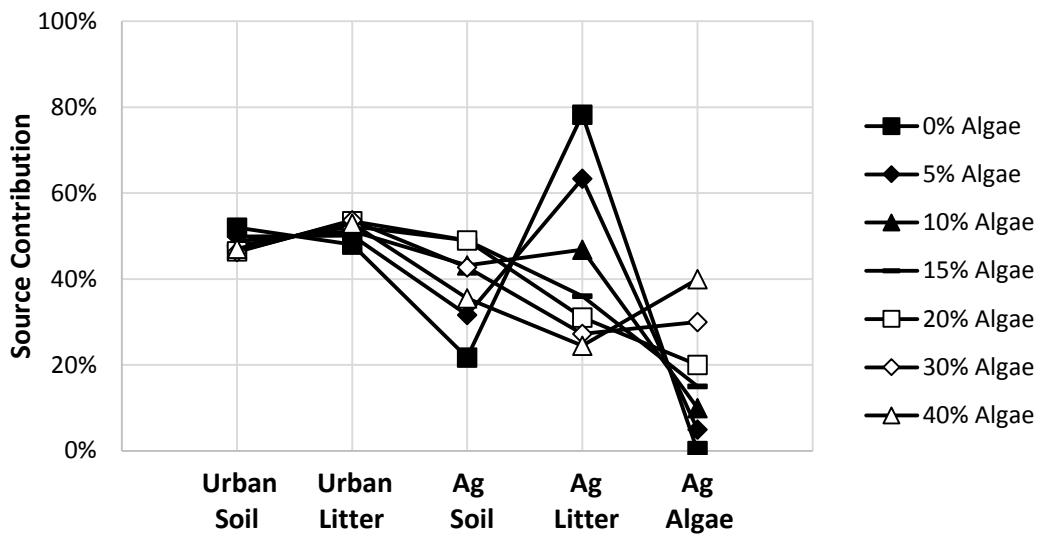


Figure 5-5: Monte Carlo Simulation (n = 10,000) Source Contribution Results for Fixed Algae Percentage

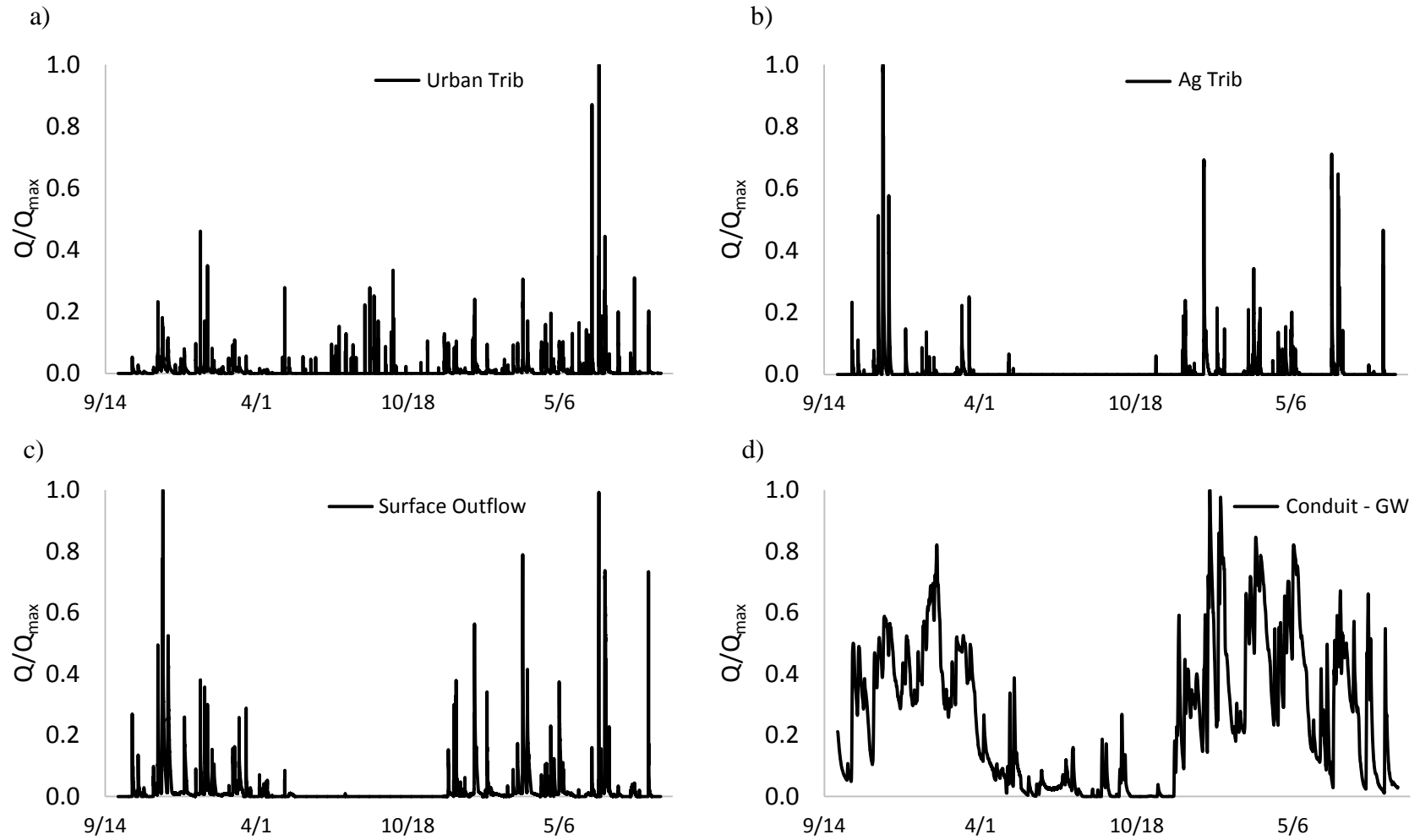


Figure 5-6: Inflows (a and b) and Outflows (c and d) to the Coupled Drainage Network Normalized by Maximum Flow Rate at Each Location

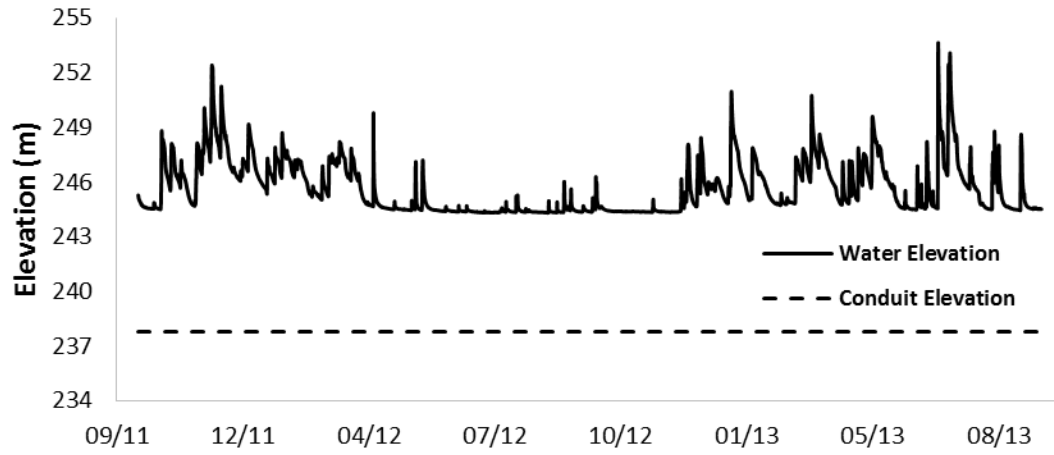


Figure 5-7: Well stage at the Groundwater Station (Cell #10)

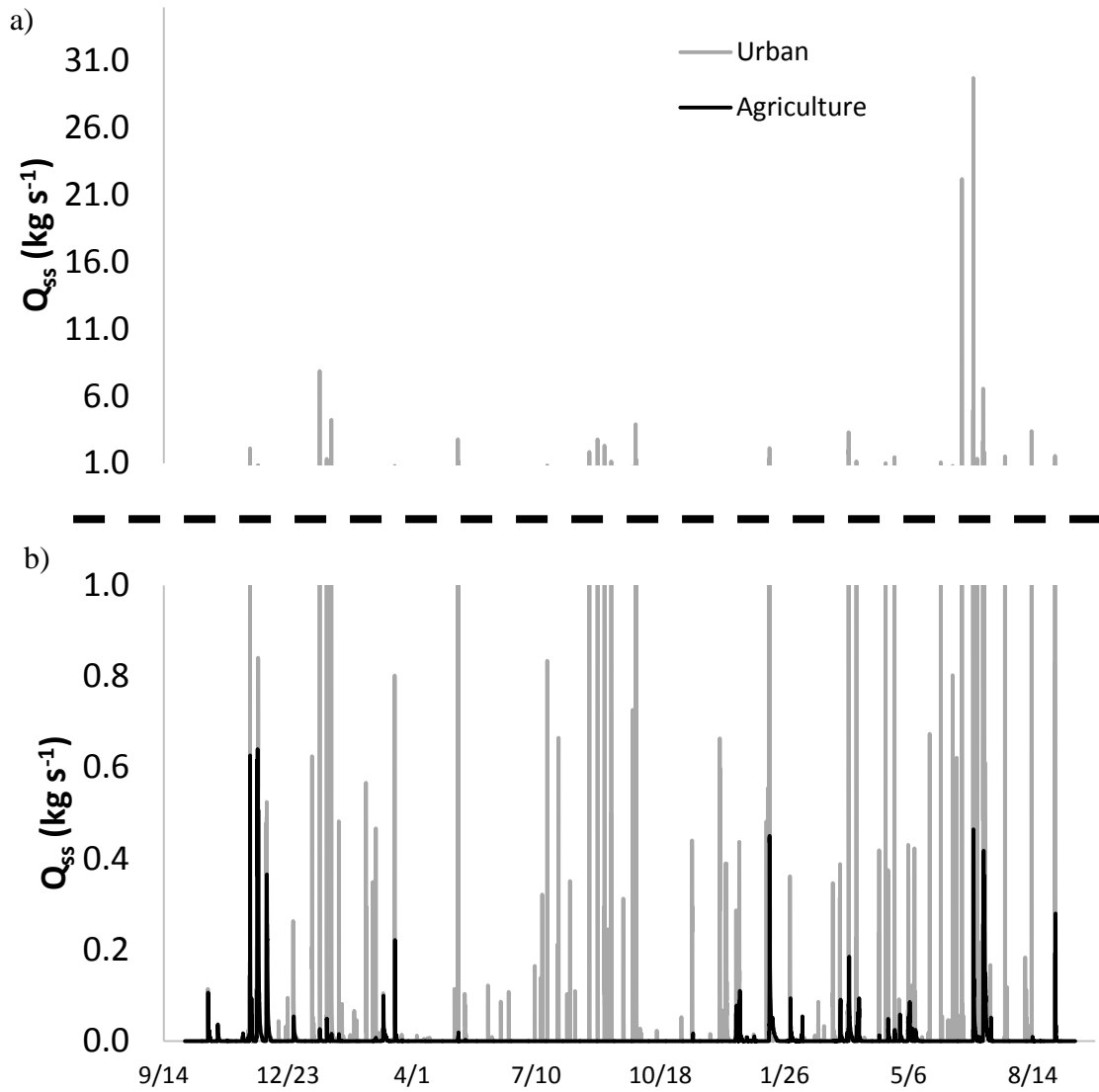


Figure 5-8: Tributary Suspended Sediment Flux with a) high flows and b) low flows

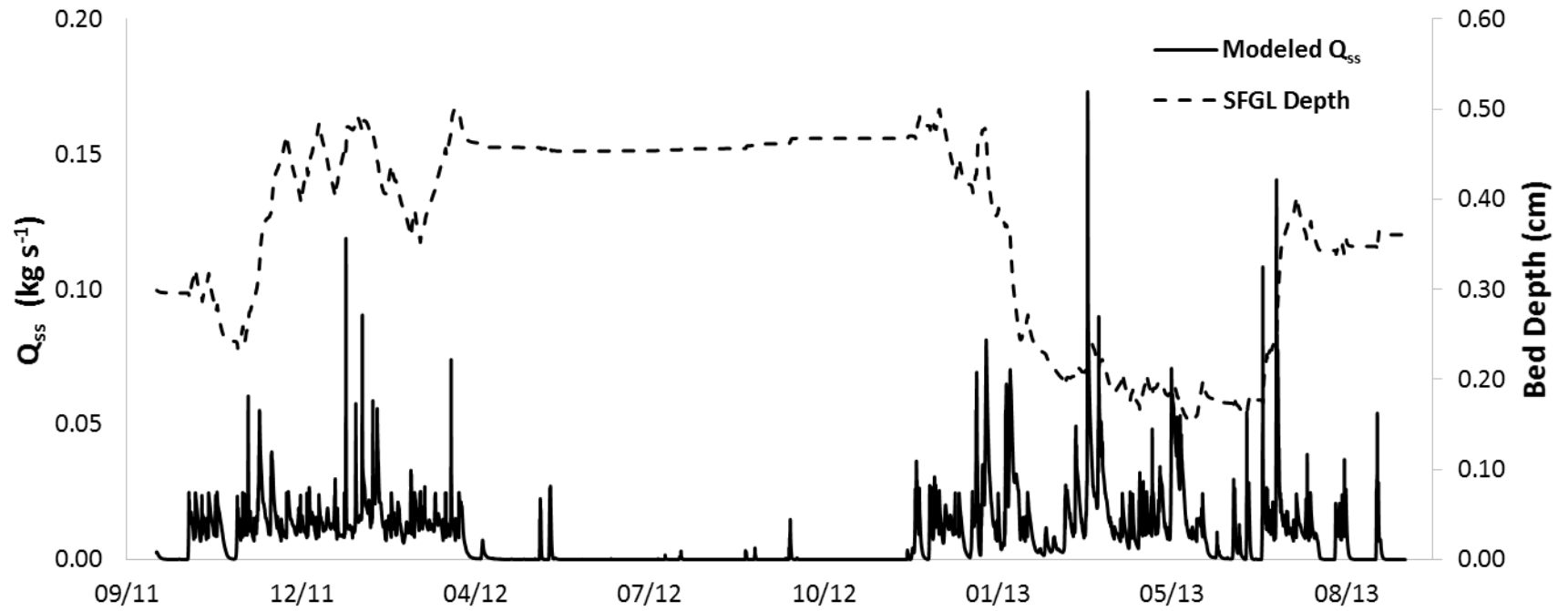


Figure 5-9: Model Results (Groundwater Station) for 2011-2013 Water Years

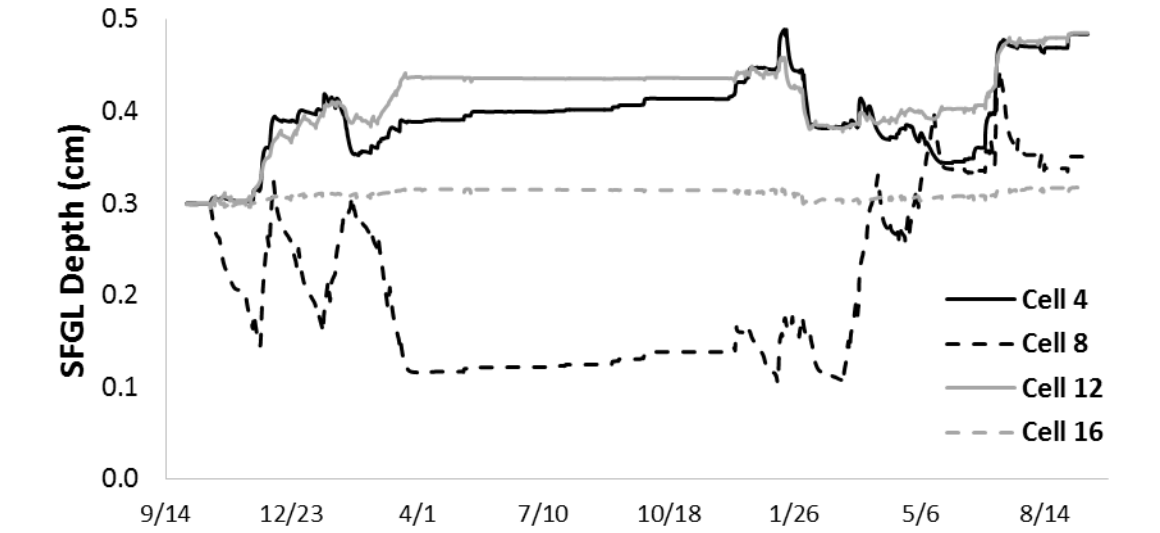


Figure 5-10: Longitudinal Bed Depth Changes in Conduit

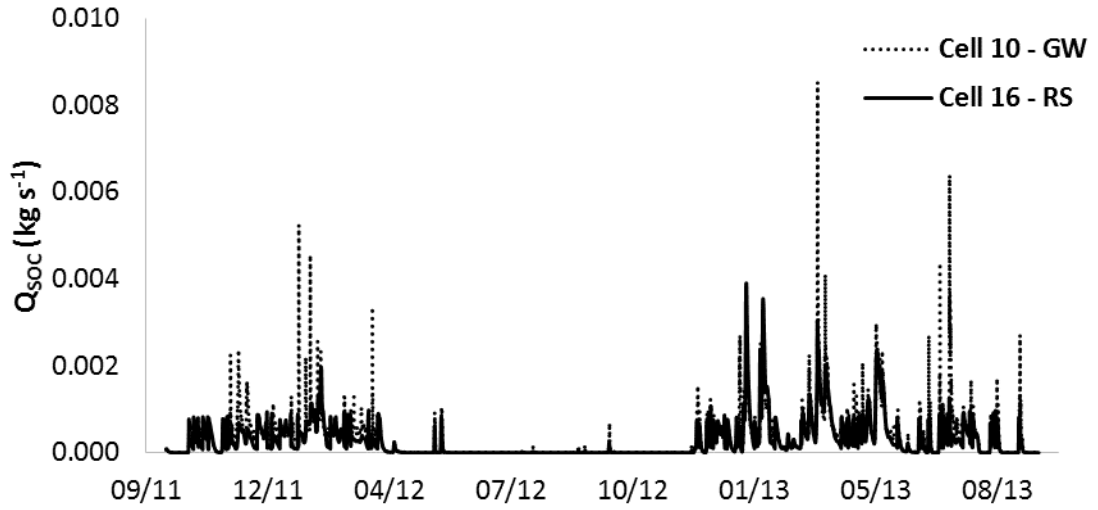


Figure 5-11: Sediment Organic Carbon Flux in Subsurface Conduit

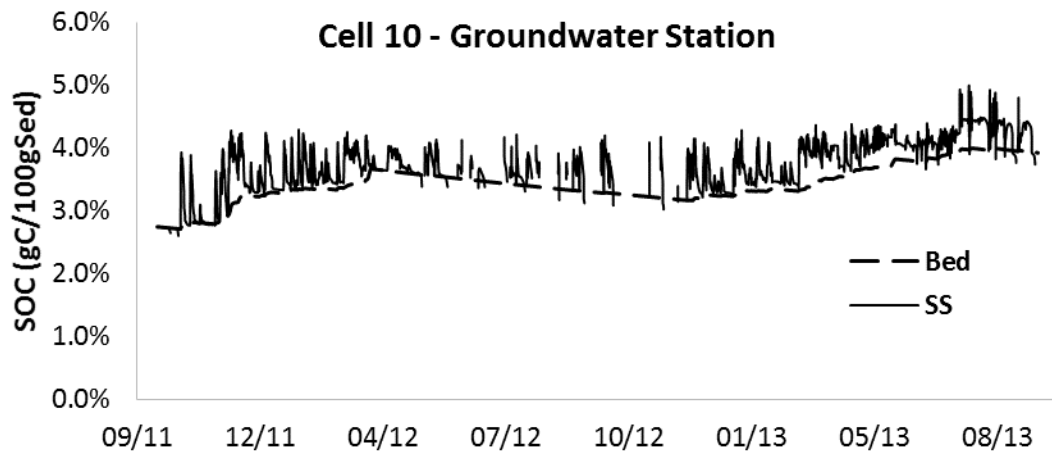


Figure 5-12: Organic Carbon Percentage in Suspended Sediment and Bed Sediment

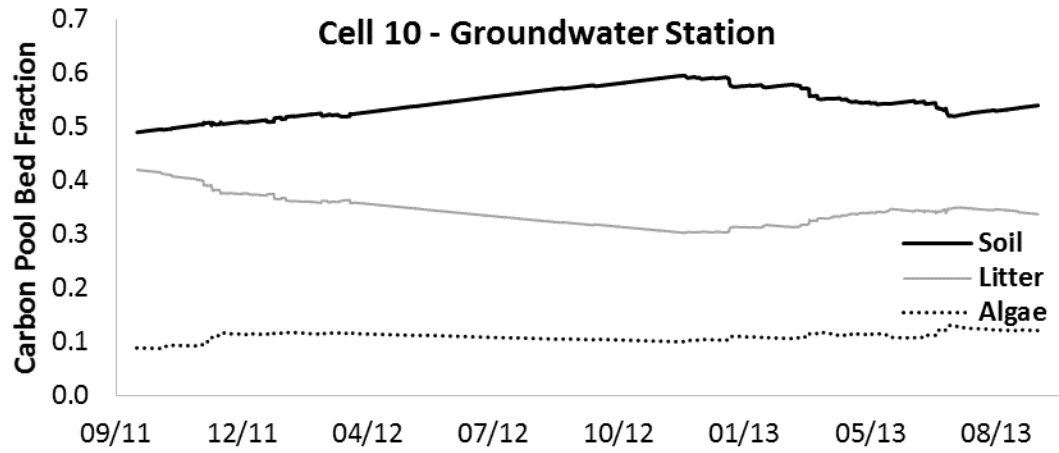


Figure 5-13: Fractioning of Carbon Pools in Conduit Bed

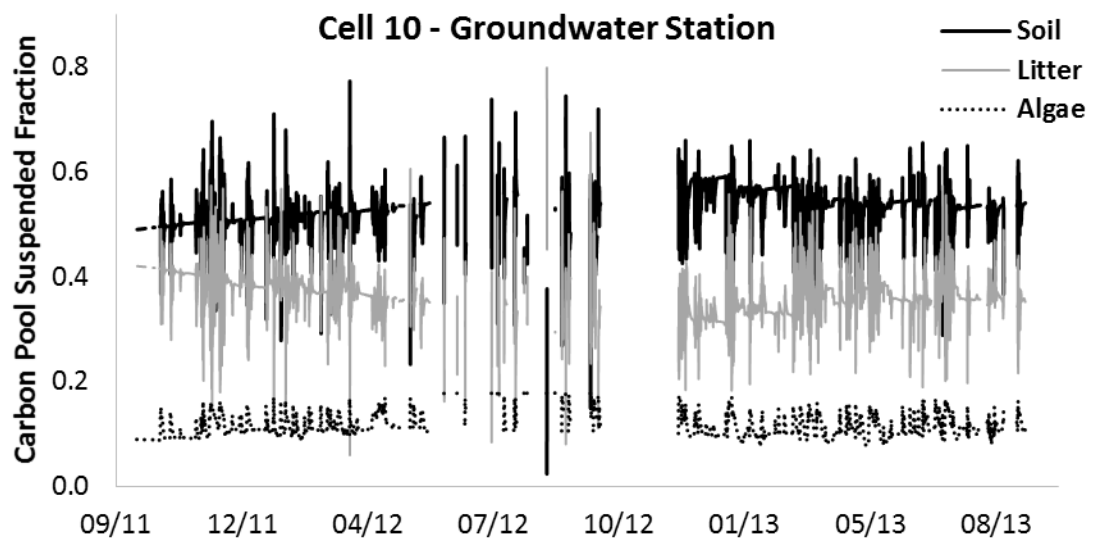


Figure 5-14: Fractioning of Carbon Sources in Suspended Conduit Load

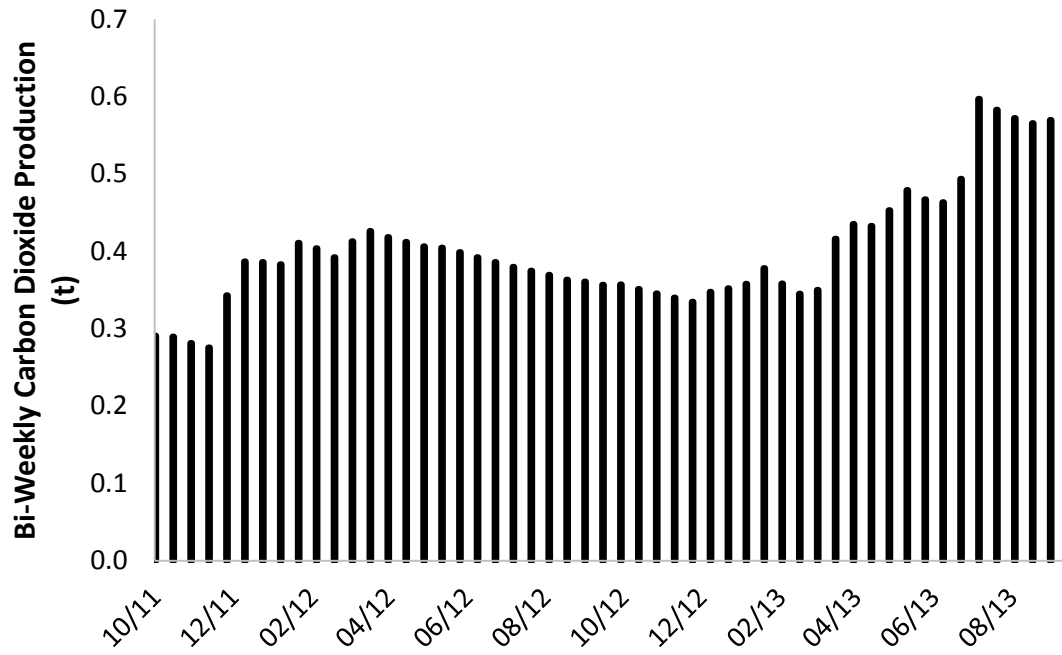


Figure 5-15: Bi-weekly Carbon Decomposition Yield in Subsurface Conduit

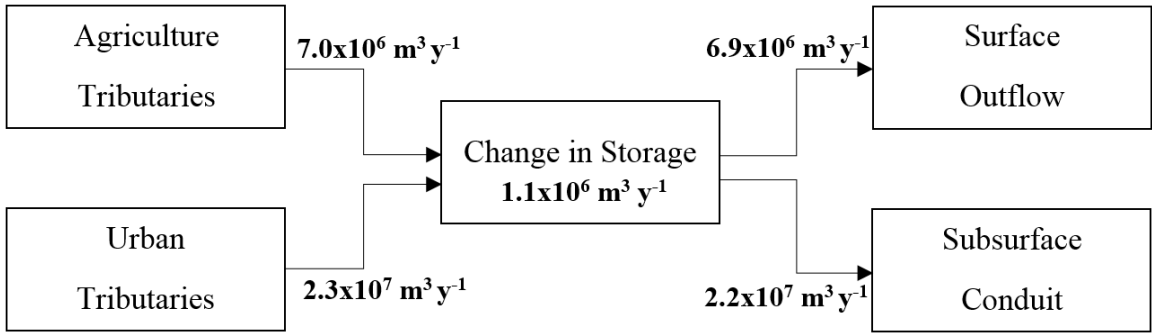


Figure 5-16: Water Budget for Cane Run Fluviokarst Watershed

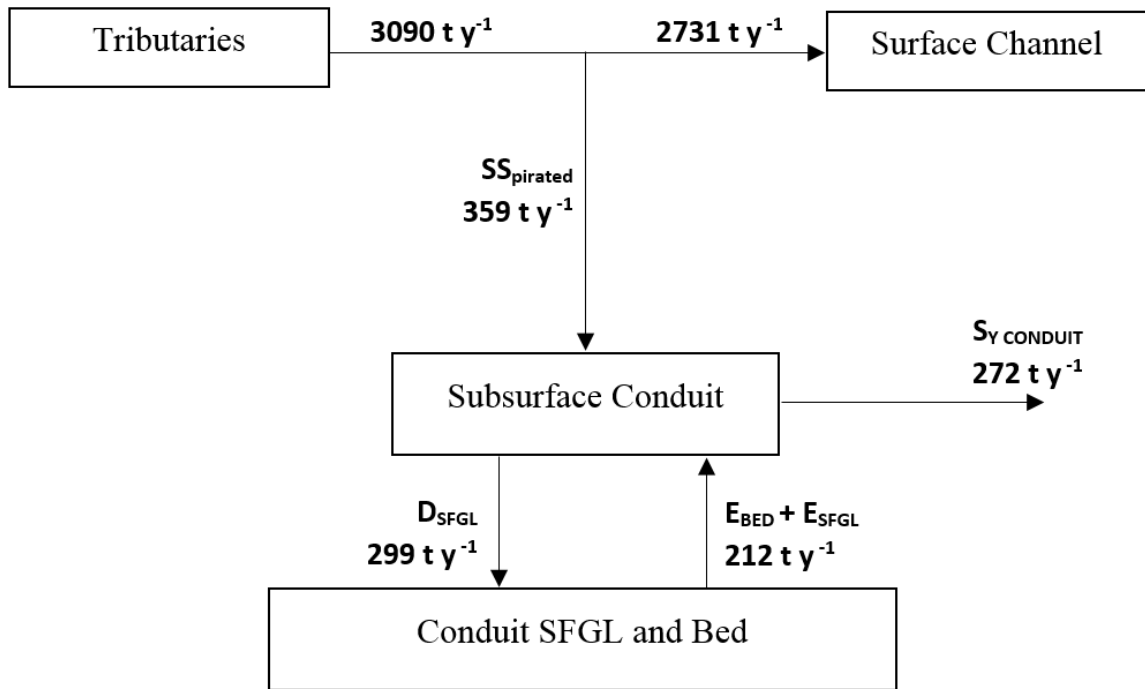


Figure 5-17: Sediment Budget for Cane Run Fluviokarst Watershed

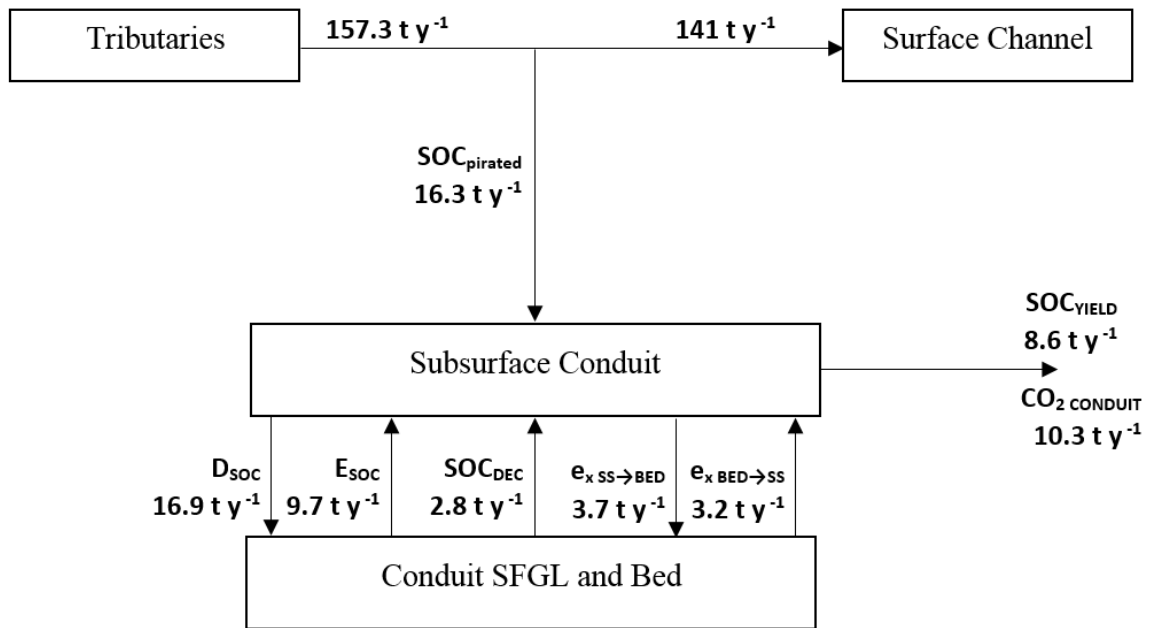


Figure 5-18: Carbon Budget for Cane Run Fluviokarst Watershed

Chapter 6 Discussion

6.1 Karst Conduits as Active Biologic Conveyors

Data and numerical modeling results from this research provide evidence that supports the hypothesis that the subsurface karst conduit acts as an active biological conveyor of sediment carbon. In this manner, the behavior of karst pathways can be extended to considering not only the traditional ideas of CO₂ dissolution/precipitation processes, but also the oxidation of terrestrial derived carbon. Biologically active karst conveyors should be considered in fluvial studies in karst terrain given that the karst conduits turnover carbon at a much higher rate as compared to their surface stream counterparts. Both data and modeling point towards support of the hypothesis that the karst conduit is an active conveyor. Results of sediment organic carbon measurement show a 29.7% loss of sediment carbon when comparing inputs to the karst conduit with outflowing sediment at the springhead. Carbon inputs and outputs were significantly different (p-value < 1×10⁻⁶). Numerical modeling results also show similar net results with a 26.8% loss of sediment carbon when comparing inputs and outputs. This contrasts surface dominated systems in this region which show a 50% enrichment in the carbon signature of transported sediment (Ford and Fox, 2012).

Further support of the hypothesis that the karst conduit in this study is acting as a conveyor is justified based on the fact that we can marginalize alternative explanations of the results. Data-driven results of the sediment budget (see Figure 5-18) resulted in 359 and 272 t y⁻¹ of sediment input to and output from, respectively, the karst conduit suggesting that the system is not substantially gaining or losing sediment and therefore is

in near quasi-equilibrium with the same sediment continuously being transported through the system. Further, the near identical particle size distributions (see Figure 4-5) of source sediments from tributaries in the watershed and sediments collected from the karst conduit justify the idea that the same sediments are being studied at both source and sink locations and that the additional sediment sources have not been erroneously omitted. As final evidence of this concept, we found that the $\delta^{13}C$ of inflowing source sediments and $\delta^{13}C$ of outflowing conduit sediments were not significantly different (p-value = 0.79) (Table 4-6). The lack of difference of the carbon isotope signatures suggests again that the same sediments are being studied at both source and sink locations. The carbon budget shows that the mass of carbon input (16.3 t y^{-1}) to the system is nearly equal to the mass of carbon deposited (16.9 t y^{-1}) within the system which suggests a thorough mixing and assimilation of sediment within the conduit (Figure 5-19). The sediments are temporarily stored in the karst conduit and sediment organic carbon undergoes microbial oxidation. However, past studies have suggested that the enrichment ratios are relatively small and $\delta^{13}C$ is fairly conservative (Ford et al., 2015). In the present study, isotopic enrichment of temporarily stored karst sediments would result in a conservative estimate of 0 to 0.5‰ change in the carbon isotopic carbon composition. As mentioned, data results did not reflect any changes in $\delta^{13}C$ when comparing karst inputs ($-26.64 \pm 0.80\text{‰}$) and outputs ($-26.61 \pm 0.86\text{‰}$).

6.2 Physical and Biogeochemical Processes in Karst Systems

The coupling of our model and data results provides insight into the processes controlling sediment organic carbon fate and transport in the karst conduit which could also play a role in other karst systems and deserve recognition and further attention. Results suggest the importance of highly coupled physical and biogeochemical processes.

Processes for which discussion is warranted for this karst system include the limited capacity of karst conduits to transport fluid and sediment, the exchange rate of suspended and bed sediment, and the decomposition rates of carbon in karst.

Within the karst phreatic conduit, the sediment transport carrying capacity of the fluid is limited during hydrologic events but sustained in the long term, which considerably contrasts typical unregulated surface water streamflow. The behavior of the karst conduit is particularly worthy of attention when considering that the conduit transports approximately 75% of the water that transports through the watershed and 12% of the watershed's sediment. During storm events, the downstream adverse hydraulic gradient limits the sediment transport carrying capacity and results in net deposition of pirated surface-derived sediments. The piezometric head of the karst groundwater basin and phreatic outflow from the conduit results in the sediment transport carrying capacity being sustained for days to weeks beyond the corresponding hydrologic peak flow of the surface stream. In turn, clear water in the karst conduit is erosive with excess carrying capacity to transport sediment and eroded previously deposited sediments during relatively inactive hydrologic time periods. The storm flow deposition and low to moderate flow erosion within the karst conduit results in a near long term equilibrium of the temporary sediment storage in the streambed of the subsurface conduit. In the study period, extreme hydrologic activity during the second year provided large quantities of sediment to the subsurface that are expected to gradually erode toward equilibrium given enough time. However, the pronounced temporary deposition of high-quality surface sediment promotes the biogeochemical processes that turnover carbon in the conduit.

In addition to the behavior of the sediment transport carrying capacity of the flow, model results suggest the potential importance of a less studied sediment transport physical process associated with the exchange of sediment during equilibrium sediment transport, i.e., net zero erosion from or deposition to the bed. Sediment exchange during equilibrium is a physical mechanism that in turn impacts sediment organic carbon turnover in the conduit temporary storage zones by exchanging the higher carbon density sediment in suspension with more depleted sediment from within the conduit bed. Sediment transport scientists have long understood that suspended sediments in turbulent flow can actively exchange with stored bed sediments although during equilibrium transport it is recognized that the net exchange is zero (e.g., Chang, 1998). The physics of the sediment exchange process has been more recently justified using advanced visualization techniques and it has been found that sediment erosion and deposition is coupled to flow coherency (Cellino and Lemmin, 2004). Cellino and Lemmin (2004) showed that low momentum zones of coherent fluid that transports settling sediment episodically deposits sediment to the bed while fluid ejections associated with the shedding phenomena at the bed episodically re-suspends bed sediment into the water column. However, sediment exchange processes between the water column and bed during equilibrium transport have been rarely included in sediment transport models. One reason for omitting the equilibrium exchange process from models is a lack of need for such detailed information given that the net results sought after for sediment transport models have been the downstream transport rates distributed over time and the net change in the streambed elevation. A second reason for omitting the exchange process has likely been a lack of methods to help parameterize the exchange

process, as studies such as those by Cellino and Lemmin (2004) were experimental in nature and limited to the laboratory scale.

While perhaps understudied, the equilibrium exchange of sediment is potentially of high interest in the recent class of scientific studies that emphasize elucidating the role of carbon processes in the inland freshwater carbon budget (Battin et al., 2008; Regnier et al., 2013). In the case of sediment organic fate and transport in the fluvial system studied here, the exchange rate appears important given the potential to exchange labile carbon with recalcitrant carbon, the former being temporarily stored and turned over and the latter being transported downstream and out of the reach. Further, the sensitivity of the exchange rate upon the net sediment organic carbon transported out of the karst conduit highlights the potential of the exchange process to be at least partially controlling in terms of sediment organic carbon fate in fluvial systems. While equilibrium exchange showed sensitivity in the present study, it is not fully clear the net importance of the exchange process upon sediment organic carbon fate during equilibrium flows in other fluvial systems. For example, in surface streams equilibrium transport can be of short duration as bed sediments are eroded to the water column during the rising limb of the hydrograph and upstream conveyed sediment are deposited to the bed during the falling limb of the hydrograph. For such occurrences, the exchange during equilibrium may be marginalized in importance relative to non-equilibrium exchanges. In this manner, it is possible that the phreatic karst conduits represents a class of fluvial systems in which equilibrium exchange is significant due to the fairly limited range of the sediment transport carrying capacity of the flow dictated by the downstream hydraulic control. Nevertheless, given the importance of the equilibrium exchange within this study, we suggest further research is needed in fluvial

systems with both field based sensor method and models to gain an understanding of the exchange process.

The sensitivity of carbon decomposition rates and their needed inclusion in the sediment carbon continuity equation suggest the prevalence of microbial oxidation in the temporarily stored sediments. Three sub-pools of carbon are associated with the transported sediments including autochthonous carbon produced in the surface stream channels, litter and terrestrial detritus, and the more recalcitrant soil-derived carbon pool. The calibrated reaction rates of the three carbon pools used within the numerical model were well within their literature range (Webster et al., 1999; Alvarez and Guerrero, 2000; Six and Jastrow, 2002; Ford and Fox, 2012) and agreed well with the sediment carbon turnover analysis in surface streams of this region (Ford and Fox, 2015). The decomposition rate for soil organic carbon is typically two orders of magnitude less than that of other carbon pools, but in the studied karst system the soil decomposition rate is only one order of magnitude smaller than that of the litter detritus and autochthonous algae decomposition rates which shows that ability of the fluvio-karst environment to promote accelerated decomposition of carbon sources. The heterotrophic bacteria decomposition of carbon provides a carbon loss mechanism within the sediment during temporary storage.

The subsurface conduit drainage system provides a fairly unique environment in this temperate climate that justifies a decomposition of sediment carbon for a number of reasons as follows: (i) the constant influx of surface water promotes aerobic conditions in the surficial layer of sediments deposited in the subsurface conduits as opposed to anaerobic conditions; (ii) there is a lack of autochthonous growth to offset respired carbon due to the lack of sunlight in the subsurface environment; (iii) the temporary sediment

storage deposits coupled with relatively high water temperatures (mean water temperature = 16.2°C) promote an active microbial pool; (iv) agricultural drainage promote high nutrient conditions to sustain the microbial pool in the absence of algal organic matter; and (v) regular deposition of carbon rich tributary sediment would suggest potential for active carbon turnover.

6.3 Advancement of Water Quality Modeling

As final contribution of this paper, a note regarding the advancement of water quality modeling is warranted. The progressive method adopted in this paper shows how the novel use of stable isotope data can be coupled with more traditional water quality modeling in order to assist with understanding the non-linear behavior of sediment carbon source, fate and transport in fluviokarst watersheds. In the present contribution, the stable carbon isotopic composition of sediment provides an independent method to assist with allocating sources of surface derived sediments to the karst subsurface and justify the consistency of the sediment pool studied in the surface and subsurface environments. Together with the sediment organic carbon concentration data, the stable isotope datasets assisted as inputs and calibration methods for the water quality modeling based on the continuity of water, sediment and carbon over the two year modeling duration.

The research method provides another example of a branch of hydrologic modeling that relies on the application of stable isotopes for inputs and verification purposes. The stable isotope composition of sediments has been long used for gaining an understanding of sediment carbon provenance in estuary and marine sciences (Martinotti et al., 1997; Sigleo and Macko, 2002). Over the past decade or so, stable isotopes have been

increasingly applied within the sediment fingerprinting methodology in order to understand erosion sources at catchment and watershed scales (Papanicolaou et al., 2003; Bellanger et al., 2004; Fox, 2005, 2009; Fox and Papanicolaou, 2007, 2008; Jacinthe et al., 2009; Mukundan et al., 2010; Collins et al., 2013; Jiang and Ji, 2013; Imberger et al., 2014; Ford et al., 2015). The coupling of sediment fingerprinting technology where stable isotopes are used as tracers with traditional water quality modeling that simulates sediment and sediment carbon continuity is now being published in the recent literature. Ford and Fox (2015) showed using the *ISOFLOC* model how algal growth and sloughing could be calibrated with stable carbon isotopes in order to simulate the fluvial organic carbon budget for streams. Fox and Martin (2015) showed how stable isotopes could be used to assist with calibration of model parameters including the sediment delivery ratio and sediment transport capacity with a soil erosion and sediment yield model applicable to watersheds with mixed land uses. Coupling of stable isotopes and water quality modeling is a fairly new class of research, and it is expected that model advancement and lessons learned from the present study as well as the aforementioned studies will assist researchers as they apply the stable isotope tools to assist with reducing numerical model uncertainties.

Chapter 7 Conclusions

In this thesis research, coupled biogeochemical and physical processes of water, sediment, and carbon are investigated in a temperate, low order fluviokarst watershed in central Kentucky, USA. A framework is developed that links surface and subsurface sediment transport mechanisms with sediment organic carbon decomposition to estimate the flux of sediment in the phreatic conduit and to approximate the extent to which carbon dioxide is degassed from stored sediments.

The physical processes controlling flow and sediment transport in the subsurface are a function of the transport carrying capacity of the karst conduit which is limited by a downstream subsurface hydraulic dam that results in deposition of pirated surface sediment during storm events in the subsurface. Results of the water budget show that 76% of the water flow out of the watershed is through the karst conduit. Approximately 12% of the tributary produced sediment that is introduced to the main surface channel is pirated from the surface to the subterranean conduit. Sensitive parameters in the hydraulic model are transport carrying capacity and the settling depth coefficient.

The biological processes controlling sediment organic carbon flux and transformations are driven by the temporary trapping of carbon-rich surface sediments within the karst conduit. Litter and soil are the dominant sources of organic carbon into the subsurface conduit with algae being a minor source. Sediment organic carbon in the karst environment undergo heterotrophic bacteria decomposition resulting in a 30% net loss in sediment carbon density. A new parameter, the exchange rate, has been developed to represent the net-zero mass exchange mixing of suspended and bed sediments. Sensitive

parameters in the sediment organic carbon model include the exchange factor and the litter decomposition rate. The subsurface karst drainage network exports $0.15 \text{ tC km}^{-2} \text{ y}^{-1}$.

A comparison with a neighboring immature karst would suggest that decomposition in karst dominated watersheds results in a loss of carbon density within temporarily trapped sediment rather than an enrichment (Ford and Fox, 2012). As a result, sediment within karst topography can be seen as a source of carbon dioxide to the atmosphere. From this study, carbon dioxide efflux rates for similar fluviokarst watersheds can be estimated at $0.18 \text{ tCO}_2\text{km}^{-2}\text{y}^{-1}$. The magnitude of the number is low compared to that of surface-dominated watersheds (Hope et al., 2001; Ford and Fox, 2015), but when considering that 12% of the earth's surface is karst, the collective efflux from karst should be included when formulating global climate models.

There are several limitations within the model that if ameliorated could close results and provide a cleaner analysis. Data collection efforts within karst watersheds can be difficult due to added complexity of physical and hydraulic heterogeneity. More consistent and reliable stream gages and velocity probes could remove the need for using surrogate gages. Gaging directly upstream and downstream of a large swallet could help to better estimate direct flow loss to the subsurface. Instrumentation of swallets with velocity sensors to collect flow, sediment, and carbon data. Periodic conduit bed samples would allow for direct measurements of conduit bed carbon composition to be used as an extra tool for calibration.

To more fully understand how sediment is transported and transformed through fluviokarst watersheds, additional work has to be performed to more tightly couple

different models and processes, to account for uncertainty in estimating parameters, and to extend this analysis to other systems and into the future. A complete hydraulic model coupling open channel flow in the surface with pipe flow in the subsurface is needed in the future to more closely represent flow dynamics in fluvio karst. Modelling the nitrogen cycle in conduit-dominated karst aquifers is another need that may have many implications to regional and global nitrogen budgets. Lab experiments should be developed to more closely investigate the relationship between the friction factor and other variables in karst rocks. Finally, upscaling the results of this research to regional and global scales will provide a tool representing fluvio karst processes to researchers that can be used in future water, sediment, and carbon budgeting.

References

- Abril, G., Etcheber, H., Borges, A. V., & Frankignoulle, M. (2000). Excess atmospheric carbon dioxide transported by rivers into the Scheldt estuary. *Comptes Rendus de l'Academie des Sciences-Series IIA-Earth and Planetary Science*, 330(11), 761-768.
- Acton, P., Fox, J., Campbell, E., Rowe, H., & Wilkinson, M. (2013). Carbon isotopes for estimating soil decomposition and physical mixing in well-drained forest soils. *Journal of Geophysical Research: Biogeosciences*, 118(4), 1532-1545.
- Ahmadi, S. H., Amin, S., Keshavarzi, A. R., & Mirzamostafa, N. (2006). Simulating watershed outlet sediment concentration using the ANSWERS model by applying two sediment transport capacity equations. *Biosystems engineering*, 94(4), 615-626.
- Aldrian, E., Chen, C. T. A., Adi, S., Sudiana, N., & Nugroho, S. P. (2008). Spatial and seasonal dynamics of riverine carbon fluxes of the Brantas catchment in East Java. *Journal of Geophysical Research: Biogeosciences (2005–2012)*, 113(G3).
- Allan, J. D., & Castillo, M. M. (2007). *Stream ecology: structure and function of running waters*. Springer Science & Business Media.
- Allen, J. R. (1971). Transverse erosional marks of mud and rock: their physical basis and geological significance. *Sedimentary Geology*, 5(3), 167-385.
- Allen, J. J., Shockling, M. A., Kunkel, G. J., & Smits, A. J. (2007). Turbulent flow in smooth and rough pipes. *Philosophical Transactions of the Royal Society of London A: Mathematical, Physical and Engineering Sciences*, 365(1852), 699-714.
- Alvarez, S., & Guerrero, M. C. (2000). Enzymatic activities associated with decomposition of particulate organic matter in two shallow ponds. *Soil Biology and Biochemistry*, 32(13), 1941-1951.
- Alvarez-Cobelas, M., Angeler, D. G., Sánchez-Carrillo, S., & Almendros, G. (2012). A worldwide view of organic carbon export from catchments. *Biogeochemistry*, 107(1-3), 275-293.
- Anchuela, Ó. P., Juan, A. P., Casas-Sainz, A. M., Ansón-López, D., & Gil-Garbi, H. (2013). Actual extension of sinkholes: considerations about geophysical, geomorphological, and field inspection techniques in urban planning projects in the Ebro basin (NE Spain). *Geomorphology*, 189, 135-149.
- Aquilina, L., Ladouche, B., & Dörfliger, N. (2006). Water storage and transfer in the epikarst of karstic systems during high flow periods. *Journal of Hydrology*, 327(3), 472-485.
- American Society of Civil Engineers (ASCE). (1993). The ASCE task committee on definition of criteria for evaluation of watershed models of the watershed

- management committee Irrigation and Drainage Division, Criteria for evaluation of watershed models. *J. Irri. Drain. Engng, ASCE*, 119(3), 429-442.
- Ashton, K. (1966). The analysis of flow data from karst drainage systems. *Trans. Cave Res. Group GB*, 7(2), 161-203.
- Atkinson, T. C. (1977). Diffuse flow and conduit flow in limestone terrain in the Mendip Hills, Somerset (Great Britain). *Journal of hydrology*, 35(1), 93-110.
- Aufdenkampe, A. K., Mayorga, E., Raymond, P. A., Melack, J. M., Doney, S. C., Alin, S. R., ... & Yoo, K. (2011). Riverine coupling of biogeochemical cycles between land, oceans, and atmosphere. *Frontiers in Ecology and the Environment*, 9(1), 53-60.
- Bača, P. (2008). Hysteresis effect in suspended sediment concentration in the Rybárik basin, Slovakia/Effet d'hystérèse dans la concentration des sédiments en suspension dans le bassin versant de Rybárik (Slovaquie). *Hydrological Sciences Journal*, 53(1), 224-235.
- Baedke, S. J., & Krothe, N. C. (2001). Derivation of effective hydraulic parameters of a karst aquifer from discharge hydrograph analysis. *Water Resources Research*, 37(1), 13-19.
- Bai, X., Zhang, X., Long, Y., Liu, X., & Siyu, Z. (2013). Use of ¹³⁷Cs and ²¹⁰Pbex measurements on deposits in a karst depression to study the erosional response of a small karst catchment in Southwest China to land-use change. *Hydrological Processes*, 27(6), 822-829.
- Bailly-Comte, V., Jourde, H., Roesch, A., & Pistre, S. (2008). Mediterranean flash flood transfer through karstic area. *Environmental Geology*, 54(3), 605-614.
- Bakalowicz, M. (2004). The epikarst, the skin of karst. *Jones, WK, Culver, DC and Herman, J.(Eds.)*, 16-22.
- Bakalowicz, M. (2005). Karst groundwater. A challenge for new resources *Hydrogeology Journal*, 13 (1), 148-160.
- Bakalowicz, M., El Hakim, M., & El-Hajj, A. (2008). Karst groundwater resources in the countries of eastern Mediterranean: the example of Lebanon. *Environmental geology*, 54(3), 597-604.
- Baldini, J. U., Baldini, L. M., McDermott, F., & Clipson, N. (2006). Carbon dioxide sources, sinks, and spatial variability in shallow temperate zone caves: evidence from Ballynamindra Cave, Ireland. *Journal of Cave and Karst Studies*, 68(1), 4-11.
- Battin, T. J., Kaplan, L. A., Newbold, J. D., & Hansen, C. M. (2003). Contributions of microbial biofilms to ecosystem processes in stream mesocosms. *Nature*, 426(6965), 439-442.

- Battin, T. J., Kaplan, L. A., Findlay, S., Hopkinson, C. S., Marti, E., Packman, A. I., ... & Sabater, F. (2008). Biophysical controls on organic carbon fluxes in fluvial networks. *Nature Geoscience*, 1(2), 95-100.
- Bellanger, B., Huon, S., Velasquez, F., Vallès, V., Girardin, C., & Mariotti, A. (2004). Monitoring soil organic carbon erosion with $\delta^{13}\text{C}$ and $\delta^{15}\text{N}$ on experimental field plots in the Venezuelan Andes. *Catena*, 58(2), 125-150.
- Benischke R., Goldscheider N. & Smart C.C., (2007). Tracer techniques. In: Goldscheider N. & Drew D. (Eds.) – *Methods in Karst Hydrogeology*. International Contributions to Hydrogeology. Taylor & Francis, London, UK: 147-170.
- Biggs, B. J., Goring, D. G., & Nikora, V. I. (1998). Subsidy and stress responses of stream periphyton to gradients in water velocity as a function of community growth form. *Journal of Phycology*, 34(4), 598-607.
- Birdwell, J. E., & Engel, A. S. (2009). Variability in terrestrial and microbial contributions to dissolved organic matter fluorescence in the Edwards Aquifer, Central Texas. *Journal of Cave and Karst Studies*, 71(2), 144-156.
- Bögli, A. (2012). *Karst hydrology and physical speleology*. Springer Science & Business Media.
- Bonacci, O. (2001). Analysis of the maximum discharge of karst springs. *Hydrogeology Journal*, 9(4), 328-338.
- Bonacci, O., & Magdalenic, A. (1993). The catchment area of the Sv. Ivan Karst spring in Istria (Croatia). *Groundwater*, 31(5), 767-773.
- Bonacci, O., Pipan, T., & Culver, D. C. (2009). A framework for karst ecohydrology. *Environmental Geology*, 56(5), 891-900.
- Brookes, A. (1986). Response of aquatic vegetation to sedimentation downstream from river channelisation works in England and Wales. *Biological Conservation*, 38(4), 351-367.
- Brown, G. O. (2002). The history of the Darcy-Weisbach equation for pipe flow resistance. *Environmental and Water Resources History*, 38(7), 34-43.
- Bruno E., Calcaterra, D., Parise, M. (2008). Development And Morphometry Of Sinkholes In Coastal Plains Of Apulia, Southern Italy. Preliminary Sinkhole Susceptibility Assessment. *Engineering Geology* 99 (2008) 198–209.
- Brussaard, L. (1994). An appraisal of the Dutch programme on soil ecology of arable farming systems (1985–1992). *Agriculture, ecosystems & environment*, 51(1), 1-6.
- Butman, D., & Raymond, P. A. (2011). Significant efflux of carbon dioxide from streams and rivers in the United States. *Nature Geoscience*, 4(12), 839-842.

- Campbell, C. W., & Sullivan, S. M. (2002). Simulating time-varying cave flow and water levels using the Storm Water Management Model. *Engineering Geology*, 65(2), 133-139.
- Carey, A. E., Gardner, C. B., Goldsmith, S. T., Lyons, W. B., & Hicks, D. M. (2005). Organic carbon yields from small, mountainous rivers, New Zealand. *Geophysical research letters*, 32(15).
- Cellino, M., & Lemmin, U. (2004). Influence of coherent flow structures on the dynamics of suspended sediment transport in open-channel flow. *Journal of Hydraulic Engineering*, 130(11), 1077-1088.
- Chadwick, M., Huryn, A., Benke, A., & Dobberfuhl, D. (2010). Coarse organic matter dynamics in urbanised tributaries of the St. Johns River, Florida. In *Freshwater Forum (Vol. 28)*.
- Chang, H. H. (1988). *Fluvial Processes in River Engineering*. Krieger Publishing Company: Malabar, Florida.
- Chapelle, F. (2001). *Ground-water microbiology and geochemistry*. John Wiley & Sons.
- Clemens, T., Hueckinghaus, D., Sauter, M., Liedl, R., & Teutsch, G. (1997). Modelling the genesis of karst aquifer systems using a coupled reactive network model. *IAHS PUBLICATION*, 241, 3-10.
- Clepper, M. L. (2011). *Lithostratigraphic and paleoenvironmental framework of The Upper Ordovician Lexington Limestone, Bluegrass Region, Central Kentucky*. University of Kentucky.
- Cole, J. J., Prairie, Y. T., Caraco, N. F., McDowell, W. H., Tranvik, L. J., Striegl, R. G., ... & Melack, J. (2007). Plumbing the global carbon cycle: integrating inland waters into the terrestrial carbon budget. *Ecosystems*, 10(1), 172-185.
- Collins, A. L., Zhang, Y. S., Duethmann, D., Walling, D. E., & Black, K. S. (2013). Using a novel tracing-tracking framework to source fine-grained sediment loss to watercourses at sub-catchment scale. *Hydrological Processes*, 27(6), 959-974.
- Conant, R. T., Paustian, K., & Elliott, E. T. (2001). Grassland management and conversion into grassland: effects on soil carbon. *Ecological Applications*, 11(2), 343-355.
- Coulter, C. B., Kolka, R. K., & Thompson, J. A. (2004). Water quality in agricultural, urban, and mixed land use watersheds. *Journal of the American Water Resources Association* 40, 1593-1601.
- Creamer, C. A., de Menezes, A. B., Krull, E. S., Sanderman, J., Newton-Walters, R., & Farrell, M. (2015). Microbial community structure mediates response of soil C decomposition to litter addition and warming. *Soil Biology and Biochemistry*, 80, 175-188.

- Crenshaw, C. L., Valett, H. M., & Webster, J. R. (2002). Effects of augmentation of coarse particulate organic matter on metabolism and nutrient retention in hyporheic sediments. *Freshwater Biology*, 47(10), 1820-1831.
- Cressman, E. R. (1967). Geologic map of the Georgetown quadrangle, Scott and Fayette counties, Kentucky (No. 605).
- Cressman, E. R. (1973). *Lithostratigraphy and depositional environments of the Lexington Limestone (Ordovician) of central Kentucky* (No. 768). US Govt. Print. Off.,.
- Cressman, E. R., & Peterson, W. L. (1986). Ordovician system. In: McDowell, R.C. (Ed.), *The Geology Of Kentucky: A Text To Accompany The Geologic Map Of Kentucky*. U.S. Geological Survey Professional Paper 1151-H.
- Curl, R. L. (1974). Deducing flow velocity in cave conduits from scallops. *National Speleological Society Bulletin*, 36(2), 1-5.
- Currens, J. C., & Paylor, R. L. (2009). Karst groundwater basins in Kentucky; Kentucky Geological Survey, unpublished map, scale 1:500,000.
- Currens, J. C., Taylor, C. J., Webb, S., Zhu, J., Workman, S., Agouridis, C., Fox, J., & Husic, A. (2015). Initial Findings from the Karst Water Instrumentation System Station, Royal Spring Groundwater Basin, Kentucky Horse Park 2010-2014, *Proceedings Kentucky Water Resources Annual Symposium, Kentucky Water Resources Research Institute*, Lexington, Kentucky, p. 9-10.
- Cyr, A. J., & Granger, D. E. (2008). Dynamic equilibrium among erosion, river incision, and coastal uplift in the northern and central Apennines, Italy. *Geology*, 36(2), 103-106.
- Danovaro, R., Dell'Anno, A., & Fabiano, M. (2001). Bioavailability of organic matter in the sediments of the Porcupine Abyssal Plain, northeastern Atlantic. *Marine ecology. Progress series*, 220, 25-32.
- Davies-Colley, R. J., Hickey, C. W., Quinn, J. M., & Ryan, P. A. (1992). Effects of clay discharges on streams. *Hydrobiologia*, 248(3), 215-234.
- Davis, C. M., & Fox, J. F. (2009). Sediment fingerprinting: review of the method and future improvements for allocating nonpoint source pollution. *Journal of Environmental Engineering*.
- De Chant, L. J. (2005). The venerable 1/7th power law turbulent velocity profile: a classical nonlinear boundary value problem solution and its relationship to stochastic processes. *Applied Mathematics and Computation*, 161(2), 463-474.
- de Rooij, R., Perrochet, P., & Graham, W. (2013). From rainfall to spring discharge: Coupling conduit flow, subsurface matrix flow and surface flow in karst systems using a discrete–continuum model. *Advances in Water Resources*, 61, 29-41.

- Decho, A. W. (1990). Microbial exopolymer secretions in ocean environments: their role (s) in food webs and marine processes. *Oceanogr. Mar. Biol. Annu. Rev.*, 28(7), 73-153.
- Depetris, P. J., & Kempre, S. (1993). Carbon dynamics and sources in the Parani River. *Limnology and Oceanography*, 38(2), 382-395.
- Dodds, W. K., & Biggs, B. J. (2002). Water velocity attenuation by stream periphyton and macrophytes in relation to growth form and architecture. *Journal of the North American Benthological Society*, 21(1), 2-15.
- Doerfliger, N., Jeannin, P. Y., & Zwahlen, F. (1999). Water vulnerability assessment in karst environments: a new method of defining protection areas using a multi-attribute approach and GIS tools (EPIK method). *Environmental Geology*, 39(2), 165-176.
- Dogwiler, T., & Wicks, C. M. (2004). Sediment entrainment and transport in fluvio-karst systems. *Journal of Hydrology*, 295(1), 163-172.
- Donigian, A. S. (2002). Watershed model calibration and validation: The HSPF experience. *Proceedings of the Water Environment Federation*, 2002(8), 44-73.
- Dou, G. R. (1974). Similarity theory and its application to the design of total sediment transport model. *Research Bulletin of Nanjing Hydraulic Research Institute*.
- Drahovzal, J. A., Harris, D. C., Wickstrom, L. H., Walker, D., Keith, B., Furer, L. C. (1992). The East Continental Rift basin: A New Discovery. Kentucky Geological Survey Special Publication 18, Series XI.
- Drahovzal, J.A., Noger, M. C. (1995). Preliminary map of the structure of the Precambrian surface in eastern Kentucky. Kentucky Geological Survey Map and Chart Series 8, Series XI.
- Dreiss, S. J. (1989). Regional scale transport in a karst aquifer: 1. Component separation of spring flow hydrographs. *Water Resources Research*, 25(1), 117-125.
- Droppo, I. G., & Stone, M. (1994). In-channel surficial fine-grained sediment laminae. Part I: Physical characteristics and formational processes. *Hydrological Processes*, 8(2), 101-111.
- Droppo, I. G., & Amos, C. L. (2001). Structure, stability, and transformation of contaminated lacustrine surface fine-grained laminae. *Journal of Sedimentary Research*, Vol. 71, No. 5, pp 717-726.
- Einsiedl, F. (2005). Flow system dynamics and water storage of a fissured-porous karst aquifer characterized by artificial and environmental tracers. *Journal of Hydrology*, 312(1), 312-321.
- Einstein, H. A. (1950). *The bed-load function for sediment transportation in open channel flows* (No. 1026). US Department of Agriculture.

- Eisenlohr, L., Bouzelboudjen, M., Király, L., & Rossier, Y. (1997). Numerical versus statistical modelling of natural response of a karst hydrogeological system. *Journal of hydrology*, 202(1), 244-262.
- El-Swaify, S. A. (1994). State-of-the-art for assessing soil and water conservation needs and technologies. *Adopting conservation on the farm. An international perspective on the socioeconomics of soil and water conservation. Soil and Water Conservation Society, Ankeny, IA*, 13-27.
- Emblanch, C., Zuppi, G. M., Mudry, J., Blavoux, B., & Batiot, C. (2003). Carbon 13 of TDIC to quantify the role of the unsaturated zone: the example of the Vaucluse karst systems (Southeastern France). *Journal of Hydrology*, 279(1), 262-274.
- Evans, D. J., Gibson, C. E., & Rossell, R. S. (2006). Sediment loads and sources in heavily modified Irish catchments: A move towards informed management strategies. *Geomorphology*, 79(1), 93-113.
- Farnleitner, A. H., Wilhartitz, I., Ryzinska, G., Kirschner, A. K., Stadler, H., Burtscher, M. M., ... & Mach, R. L. (2005). Bacterial dynamics in spring water of alpine karst aquifers indicates the presence of stable autochthonous microbial endokarst communities. *Environmental Microbiology*, 7(8), 1248-1259.
- Field, M. S., & Nash, S. G. (1997). Risk assessment methodology for karst aquifers:(1) Estimating karst conduit-flow parameters. *Environmental Monitoring and Assessment*, 47(1), 1-21.
- Findlay, S. E. G., Mulholland, P. J., Hamilton, S. K., Tank, J. L., Bernot, M. J., Burgin, A. J., ... & Sobota, D. J. (2011). Cross-stream comparison of substrate-specific denitrification potential. *Biogeochemistry*, 104(1-3), 381-392.
- Fiorillo, F. (2011). Tank-reservoir drainage as a simulation of the recession limb of karst spring hydrographs. *Hydrogeology Journal*, 19(5), 1009-1019.
- Fleury, P., Plagnes, V., & Bakalowicz, M. (2007). Modelling of the functioning of karst aquifers with a reservoir model: Application to Fontaine de Vaucluse (South of France). *Journal of Hydrology*, 345(1), 38-49.
- Fleury, P., Maréchal, J. C., & Ladouche, B. (2013). Karst flash-flood forecasting in the city of Nîmes (southern France). *Engineering Geology*, 164, 26-35.
- Fleury, S. (2009). *Land use policy and practice on karst terrains: Living on limestone*. Springer Science & Business Media.
- Ford, D. C., & Williams, P. W. (1989). *Karst Geomorphology and Hydrology* (Vol. 601). London: Unwin Hyman.
- Ford, D. C., & Williams, P. W. (2007). *Karst Hydrogeology and Geomorphology*. Chichester, John Wiley & Sons.

- Ford, W. I., & Fox, J. F. (2012). Model of particulate organic carbon transport in an agriculturally impacted stream. *Hydrological Processes*, 28(3), 662-675.
- Ford, W. I., & Fox, J. F. (2014). Benthic control on the statistical distribution of transported sediment carbon in a low-gradient stream. *Journal of Hydrology*, 515, 316-329.
- Ford, W. I., & Fox, J. F. (2015). Isotope-based Fluvial Organic Carbon (ISOFLOC) Model: Model Formulation, Sensitivity and Evaluation. *Water Resources Research*, 51(6), 4046-4064.
- Ford, W. I., Fox, J. F., & Rowe, H. (2015). Impact of extreme hydrologic disturbance upon the sediment carbon quality in agriculturally impacted temperate streams. *Ecohydrology*, 8(3), 438-449.
- Fox, J. F. (2005). Fingerprinting Using Biogeochemical Tracers to Investigate Watershed Processes. PhD Thesis, University of Iowa, Iowa City, Iowa.
- Fox, J. F. (2009). Measurements of sediment transport processes in forested watersheds with surface coal mining disturbance using carbon and nitrogen isotopes, *Journal of the American Water Resources Association*, 45(5), 1273-1289.
- Fox, J. F., & Papanicolaou, A. N. (2007). The Use of Carbon and Nitrogen Isotopes to Study Watershed Erosion Processes1. *JAWRA Journal of the American Water Resources Association*, 43(4), 1047-1064.
- Fox, J. F., & Papanicolaou, A. N. (2008). An un-mixing model to study watershed erosion processes. *Advances in water resources*, 31(1), 96-108.
- Fox, J. F., Davis, C. M., & Martin, D. K. (2010). Sediment source assessment in a lowland watershed using nitrogen stable isotopes. *Journal of American Water Resources Association* 46:1192-1204.
- Fox, J. F., & Martin, D. K. (2015). Sediment fingerprinting for calibrating a soil erosion and sediment-yield model in mixed land-use watersheds. *Journal of Hydrologic Engineering*, C4014002.
- Gale, S. J. (1984). The hydraulics of conduit flow in carbonate aquifers. *Journal of Hydrology*, 70(1), 309-327.
- Gao, Q., Tao, Z., Yao, G., Ding, J., Liu, Z., & Liu, K. (2007). Elemental and isotopic signatures of particulate organic carbon in the Zengjiang River, southern China. *Hydrological processes*, 21(10), 1318-1327.
- Geyer, T., Birk, S., Licha, T., Liedl, R., & Sauter, M. (2007). Multitracer test approach to characterize reactive transport in karst aquifers. *Groundwater*, 45(1), 36-45.
- Gibert, J. (1986). Ecologie d'un système karstique jurassien. Hydrogéologie, de rive animale, transits de matières, dynamique de la population de Niphargus (Crustacé Amphipode): *Memoires de Biospeologie*, v. 13, p. 1-379.

- Goldman, J. H., Rounds, S. A., Keith, M. K., & Sobieszczyk, S. (2014). Investigating organic matter in Fanno Creek, Oregon, Part 3 of 3: Identifying and quantifying sources of organic matter to an urban stream. *Journal of Hydrology*, 519, 3028-3041.
- Goldscheider, N. (2005). Karst groundwater vulnerability mapping: application of a new method in the Swabian Alb, Germany. *Hydrogeology Journal*, 13(4), 555-564.
- Goldscheider, N., & Drew, D. (Eds.). (2007). *Methods in Karst Hydrogeology: IAH: International Contributions to Hydrogeology*, 26. CRC Press.
- Goldscheider, N., Meiman, J., Pronk, M., & Smart, C. (2008). Tracer tests in karst hydrogeology and speleology. *International Journal of Speleology*, 37(1), 3.
- Gomez, B., Trustrum, N. A., Hicks, D. M., Rogers, K. M., Page, M. J., & Tate, K. R. (2003). Production, storage, and output of particulate organic carbon: Waipaoa River basin, New Zealand. *Water Resources Research*, 39(6).
- Graça, M. A., Ferreira, V., Canhoto, C., Encalada, A. C., Guerrero-Bolaño, F., Wantzen, K. M., & Boyero, L. (2015). A conceptual model of litter breakdown in low order streams. *International Review of Hydrobiology*, 100(1), 1-12.
- Griffiths, N. A., Tank, J. L., Royer, T. V., Warrner, T. J., Frauendorf, T. C., Rosi-Marshall, E. J., & Whiles, M. R. (2012). Temporal variation in organic carbon spiraling in Midwestern agricultural streams. *Biogeochemistry*, 108(1-3), 149-169.
- Grünheid, S., Amy, G., & Jekel, M. (2005). Removal of bulk dissolved organic carbon (DOC) and trace organic compounds by bank filtration and artificial recharge. *Water research*, 39(14), 3219-3228.
- Guo, Q., Wang, Y., Ma, T., & Li, L. (2005). Variation of karst spring discharge in the recent five decades as an indicator of global climate change: A case study at Shanxi, northern China. *Science in China Series D: Earth Sciences*, 48(11), 2001-2010.
- Gupta, R. S. (2008). *Hydrology and Hydraulic Systems*. 3rd ed. Long Grove, IL: Waveland Press, Inc.
- Guy, B. T., Dickenson, W. T., Sohrabi, T. M., & Rudra, R. P. (2009). Development of an empirical model for calculating sediment-transport capacity in shallow overland flows: Model calibration. *Biosystems engineering*, 103(2), 245-255.
- Hanson, G. J., & Simon, A. (2001). Erodibility of cohesive streambeds in the loess area of the midwestern USA. *Hydrological processes*, 15(1), 23-38.
- Hart, E. A., & Schurger, S. G. (2005). Sediment storage and yield in an urbanized karst watershed. *Geomorphology*, 70(1), 85-96.
- Hauns, M., Jeannin, P. Y., & Atteia, O. (2001). Dispersion, retardation and scale effect in tracer breakthrough curves in karst conduits. *Journal of hydrology*, 241(3), 177-193.

- Hélie, J. F., & Hillaire-Marcel, C. (2006). Sources of particulate and dissolved organic carbon in the St Lawrence River: isotopic approach. *Hydrological processes*, 20(9), 1945-1959.
- Herman, E. K., Toran, L., & White, W. B. (2008). Threshold events in spring discharge: evidence from sediment and continuous water level measurement. *Journal of Hydrology*, 351(1), 98-106.
- Hollis, G. E. (1975). The effect of urbanization on floods of different recurrence interval. *Water Resources Research*, 11(3), 431-435.
- Hope, D., Palmer, S. M., Billett, M. F., & Dawson, J. J. (2001). Carbon dioxide and methane evasion from a temperate peatland stream. *Limnology and Oceanography*, 46(4), 847-857
- Howarth, R. W., Fruci, J. R., & Sherman, D. (1991). Inputs of sediment and carbon to an estuarine ecosystem: influence of land use. *Ecological applications*, 27-39.
- Humphreys, W. F. (2006). Aquifers: the ultimate groundwater-dependent ecosystems. *Australian Journal of Botany*, 54(2), 115-132.
- Imberger, S. J., Cook, P. L., Grace, M. R., & Thompson, R. M. (2014). Tracing carbon sources in small urbanising streams: catchment-scale stormwater drainage overwhelms the effects of reach-scale riparian vegetation. *Freshwater Biology*, 59(1), 168-186.
- Islam, M. R., & Chaudhry, M. H. (1997). Numerical solution of transport equation for applications in environmental hydraulics and hydrology. *Journal of hydrology*, 191(1), 106-121.
- Ittekkot, V., Safiullah, S., & Arain, R. (1986). Nature of organic matter in rivers with deep sea connections: The Ganges-Brahmaputra and Indus. *Science of the Total Environment*, 58(1), 93-107.
- Jacinte, P. A., Lal, R., & Owens, L. B. (2009). Application of stable isotope analysis to quantify the retention of eroded carbon in grass filters at the North Appalachian experimental watersheds. *Geoderma*, 148(3), 405-412.
- Jackson, C. R., & Vallaire, S. C. (2007). Microbial activity and decomposition of fine particulate organic matter in a Louisiana cypress swamp. *Journal of the North American Benthological Society*, 26(4), 743-753.
- Jeannin, P. Y. (2001). Modeling flow in phreatic and epiphreatic karst conduits in the Hölloch cave (Muotatal, Switzerland). *Water Resources Research*, 37(2), 191-200.
- Jeannin, P. Y., & Marechal, J. C. (1995). Lois de pertes de charge dans les conduits karstiques: base théorique et observations. *Bull. Hydrogeol.*, 14, 149-176.
- Jeannin, P.-Y., and J.-C. Marechal, Lois de pertes de charge dans les con-

- Jeannin, P.-Y., and J.-C. Marechal, Lois de pertes de charge dans les con-
- Jewell, H. E., & Etensohn, F. R. (2004). An ancient seismite response to Taconian far-field forces: the Cane Run Bed, Upper Ordovician (Trenton) Lexington Limestone, Central Kentucky (USA). *Journal of Geodynamics*, 37(3), 487-511.
- Jiang, Y., & Ji, H. (2013). Isotopic indicators of source and fate of particulate organic carbon in a karstic watershed on the Yunnan-Guizhou Plateau. *Applied Geochemistry*, 36, 153-167.
- Jobbágy, E. G., & Jackson, R. B. (2000). The vertical distribution of soil organic carbon and its relation to climate and vegetation. *Ecological applications*, 10(2), 423-436.
- Jukić, D., & Denić-Jukić, V. (2009). Groundwater balance estimation in karst by using a conceptual rainfall-runoff model. *Journal of hydrology*, 373(3), 302-315.
- Kaftori, D., Hetsroni, G., & Banerjee, S. (1998). The effect of particles on wall turbulence. *International Journal of Multiphase Flow*, 24(3), 359-386.
- Kaufmann, G. (2009). Modelling karst geomorphology on different time scales. *Geomorphology*, 106(1), 62-77.
- Keith, M. K., Sobieszczyk, S., Goldman, J. H., & Rounds, S. A. (2014). Investigating organic matter in Fanno Creek, Oregon, Part 2 of 3: Sources, sinks, and transport of organic matter with fine sediment. *Journal of Hydrology*, 519, 3010-3027.
- Kemmerly, P. R. (1982). Spatial analysis of a karst depression population: clues to genesis. *Geological Society of America Bulletin*, 93(11), 1078-1086.
- Kentucky Geological Survey (KGS). (2002). Karst Is a Landscape. Retrieved from http://www.uky.edu/KGS/water/general/karst/karst_landscape.htm.
- Khomenko, V. P. (2006). Suffosion hazard: Today's and tomorrow's problem for cities. *Proceedings of IAEG2006, Nottingham, UK*, 610, 8.
- Kiraly, L. (1998). Modelling karst aquifers by the combined discrete channel and continuum approach. *Bulletin d'Hydrogéologie*, 16, 77-98.
- Klimchouk, A. B. (2000). The formation of epikarst and its role in vadose speleogenesis. *Speleogenesis: Evolution of karst aquifers. Huntsville: Natl. Speleol. Soc.*, 91-99.
- Konrad, C. P. (2003). Effects of urban development on floods. U.S. Geological Survey Fact Sheet FS-076-03.
- Lacroix, M., Rodet, J., Wang, H. Q., Masséi, N., & Dupont, J. (2000). Origin of suspended particulate matter in a karstic aquifer system: contribution of the microgranulometry. *Comptes Rendus de l'Academie des Sciences Series IIA Earth and Planetary Science*, 330(5), 347-354.

- Lal, R. (2004). Soil carbon sequestration to mitigate climate change. *Geoderma*, 123(1), 1-22.
- Lam, C. H., & Horváth, V. K. (2000). Pipe network model for scaling of dynamic interfaces in porous media. *Physical review letters*, 85(6), 1238.
- Lane, C. S., Lyon, D. R., & Ziegler, S. E. (2013). Cycling of two carbon substrates of contrasting lability by heterotrophic biofilms across a nutrient gradient of headwater streams. *Aquatic sciences*, 75(2), 235-250.
- Lapcevic, P. A., Novakowski, K. S., & Sudicky, E. A. (1999). The interpretation of a tracer experiment conducted in a single fracture under conditions of natural groundwater flow. *Water resources research*, 35(8), 2301-2312.
- Lauritzen, S. E., Abbott, J., Arnesen, R., Crossley, G., Grepperud, D., Ive, A., & Johnson, S. (1985). Morphology and hydraulics of an active phreatic conduit. *Cave Science*, 12, 139-146.
- Lee, E. S., & Krothe, N. C. (2001). A four-component mixing model for water in a karst terrain in south-central Indiana, USA. Using solute concentration and stable isotopes as tracers. *Chemical Geology*, 179(1), 129-143.
- Lee, S. C. (2012). Identifying Hot-Spots of Fecal Contamination in the Royal Spring Karstshed. Master's Thesis, University of Kentucky, Lexington, Kentucky.
- Leibundgut, C. (1998). Vulnerability of karst aquifers. *IAHS PUBLICATION*, 45-60.
- Leithold, E. L., Perkey, D. W., Blair, N. E., & Creamer, T. N. (2005). Sedimentation and carbon burial on the northern California continental shelf: the signatures of land-use change. *Continental Shelf Research*, 25(3), 349-371.
- Liedl, R., Sauter, M., Hückinghaus, D., Clemens, T., & Teutsch, G. (2003). Simulation of the development of karst aquifers using a coupled continuum pipe flow model. *Water Resources Research*, 39(3).
- Long, A. J. (2009). Hydrograph separation for karst watersheds using a two-domain rainfall–discharge model. *Journal of Hydrology*, 364(3), 249-256.
- MacIntyre, S., Lick, W., & Tsai, C. H. T. H. (1990). Variability of entrainment of cohesive sediments in freshwater. *Biogeochemistry*, 9(3), 187-209.
- Madej, M. A., Sutherland, S. G., Lisle, T. E., & Pryor, B. (2009). Channel responses to varying sediment input: a flume experiment modeled after Redwood Creek, California. *Geomorphology*, Vol. 103, pp. 507-519.
- Mahler, B. J., Lynch, L., & Bennett, P. C. (1999). Mobile sediment in an urbanizing karst aquifer: implications for contaminant transport. *Environmental geology*, 39(1), 25-38.

- Maloszewski, P., Stichler, W., Zuber, A., & Rank, D. (2002). Identifying the flow systems in a karstic-fissured-porous aquifer, the Schneetalpe, Austria, by modelling of environmental ^{18}O and ^3H isotopes. *Journal of Hydrology*, 256(1), 48-59.
- Martin, C. H. (2009). Lexington Consent Decree—A Unique Enforcement Action (SSO & MS4 Violations). *Proceedings of the Water Environment Federation*, 2009(2), 30-40.
- Martinotti, W., Camusso, M., Guzzi, L., Patrolecco, L., & Pettine, M. (1997). C, N and their stable isotopes in suspended and sedimented matter from the Po estuary (Italy). In *The Interactions Between Sediments and Water* (pp. 325-332). Springer Netherlands.
- Masiello, C. A., & Druffel, E. R. (2001). Carbon isotope geochemistry of the Santa Clara River. *Global Biogeochemical Cycles*, 15(2).
- Massei, N., Wang, H. Q., Field, M. S., Dupont, J. P., Bakalowicz, M., & Rodet, J. (2006). Interpreting tracer breakthrough tailing in a conduit-dominated karstic aquifer. *Hydrogeology Journal*, 14(6), 849-858.
- Matson, G. C., & Palmer, C. (1909). *Water resources of the Blue Grass region, Kentucky, with a chapter on the quality of the waters* (No. 233). Govt. Print. Off.,.
- McLusky, D.S. (1971). *Ecology of Estuaries*. Heinemann, London.
- Meiman, J., & Ryan, M. T. (1999). The development of basin-scale conceptual models of the active flow conduit system. In *Proceedings of the Karst Modeling Symposium. Karst Waters Institute Special Publication (Vol. 5, pp. 203-212)*.
- Meybeck, M. (1982). Carbon, nitrogen, and phosphorus transport by world rivers. *Am. J. Sci*, 282(4), 401-450.
- Mikac, I., Fiket, Ž., Terzić, S., Barešić, J., Mikac, N., & Ahel, M. (2011). Chemical indicators of anthropogenic impacts in sediments of the pristine karst lakes. *Chemosphere*, 84(8), 1140-1149.
- Milanovic, P. (2004). *Water resources engineering in karst*. CRC press, Taylor & Francis, London.
- Miller, G. (1990). Jr. *Living in the Environment*. The Annenberg/CPB project, Belmont: Wadsworth Inc.
- Miller, R. W., & Donahue, R. L. (1990). *Soils: an introduction to soils and plant growth* (No. Ed. 6). Prentice-Hall International Inc.
- Minshall, G. W., Petersen, R. C., Cummins, K. W., Bott, T. L., Sedell, J. R., Cushing, C. E., & Vannote, R. L. (1983). Interbiome comparison of stream ecosystem dynamics. *Ecological Monographs*, 2-25.

- Minshall, G.W., Petersen, R.C., Bott, T.L., Cushing, C.E., Cummins, K.W., Vannote, R.L., & Sedell, J.R. (1992). Stream ecosystem dynamics of the Salmon River, Idaho: an 8th-order system. *J. N. Am. Benthol. Soc.* 11, 111–137.
- Moody, L. F. (1944). Friction factors for pipe flow. *Trans. Asme*, 66(8), 671-684.
- Moore, J. C., Berlow, E. L., Coleman, D. C., Ruitter, P. C., Dong, Q., Hastings, A., ... & Wall, D. H. (2004). Detritus, trophic dynamics and biodiversity. *Ecology letters*, 7(7), 584-600.
- Moorhead, D. L., Sinsabaugh, R. L., Linkins, A. E., & Reynolds, J. F. (1996). Decomposition processes: modelling approaches and applications. *Science of the Total Environment*, 183(1), 137-149.
- Morgan, R. P. C. (1995). *Soil Erosion and Conservation*. Longman, London.
- Moriasi, D. N., Arnold, J. G., Van Liew, M. W., Bingner, R. L., Harmel, R. D., & Veith, T. L. (2007). Model evaluation guidelines for systematic quantification of accuracy in watershed simulations. *Trans. Asabe*, 50(3), 885-900.
- Morris, G. L., & Fan, J. (1998). *Reservoir sedimentation handbook: design and management of dams, reservoirs, and watersheds for sustainable use*. McGraw Hill Professional.
- Mukundan, R., Radcliffe, D. E., Ritchie, J. C., Risse, L. M., & McKinley, R. A. (2010). Sediment fingerprinting to determine the source of suspended sediment in a southern Piedmont stream. *Journal of environmental Quality*, 39(4), 1328-1337.
- Mulholland, P. J., Helton, A. M., Poole, G. C., Hall, R. O., Hamilton, S. K., Peterson, B. J., ... & Thomas, S. M. (2008). Stream denitrification across biomes and its response to anthropogenic nitrate loading. *Nature*, 452(7184), 202-205.
- Naiman, R., Bilby, R. E., & Kantor, S. (2001). *River ecology and management: lessons from the Pacific coastal ecoregion*. Springer Science & Business Media.
- Nash, J., & Sutcliffe, J. V. (1970). River flow forecasting through conceptual models part I—A discussion of principles. *Journal of hydrology*, 10(3), 282-290.
- Newcomer, T. A., Kaushal, S. S., Mayer, P. M., Shields, A. R., Canuel, E. A., Groffman, P. M., & Gold, A. J. (2012). Influence of natural and novel organic carbon sources on denitrification in forest, degraded urban, and restored streams. *Ecological Monographs*, 82(4), 449-466.
- Owens, P. N., Walling, D. E., Carton, J., Meharg, A. A., Wright, J., & Leeks, G. J. L. (2001). Downstream changes in the transport and storage of sediment-associated contaminants (P, Cr and PCBs) in agricultural and industrialized drainage basins. *Science of the total environment*, 266(1), 177-186.

- Palanisamy, B., & Workman, S. R. (2014). Hydrologic Modeling of Flow through Sinkholes Located in Streambeds of Cane Run Stream, Kentucky. *Journal of Hydrologic Engineering*, 20(5), 04014066.
- Papanicolaou, A. N., Diplas, P., Dancey, C. L., & Balakrishnan, M. (2001). Surface roughness effects in near-bed turbulence: Implications to sediment entrainment. *Journal of Engineering Mechanics*, 127(3), 211-218.
- Papanicolaou, A. N., & Hildale, R. (2002). Turbulence characteristics in gradual channel transition. *ASCE J. Engineering Mechanics*, 128(9), 948-960.
- Papanicolaou, A. N., Fox, J. F., & Marshall, J. (2003). Soil fingerprinting in the Palouse Basin, USA using stable carbon and nitrogen isotopes: *International Journal of Sediment Research*, v. 18, no.2, p. 291–297.
- Paylor, R. & Currens, J. (2004). Royal spring karst groundwater travel time investigation. Report prepared for Georgetown Municipal Water and Sewer Services, Kentucky Geological Survey, University of Kentucky, 15p.
- Perrin, J., Jeannin, P. Y., & Zwahlen, F. (2003). Epikarst storage in a karst aquifer: a conceptual model based on isotopic data, Milandre test site, Switzerland. *Journal of hydrology*, 279(1), 106-124.
- Personné, J. C., Poty, F., Mahler, B. J., & Drogue, C. (2004). Colonization by aerobic bacteria in karst: laboratory and in situ experiments. *Groundwater*, 42(4), 526-533.
- Peterson, E. W. (2002). Fate and transport of 17b-estradiol in karst aquifers. PhD Thesis, University of Missouri Columbia, Columbia, MO, United States.
- Peterson, E. W., & Wicks, C. M. (2006). Assessing the importance of conduit geometry and physical parameters in karst systems using the storm water management model (SWMM). *Journal of hydrology*, 329(1), 294-305.
- Pflüger, Y., Rackham, A., & Larned, S. (2010). The aesthetic value of river flows: An assessment of flow preferences for large and small rivers. *Landscape and Urban Planning*, 95(1), 68-78.
- Phillips, J. M., Russell, M. A., & Walling, D. E. (2000). Time-integrated sampling of fluvial suspended sediment: a simple methodology for small catchments. *Hydrological Processes*, 14, 2589-2602.
- Piest, R. F., Kramer, L. A., & Heinemann, H. G. (1975). Sediment movement from loessial watersheds. *Present and prospective technology for predicting sediment yields and sources*, 130-141.
- Proffitt, A. P. B., & Rose, C. W. (1991). Soil erosion processes. I. The relative importance of rainfall detachment and runoff entrainment. *Soil Research*, 29(5), 671-683.

- Pronk, M., Goldscheider, N., & Zopfi, J. (2006). Dynamics and interaction of organic carbon, turbidity and bacteria in a karst aquifer system. *Hydrogeology Journal*, 14(4), 473-484.
- Pronk, M., Goldscheider, N., Zopfi, J., & Zwahlen, F. (2009). Percolation and particle transport in the unsaturated zone of a karst aquifer. *Groundwater*, 47(3), 361-369.
- Qian, J., Zhao, W., Liu, Y., & Sun, F. (1999). The average velocity test of bedrock water flow in a single fracture within 3 mm width. *Coal Geology & Exploration*, 27(2), 35-38.
- Qian, J., Zhan, H., Zhao, W., & Sun, F. (2005). Experimental study of turbulent unconfined groundwater flow in a single fracture. *Journal of Hydrology*, 311(1), 134-142.
- Ray, J. A. (2005). Sinking streams and losing streams. *Encyclopedia of Caves*. Elsevier, Amsterdam, 509-513.
- Ray, J. A., Webb, J. S & O'dell, P. W. (1994). Groundwater sensitivity regions of Kentucky: map sheet, Kentucky Dept. for Environmental Protection.
- Raymond, P. A., Hartmann, J., Lauerwald, R., Sobek, S., McDonald, C., Hoover, M., ... & Guth, P. (2013). Global carbon dioxide emissions from inland waters. *Nature*, 503(7476), 355-359.
- Reed, T. M., McFarland, J. T., Fryar, A. E., Fogle, A. W., & Taraba, J. L. (2010). Sediment discharges during storm flow from proximal urban and rural karst springs, central Kentucky, USA. *Journal of Hydrology*, 383(3), 280-290.
- Regnier, P., Friedlingstein, P., Ciais, P., Mackenzie, F. T., Gruber, N., Janssens, I. A., ... & Thullner, M. (2013). Anthropogenic perturbation of the carbon fluxes from land to ocean. *Nature Geoscience*, 6(8), 597-607.
- Rier, S. T., Kuehn, K. A., & Francoeur, S. N. (2007). Algal regulation of extracellular enzyme activity in stream microbial communities associated with inert substrata and detritus. *Journal of the North American Benthological Society*, 26(3), 439-449.
- Rouse, H. (1937). Nomograph for the Settling Velocity of Spheres. *Report of the Committee on Sedimentation*, 57.
- Rouse, H. (1976). Hydraulics' latest golden age. *Annual Review of Fluid Mechanics*, 8(1), 1-13.
- Rowe, J. M., Meegan, S. K., Engstrom, E. S., Perry, S. A., & Perry, W. B. (1996) Comparison of leaf processing rates under different temperature regimes in three headwater streams. *Freshwater Biol.* 36, 277-288.
- Russo, J., & Fox, J. (2012). The role of the surface fine-grained laminae in low-gradient streams: A model approach. *Geomorphology*, 171, 127-138.

- Salaheldin, T. M., Imran, J., Chaudhry, M. H., & Reed, C. (2000). Role of fine-grained sediment in turbidity current flow dynamics and resulting deposits. *Marine Geology*, 171(1), 21-38.
- Sand-Jensen, K., & Pedersen, O. (1999). Velocity gradients and turbulence around macrophyte stands in streams. *Freshwater Biology*, 42(2), 315-328.
- Sanford, L. P., & Maa, J. P. Y. (2001). A unified erosion formulation for fine sediments. *Marine Geology*, Vol. 179, pp. 9-23.
- Sarbu, S. M., Kane, T. C., & Kinkle, B. K. (1996). A chemoautotrophically based cave ecosystem. *Science*, 272(5270), 1953.
- Sauter, M. (1992). Quantification and forecasting of regional groundwater flow and transport in a karst aquifer (Gallusquelle, Malm, SW. Germany).
- Sawyer, A. H., Zhu, J., Currens, J. C., Atcher, C., & Binley, A. (2015). Time-lapse electrical resistivity imaging of solute transport in a karst conduit. *Hydrological Processes*, 29(23), 4968-4976.
- Scanlon, B. R., Mace, R. E., Barrett, M. E., & Smith, B. (2003). Can we simulate regional groundwater flow in a karst system using equivalent porous media models? Case study, Barton Springs Edwards aquifer, USA. *Journal of Hydrology*, 276(1), 137-158.
- Schlesinger, W. H. & Melack, J. M. (1981). Transport of organic carbon in the world's rivers. *Tellus*, 33(2), 172-187.
- Schlütter, F. (1999). A conceptual model for sediment transport in combined sewer systems. *Water science and technology*, 39(9), 39-46.
- Sharma, P. S. C. R., & Rai, S. C. (2004). Streamflow, sediment and carbon transport from a Himalayan watershed. *Journal of Hydrology*, 289(1), 190-203.
- Shields, A. (1936). Application of the theory of similarity and turbulence research to the bed load movement, *Mitt. Preuss. Vers. Wasser Schiff*, 26, 5-24.
- Short, R. A., Canton, S. P., & Ward, J. V. (1980). Detrital processing and associated macroinvertebrates in a Colorado mountain stream. *Ecology*, 728-732.
- Shuster, E. T., & White, W. B. (1971). Seasonal fluctuations in the chemistry of lime-stone springs: A possible means for characterizing carbonate aquifers. *Journal of Hydrology*, 14(2), 93-128.
- Sigleo, A. C., & S. A. Macko (2002), Carbon and nitrogen isotopes in suspended particles and colloids, Chesapeake and San Francisco estuaries, U.S.A., *Estuarine Coastal Shelf Sci.*, 54, 701 – 711.

- Simon, A., & Thomas, R.E. (2002). Processes and forms of an unstable alluvial system with resistant, cohesive streambeds. *Earth Surface Processes and Landforms*, Vol. 27, pp. 699-718.
- Simon, A., Pollen-Bankhead, N., Mahacek, V., & Langendoen, E. (2009). Quantifying reductions of mass-failure frequency and sediment loadings from streambanks using toe protection and other means: Lake Tahoe, United States. *Journal of American Water Resources Association*, Vol. 45, pp. 170-186.
- Simon, K. S., & Benfield, E. F. (2001). Leaf and wood breakdown in cave streams. *Journal of the North American Benthological Society*, 20(4), 550-563.
- Simon, K. S., Benfield, E. F., & Macko, S. A. (2003). Food web structure and the role of epilithic biofilms in cave streams. *Ecology*, 84(9), 2395-2406.
- Simon, K. S., Pipan, T., & Culver, D. C. (2007). A conceptual model of the flow and distribution of organic carbon in caves. *Journal of Cave and Karst Studies*, 69(2), 279-284.
- Sinsabaugh, R. L., Osgood, M. P., & Findlay, S. (1994). Enzymatic models for estimating decomposition rates of particulate detritus. *Journal of the North American Benthological Society*, 160-169.
- Six, J., & Jastrow, J. D. (2002). Organic matter turnover. *Encyclopedia of soil science*. Marcel Dekker, New York, 936-942.
- Smart, C. C. (1988). Quantitative tracing of the Maligne karst system, Alberta, Canada. *Journal of hydrology*, 98(3), 185-204.
- Smart, P. L., & Laidlaw, I. M. S. (1977). An evaluation of some fluorescent dyes for water tracing. *Water Resources Research*, 13(1), 15-33.
- Smart, P. L., & Hobbs, S. L. (1986). Characterization of carbonate aquifers: A conceptual base. In *Proceedings of the Environmental Problems in Karst Terranes and Their Solutions Conference, Bowling Green, KY* (pp. 1-14).
- Smith, B. P. G, Naden, P. S., Leeks, G. J. L., & Wass, P. D. (2003). The influence of storm events on fine sediment transport, erosion and deposition within a reach of the River Swale, Yorkshire, UK. *The Science of the Total Environment*, Vol. 314 –316, pp 451–474.
- Smith, D. G., Croker, G. F., & McFarlane, K. (1995). Human perception of water appearance: 1. Clarity and colour for bathing and aesthetics. *New Zealand Journal of Marine and Freshwater Research*, 29(1), 29-43.
- Sobczak, W. V., & Raymond, P. A. (2015). Watershed hydrology and dissolved organic matter export across time scales: minute to millennium. *Freshwater Science*, 34(1), 392-398.

- Sobieszczyk, S., Keith, M. K., Rounds, S. A., & Goldman, J. H. (2014). Investigating organic matter in Fanno Creek, Oregon, Part 1 of 3: estimating annual foliar biomass for a deciduous-dominant urban riparian corridor. *Journal of Hydrology*, 519, 3001-3009.
- Spangler, L. E. (1982). *Karst hydrogeology of northern Fayette and southern Scott counties, Kentucky*.
- Springer, G. S. (2004). A pipe-based, first approach to modeling closed conduit flow in caves. *Journal of Hydrology*, 289(1), 178-189.
- Stallard, R. F. (1998). Terrestrial sedimentation and the carbon cycle: coupling weathering and erosion to carbon burial. *Global Biogeochemical Cycles*, 12(2), 231-257.
- Stone, M., & Droppo, I. G. (1994). In-channel surficial fine-grained sediment laminae. Part II: Chemical characteristics and implications for contaminant transport in fluvial systems. *Hydrological Processes*, 8(2), 113-124.
- Tank, J. L., Rosi-Marshall, E. J., Griffiths, N. A., Entekin, S. A., & Stephen, M. L. (2010). A review of allochthonous organic matter dynamics and metabolism in streams. *Journal of the North American Benthological Society*, 29(1), 118-146.
- Taylor, C. J. (1992). Ground-water occurrence and movement associated with sinkhole alignments in the Inner Bluegrass Karst Region of central Kentucky. PhD Thesis, University of Kentucky, Lexington, Kentucky.
- Thraillkill, J. (1974). Pipe flow models of a Kentucky limestone aquifer. *Groundwater*, 12(4), 202-205.
- Thraillkill, J. (1985). The Inner Blue Grass karst region. Caves and karst of Kentucky: Kentucky Geological Survey, ser, 11, 28-62.
- Thraillkill, J., & Gouzie, D. R. (1984). Discharge and travel time determinations in the Royal Spring groundwater basin, Kentucky. Available from the National Technical Information Service, Springfield VA 22161 as PB 85-214765/AS, Price codes: A 04 in paper copy, A 01 in microfiche. *Research Report*, (149).
- Thraillkill, J., Sullivan, S. B., & Gouzie, D. R. (1991). Flow parameters in a shallow conduit-flow carbonate aquifer, Inner Bluegrass Karst Region, Kentucky, USA. *Journal of Hydrology*, 129(1), 87-108.
- Toy, T. J., Foster, G. R., & Renard, K. G. (2002). Soil erosion: processes, prediction, measurement, and control. John Wiley & Sons.
- Tripathi, G. N. (2009). Use of Surface Geophysical Techniques to Locate a Karst Conduit in the Cane Run-Royal Spring Basin, Kentucky. Master's Thesis, University of Kentucky, Lexington, Kentucky.

- Tritz, S., Guinot, V., & Jourde, H. (2011). Modelling the behaviour of a karst system catchment using non-linear hysteretic conceptual model. *Journal of hydrology*, 397(3), 250-262.
- Tucker, G. E. (2009). Natural experiments in landscape evolution. *Earth Surface Processes and Landforms*, 34(10), 1450.
- University of Kentucky College of Agriculture, Food, and Environment (UKAg). (2012). Cane Run and Royal Spring Watershed-Based Plan. EPA Project Number: C9994861-06.
- United States Environmental Protection Agency (USEPA). (1999). Standard operating procedure for the analysis of residue, nonfilterable (suspended solids), water, method 160.2 NS (Gravimetric, 103-105oC). <http://www.epa.gov/rmdcrl/sop/sopdoc/AIG018.pdf>
- United States Department of Agriculture (USDA). (1993). Soil Survey Manual. Revised Edition, United States Department of Agriculture Handbook No. 18, US Department of Agriculture, Washington, DC.
- Van Dijk, A. I. J. M., Bruijnzeel, L. A., & Eisma, E. H. (2003). A methodology to study rain splash and wash processes under natural rainfall. *Hydrological Processes*, 17(1), 153-167.
- Verardo, D. J., Froelich, P. N., & McIntyre, A. (1990). Determination of organic carbon and nitrogen in marine sediments using the Carlo Erba NA-1500 Analyzer. *Deep Sea Research Part A. Oceanographic Research Papers*, 37(1), 157-165.
- Wallace, J. B., Whiles, M. R., Eggert, S., Cuffney, T. F., Lugthart, G. J., & Chung, K. (1995) Long-term dynamics of coarse particulate organic matter in three Appalachian Mountain streams. *J. N. Am. Benthol. Soc.* 14, 217–232.
- Walling, D. E., & Amos, C. M. (1999). Source, storage and mobilisation of fine sediment in a chalk stream system. *Hydrological processes*, 13(3), 323-340.
- Walling, D. E., Collins, A. L., Jones, P. A., Leeks, G. J. L., & Old, G. (2006). Establishing fine-grained sediment budgets for the Pang and Lambourn LOCAR catchments, UK. *Journal of Hydrology*, 330(1), 126-141.
- Waltham, A. C., & Fookes, P. G. (2003). Engineering classification of karst ground conditions. *Quarterly Journal of Engineering Geology and Hydrogeology*, 36(2), 101-118.
- Ward, G. M. (1986). Lignin and cellulose content of benthic fine particulate organic matter (FPOM) in Oregon Cascade Mountain streams. *J. N. Am. Benthol. Soc.* 5, 127–139.
- Webster, J. R., Benfield, E. F., Ehrman, T. P., Schaeffer, M. A., Tank, J. L., Hutchens, J. J., & D'angelo, D. J. (1999). What happens to allochthonous material that falls into streams? A synthesis of new and published information from Coweeta. *Freshwater Biology*, 41(4), 687-705.

- Weiler, M., McGlynn, B. L., McGuire, K. J., & McDonnell, J. J. (2003). How does rainfall become runoff? A combined tracer and runoff transfer function approach. *Water Resources Research*, 39(11).
- White, W. B. (1988). *Geomorphology and hydrology of karst terrains* (Vol. 464). New York: Oxford university press.
- White, W. B. (2002). Karst hydrology: recent developments and open questions. *Engineering geology*, 65(2), 85-105.
- Wiberg, P. L., & Smith, J. D. (1987). Calculations of the critical shear stress for motion of uniform and heterogeneous sediments. *Water resources research*, 23(8), 1471-1480.
- Wicks, C. M., & Hoke, J. A. (2000). Prediction of the quality and quantity of Maramec Spring water. *Groundwater*, 38(2), 218-225.
- Wilson, J. F., Jr, Cobb, E. D., & Kilpatrick, F. A. (1986). Fluorometric procedures for dye tracing: U.S. Geological Survey Techniques of Water Resources Investigations, Book 3, Chapter A12, p.34.
- Woo, H. S., Julien, P. Y., & Richardson, E. V. (1986). Washload and fine sediment load. *Journal of Hydraulic Engineering*, 112(6), 541-545.
- Wood, P. J., & Armitage, P. D. (1997). Biological effects of fine sediment in the lotic environment. *Environmental management*, 21(2), 203-217.
- Worrall, F., Reed, M., Warburton, J., & Burt, T. (2003). Carbon budget for a British upland peat catchment. *Science of the Total Environment*, 312(1), 133-146.
- Worthington, R. H. S. (1991). Karst hydrogeology of the Canadian rocky mountains. PhD Thesis, McMaster University, Hamilton, Ontario.
- Wu, F. C., & Chou, Y. J. (2003). Rolling and lifting probabilities for sediment entrainment. *Journal of Hydraulic Engineering*, 129(2), 110-119.
- Wynn, T. M., Henderson, M. B., & Vaughan, D. H. (2008). Changes in streambank erodibility and critical shear stress due to subaerial processes along a headwater stream southwestern Virginia, USA. *Geomorphology*, Vol. 97, pp 260–273.
- Yan, L. J., Yu, X.X., Lei, T. W., & Qu, L. Q. (2008). Effects of transport capacity and erodibility on rill erosion processes: a model study using the Finite Element method. *Geoderma*, Vol. 146, pp. 114-120.
- Yoshimura, C., Gessner, M. O., Tockner, K., & Furumai, H. (2008). Chemical properties, microbial respiration, and decomposition of coarse and fine particulate organic matter. *Journal of the North American Benthological Society*, 27(3), 664-673.
- Yuan, Y., Bingner, R. L., & Rebich, R. A. (2001). Evaluation of AnnAGNPS on Mississippi Delta MSEA watersheds. *Transactions of the ASAE*, 44(5), 1183-1190.

Zhang, X., Zhao, X., & Liang, W. (2009). Profile distribution and storage of soil organic carbon and total nitrogen under conservation tillage in Northwest Liaoning, China. *Am.-Eurasian J. Sust. Agric.* 3 (4), 630–636.

Vita

Admin Husic, B.S.CE

Research Associate, Department of Civil Engineering at the University of Kentucky

Education: University of Kentucky, Civil Engineering, B.S. 05/2014

Publications and presentations:

Husic, A., Fox, J., Agouridis, C., Currens, J., Workman, S., Ford, W., and Taylor, C., Investigation of Source, Fate, and Transport of Sediments in a Karst Dominated Watershed. World Environmental & Water Resources Congress. Austin, Texas. May 17-21, 2015.

Husic, A., Fox, J., Agouridis, C., Currens, J., Workman, S., Ford, W., and Taylor, C., Sediment Transport Mechanisms in a Fluvial Karst System in Bluegrass Region. Kentucky Water Resources Research Institute Annual Symposium. Lexington, Kentucky. March 9, 2015.

Husic, A., Fox, J., Agouridis, C., Currens, J., Workman, S., Ford, W., and Taylor, C., Sediment Organic Carbon Fate and Transport Mechanisms in a Fluvial Karst System in the Bluegrass Region. Posters-at-the-Capitol. Frankfort, Kentucky February 19, 2015.